DETERMINING THE ROLE OF IRF6 IN OOGENESIS AND EXTRA EMBRYONIC DEVELOPMENT

By

Arianna L. Smith

A DISSERTATION

Submitted to
Michigan State University
in partial fulfillment of the requirements
for the degree of

Genetics - Doctor of Philosophy

2014

ABSTRACT

DETERMINING THE ROLE OF IRF6 IN OOGENESIS AND EXTRA EMBRYONIC DEVELOPMENT

By

Arianna L. Smith

Interferon Regulatory Factor 6 (IRF6) is a member for the IRF family of transcription factors. Mutations in *IRF6* cause two autosomal dominant Mendelian disorders characterized by cleft lip and palate. In addition, DNA variation in *IRF6* contributes risk for non-syndromic cleft lip and palate. Mouse models developed to study *Irf6* function indicate a critical role in regulation of proliferation and differentiation of keratinocytes during embryogenesis. *Irf6* has also been implicated in adult developmental processes and adult diseases. These include mammary development, breast cancer, squamous cell carcinoma, and wound healing. In addition, *Irf6* has been implicated in a number of processes surrounding reproduction. Studies using ovine models indicate a role for *Irf6* in trophoblast cell types, the cell lineage that composes the placenta. Irf6 was also found to be expressed in bovine oocytes, indicating that it is a maternally expressed gene. Maternal expression of *irf6* is conserved in zebrafish and frog. Inhibition of maternally deposited Irf6 in zebrafish results in early embryonic lethality. The aim of this work was to elucidate the role of maternally expressed *Irf6* in early embryonic development and to study the function of Irf6 in placental development.

To study the function of *Irf6* in a tissue specifc manner, a novel conditional allele of *Irf6,* carrying *LoxP* sites in introns two and four, was generated. We validated the functionality of this allele of *Irf6* using three *Cre* transgenic lines: *Gdf9-Cre, CAG–Cre and Ella-Cre*. Cre-mediated recombination of the conditional allele was sufficient to

produce a null allele of *Irf6.* However, not all *Cre* transgenic lines were able to facilitate recombination with the same efficiency. We conclude that the *Irf6* conditional allele is a novel tool for analysis of *Irf6* function in a tissues specific manner.

The conditional allele of *Irf6*, in combination with the *Gdf9-Cre* transgenic line, was utilized to generate mice with oocyte specific deletion of *Irf6.* Genetic analysis of progeny indicated that *Gdf9-Cre* efficiently recombined the *Irf6* conditional allele in oocytes prior to meiosis I despite persistence of gene products. Female mice with this oocyte specific excision of *Irf6* displayed an increase in litter size when compared to control counterparts. This increase in litter size was accompanied by an increase in ovulation. Females with oocyte specific excision of *Irf6* also displayed an increase in multiple oocyte follicles (MOFs). These MOFs did not appear to contribute to the observed increase in ovulation. MOFs are caused by impaired breakdown of germ cell nest. Irf6 expression was observed at critical time points in germ cell nest breakdown. This expression pattern suggests that *Irf6* plays a role in germ cell nest breakdown. From this work, a novel role for *Irf6* in regulating female fertility and folliculogenesis was identified. The mechanisms underlying these phenotypes have not yet been elucidated.

Lastly, a conventional knockout mouse model was used to study the role of *Irf6* in placental development. Irf6 expression was observed in the mouse placenta during embryogenesis. Analysis of *Irf6*-deficient and wildtype placenta was conducted. We observed no morphological differences in *Irf6*-deficient placenta. Along with this, there was no difference in wet weights between *Irf6*-deficient and wildtype embryos, suggesting normal placental function. We conclude that there is a non-essential role for *Irf6* in placental development.

ACKNOWLEDGEMENTS

To begin, I would like to extend my deepest gratitude to my mentor, Dr. Brian Schutte. His patience with me and confidence in my intellectual ability has been vital to my success. I thank him for teaching my not only how to be a scientist but also how to be a good, fair person. They have both been invaluable lessons. I would also like to thank the members of my committee, Will Kopachik, Jason Knott and Karen Friderici, for the continued support and scientific contribution to this work.

I would like to thank the current and past members of the Schutte Lab: Bill, Walid, Dan, Krysta, Raeuf, Larissa, Julie, Marissa, David, Nicole, Ari, Silas, Soumya, Erica, and Bryana. I could not have asked for a more outstanding group of people to share with both scientifically and socially. I would like to extend a special thank you to the undergraduate and high school students that contributed directly to this work. Jeannie, Kendra, Chelsea, Emily, and Sunny, your hard work and talents did not go unnoticed. Thank you for offering me your dedication, humor and time. I would also like to thank Paula Somohano whose kindness and wonderful spirit guided my first years here. Lastly, I would like to thank Dr. Youssef Kousa and Dr. Tamer Mansour for helping me to grow scientifically, emotionally, and socially. Your guidance, support, and friendship has been invaluable. Thank your helping to mold me, allowing me to voice my opinions, and sharing your beautiful families. To Evon, Dina, David, Elijah, Razan, and Adam, thank you for always embracing me and welcoming me into your families.

I must thank the 5th floor community, members of the Friderici, Fyfe, and Yuzbasiyan-Gurkan labs for their constant willingness to help and for making the 5th a wonderful work environment. To Karen, Meghan, Ellen, and Erin, thank you for all of

your guidance and friendship over the years. I would also like to that the Genetics Program staff and my fellow colleagues. A special thank you goes to Jeannine Lee and Dr. Barbara Sears for their support and willingness to help in any and all circumstances. I truly appreciate it.

I would also like to thank the many people who graciously contributed to this work. To Tim, Katie, Inchul, Zubing and Kai in the Knott Lab, thank you for help in learning techniques surrounding culturing and staining of blastocysts. To Sandeep in the Smith Lab, thank you for your patience and guidance in doing Western blot analysis. I must also thank members of the Histopathology laboratory, for sharing their expertise and warm attitudes, and members of ULAR, for there diligence and help with all things mouse related.

Last, but certainly not least, I would thank my family and friends. I would to thank my parents for a lifetime of love, guidance and support. Without them, none of this would be possible. To my siblings, Kira, Whitney, and Che', thank you for being sources of inspiration and laughter. To the rest of my family here in Michigan, in North Carolina, and in St. Croix, thank you for your support. To Christopher, thank you for being a source of laughter and stress relief. I owe a great deal of gratitude to all of my friends whom for fear of leaving anyone out, I will refrain from mentioning names. Undoubtedly, you have all been my sanity. I sincerely thank you all for your encouragement, insight, and friendship. This journey would not have been the same without you!

TABLE OF CONTENTS

LIST OF TABLES

LIST OF FIGURES

KEY TO ABBREVIATIONS

ART- Assistive Reproductive Technology

E – Embryonic day

PND – Postnatal day

MOF – Multiple oocyte follicle

TGFβ - Transforming Growth Factor β

Gdf9 – Growth and differentiation factor 9

Bmp15 - Bone morphogenetic protein 15

T-syn – t-synthase

Aqp8 – Aquaporin 8

ZGA – zygotic genome activation

Ap2-γ – Activating protein 2 – gamma

ICM – Inner cell mass

TE – Trophectoderm

aPKC- atypical Protein Kinase C

Par - Partitioning

ExE- Extra-embryonic Ectoderm

EPC – ectoplacental cone

LZ – labyrinth zone

JZ – junctional zone

TGC – Trophoblast giant cell

MMP-9 – matrix metalloproteinase 9

IRF – Interferon Regulatory factor

DBD – DNA Binding Domain

IRF- SG – Interferon Regulatory Factor – Supergroup

IAD – Interferon Association Domain

IRF6 – Interferon Regulatory Factor 6

VWS – Van der Woude Syndrome

PPS – Popliteal Pterygium Syndrome

CL/P – Cleft lip with or without cleft palate

SCC – squamous cell carcinoma

MCS9.7 – Multi-species conserved sequence 9.7kb upstream of the promoter

EVL – Enveloping Layer

Kb – kilobases

PCR – Polymerase Chain Reaction

M – Molar

Tg- transgene

H&E – Hematoxylin & Eosin

K14 – Keratin 14

DAPI - 4’ 6- diaminidino-2-phenylindole

cKO – Conditional knockout

PBS – Phosphate buffered saline

IP – intra-peritoneal

IU – international units

PMSG – Pregnant Mare’s Serum Gonadotropin

HCG – Human Chorionic Gonadotropin

CHAPTER ONE

Literature Review

SIGNIFICANCE

Successful pregnancy and childbirth requires the alignment of a number of critical factors and processes coming together in proper timing and space. In mammals, a developing egg cell, the oocyte, must first have the necessary developmental competency to be selected and mature until ovulation. Following ovulation, the oocyte must fuse with a sperm cell to form a diploid cell, known as the zygote. The zygote must undergo a series of timely cell divisions, ultimately giving rise to the blastocyst. The blastocyst gives rise to all cell lineages of the developing embryo and facilitates implantation into the uterine wall (Rossant and Cross, 2001). Defects in these steps underlie many of the most common pregnancy complications.

Infertility and difficulty conceiving affects approximately 12% of all women (Center For Disease Control and Prevention *et al.*, 2013). The underlying causes of such reproductive complications are multi-factorial. Oocyte quality and number are intimately linked to fertility. Poor oocyte quality is often implicated in reduced fertility and is a leading factor in age-related infertility (Navot *et al.*, 1991). Currently, assistive reproductive technologies (ARTs), such as in vitro fertilization, exist to help women overcome these complications. While ARTs are routinely used, they still have relatively low success rates. The Center for Disease Control reports that only 29% of all ART procedures conducted in 2011 resulted in live births (Center For Disease Control and Prevention *et al.*, 2013). Such low efficiency provide further impetus to refine these technologies.

Pregnancy complications, such as preterm birth, preeclampsia, intra-uterine growth restriction and spontaneous abortion, occur in 10-25% of first-time pregnancies

(Lykke *et al.*, 2009). These complications pose significant financial burden and health risk for both the fetus and the mother (Faye-Petersen, 2008; Hustin *et al.*, 1990). They often occur in the same pregnancy and have been reported to share a common causation, a dysfunctional placenta (Ness and Sibai, 2006; Sibai *et al.*, 2005). Like infertility, and difficulty conceiving, these complications often require costly medical interventions. To refine the medical technologies available for conception and pregnancy complications, the molecular players governing these developmental processes must be further explored.

FOLLICULOGENESIS

Female reproduction begins with the female germ cell, the oocyte. In mouse, oogenesis begins at embryonic day 10.5 (E10.5) as primordial germ cells begin to populate the genital ridge where the ovary will form (see Fig1.1) (Pepling, 2013). Once in the genital ridge, primordial germ cells, now called oogonia, divide via mitosis and develop into germ cell nests (Pepling and Spradling, 1998). The oogonia in a germ cell nest maintain communication with one another through intercellular bridges that result from incomplete cytokinesis (Pepling and Spradling, 1998). During germ cell nest formation, the clusters of primordial germ cells are surrounded by epithelial pre-granulosa cells and a basal lamina (Mazaud *et al.*, 2005). At E13.5, oogonia exit mitosis and enter meiosis, becoming oocytes. Oocytes undergo their first meiotic arrest in the diplotene stage of prophase I starting at E17.5, and remain in this state until just before ovulation (Pepling, 2013).

In addition to meiotic arrest, a process known as germ cell breakdown begins as early as E17.5 in the mouse (Pepling, 2013). During germ cell nest breakdown,

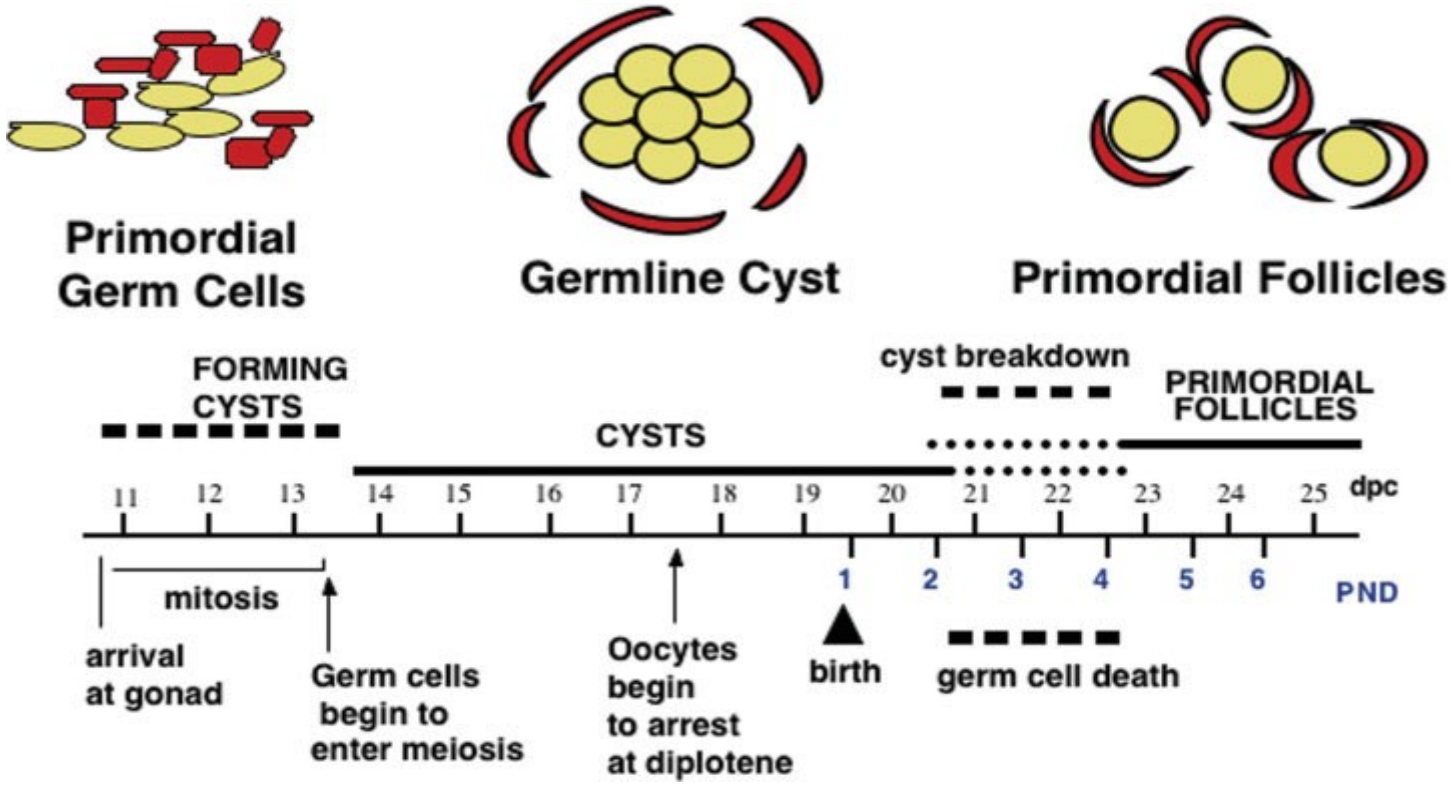

Figure 1.1: **Diagram of oocyte development in mouse**. Developmental processes occurring in utero are denoted on the days post coitum (dpc) scale. Events occurring after birth are denoted on the post natal day scale (PND-blue). Germ cell nest break down begins just before birth and ends at approximately postnatal day 5, producing primordial follicles. Figure from Pepling,M. 2006.

individual oocytes within a nest are separated and encompassed by somatic granulosa cells (Pepling and Spradling, 2001). The separation of germ cell nest requires the dissolution of intercellular bridges and intercalation of pre-granulosa cells (Jefferson *et al.*, 2006). Pre-granulosa cells become mature granulosa cells once they surround an oocyte. Concomitant with this, oocytes within each nest die. Approximately two-thirds of all oocytes undergo programmed cell death (Pepling and Spradling, 2001). Large scale oocyte death is a conserved feature in many species. While the mechanisms governing oocyte death are ill-defined, studies in mouse models indicate that it is essential for proper germ cell nest breakdown. Specifically, mice deficient for *Bax*, a pro-death protein, have more oocytes that remain in nests (Greenfeld *et al.*, 2007a; Greenfeld *et al.*, 2007b). In the mouse, germ cell nest breakdown is complete by postnatal day 7 (PND7) (Pepling, 2006). In humans, this process is complete just before birth (Konishi *et al.*, 1986). Completion of germ cell nest breakdown results in the production of primordial follicles, characterized as one oocyte surrounded by a layer of squamous granulosa cells (Pepling and Spradling, 2001) (See Fig1.1).

Multiple oocytes follicles (MOFs) are defined as more than one oocyte being encompassed in the same follicle (See Fig1.2). In many cases, MOFs arise from incomplete germ cell nest breakdown (Jefferson *et al.*, 2006). A number of mouse mutants display MOFs, suggesting their role in germ cell nest breakdown or primordial follicle formation. The Transforming Growth Factor β (TGFβ) pathway is implicated in MOF formation. Specifically, MOFs are observed in mice with mutations in two oocyte specific TGFβ family members, *growth and differentiation factor 9 (Gdf9)* and *bone morphogenetic protein 15 (Bmp15) (Yan et al., 2001).* In addition, overexpressing

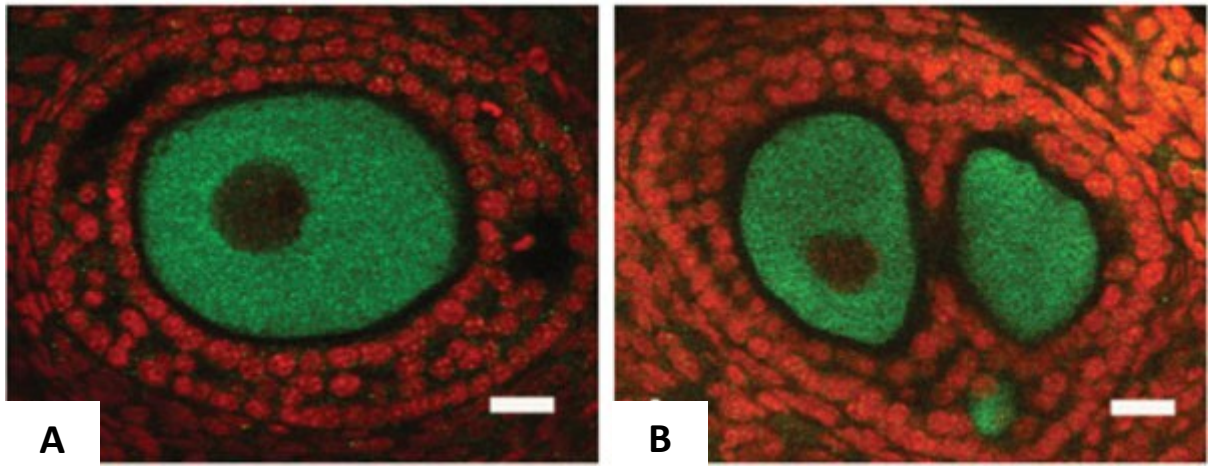

Figure 1.2: **Multiple oocyte follicles in the mouse ovary**. Confocal images of oocytes stained with VASA (green), an oocyte marker, and Propidium Iodine (Red) to mark nuclei. A) Normal follicle with one oocyte surrounded by mutliple layers of granulosa cells and a squamous basement layer. B) Multiple oocyte follicle containing three oocytes in one follicle. Figure modified from Pepling, M. 2006.

Inhibin B, an inhibitor of the TGFβ family member Activin, increases MOF production (McMullen *et al.*, 2001). Oocyte specific deletion of *t-synthase (t-syn),* a critical enzyme involved in synthesis of Core-1 derived O-glycans, leads to MOF formation. Unlike most cases of MOFs, this is a result of fusion of adjacent follicles at later stages of follicle development (Williams and Stanley, 2008).

Interestingly, MOFs are detected in mouse models with knockouts of granulosa specific genes. *Lunatic fringe* is a regulator of Notch signaling and is expressed only in the granulosa cells. Homozygosity for null alleles of *Lunatic Fringe* results in the formation of MOFs (Hahn *et al.*, 2005). In addition, mice with granulosa cell specific deletion of *Notch-2* display MOF formation due to reduced oocyte apoptosis and persistence of germ cell nests (Xu and Gridley, 2013). These data suggest a critical role for Notch signaling in germ cell nest breakdown and primordial follicle formation. Mice homozygous for a null allele of *Aquaporin 8 (Aqp8$^{-/-}$)*, which is expressed specifically in the granulosa cells, also display MOFs (Su *et al.*, 2013) . Aqp8 is a member of the aquaporin family of proteins. These proteins are intergral membrane proteins that facilitate the transport of water in and out of cells (Verkman, 2005). The formation of MOFs as a result of loss of gene function in granulosa cells highlight the critical role for granulosa cells in germ cell nest breakdown and proper follicle development and function.

Increased estrogen signaling also plays a role in MOF formation (Chen *et al.*, 2007; Hunt *et al.*, 2012; Jefferson *et al.*, 2006). Neonatal administration of the phytoestrogen, genistein, inhibits germ cell nest breakdown and leads to the formation of MOFs in mice (Jefferson *et al.*, 2006). Further exploration of genistein and other

estrogen mimetics, such as estradiol and progesterone, in organ culture and *in vivo* models indicate that increased estrogen signaling results in hindered germ cell nest breakdown and reduced oocyte loss (Chen *et al.*, 2007).

It is unclear whether multiple oocyte follicles are able to produce functional oocytes. In vitro fertilization of oocytes from mice neonatally exposed to estrogen mimetics show 30% reduction in fertilization when compared to single oocyte follicles (Iguchi *et al.*, 1991). In addition mice with mutations in *Gdf9* and *Bmp15* are sub-fertile (Yan *et al.*, 2001). However, two mouse models suggests that the presence of MOFs may not result in reduce fertility. *Aqp8*$^{-/-}$ females and mice with oocyte specific deletion of *t-syn* display increased incidence of MOFs and increased litter size (Su *et al.*, 2013; Williams and Stanley, 2008). In humans, there does not appear to be a reduction in fertilization rates in oocytes collected from multiple oocyte follicles (Dandekar *et al.*, 1988). However, the impact of MOFs of human fertility has not been assessed.

The pool of primordial follicles represents the total pool of oocytes available to a female for her entire lifespan (Peters, 1969). This number is estimated to be approximately 2000 primordial follicles at PND7 (Kerr *et al.*, 2006). Follicle activation occurs in two phases, initial recruitment and cyclic recruitment. Initial recruitment is the recruitment of pools of primordial follicles to further development (Pepling, 2013). Primordial follicles are defined as one oocyte surrounded by a single layer of squamous granulosa cells. As follicles become activated, granulosa cells undergo a morphological change, transitioning from squamous to cuboidal. At the primary follicle stage, the oocyte is surrounded by a single layer of cuboidal granulosa cells. Secondary follicles have one oocyte and multiple layers of granulosa cells (Myers *et al.*, 2004). At this

stage, theca cells, which form from fibroblast precursors in the ovary stroma begin to surround the follicle. Like granulosa cells, theca cells are somatic and function in support and growth of the oocyte (Hirshfield, 1991). As development progresses, follicles begin to develop an antrum, a fluid filled space, and become classified as antral follicles (Myers *et al.*, 2004) (See Fig1.3). Meiotic competence is re-established as the antrum begins to form, however surviving oocytes do not re-enter meiosis until just before ovulation in response to a surge of luteinizing hormone (Mehlmann, 2005). During folliculogenesis, the follicle increases greatly in size.

Cyclic recruitment refers to the selection of mature oocytes to complete development. While a large number of primordial oocytes become activated during initial recruitment, most will not make it past the antral stage (Pepling, 2013). Follicle stimulating hormone stimulation promotes further growth of only a few developing follicles to progress on to ovulation (Mehlmann, 2005). The oocyte and granulosa cells undergo apoptosis in follicles that will not make it to ovulation (Pepling, 2013).

MATERNAL CONTROL OF EARLY DEVELOPMENT

As oogenesis progresses, the oocyte grows tremendously, increasing up to 300-fold in volume (Lintern-Moore and Moore, 1979) . Concomitant with this growth is the transcription and translation of much of the maternal genome, resulting in a 300- fold and 38-fold increase in mRNA and protein content, respectively (Pepling, 2013). Some transcripts remain stored in the oocyte via polyadenylation mechanisms and association with protective protein complexes (Racki and Richter, 2006). These genes may be reserved for function later in oogenesis and early embryonic development. The storage

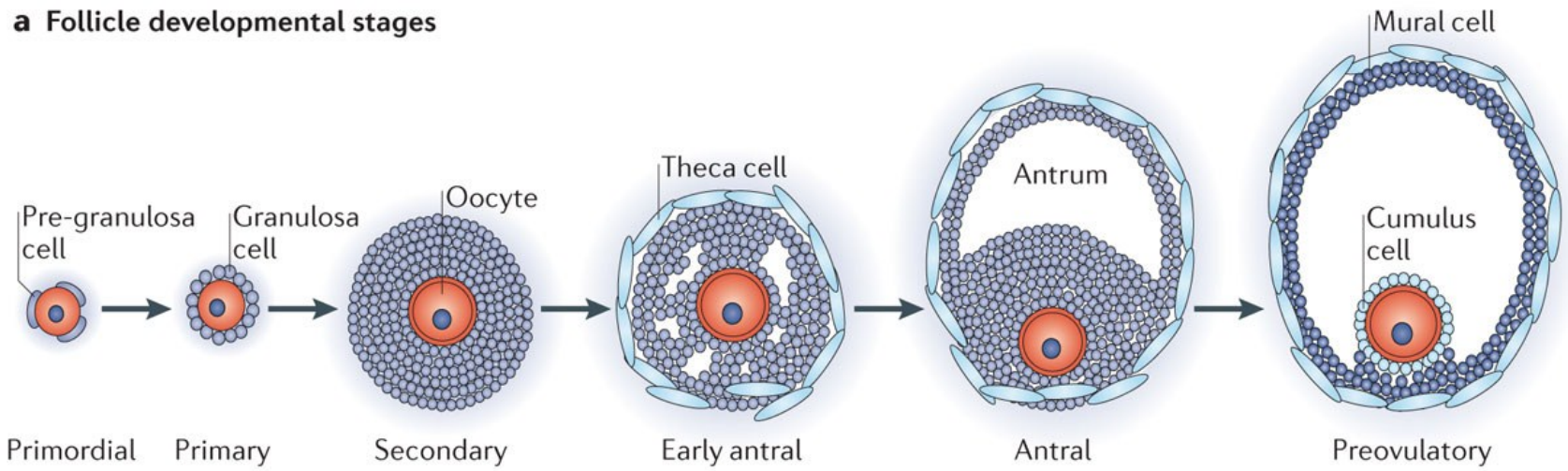

Figure 1.3: **Folliculogenesis.** Follicle development is characterized by growth of the oocyte, an expansion of the granulosa cell population, and the development of a fluid filled space, the antrum. Figure taken from Rong, L and Albertini, A.F. 2013

of maternal gene products and utilization of these products during embryogenesis is a feature conserved across a wide range of species. These genes are known as maternal effect genes (Tadros and Lipshitz, 2009).

Just prior to ovulation, the oocyte becomes transcriptionally silent and thus dependent on stored mRNAs and proteins (Li *et al.*, 2010). Once fusion of the oocyte and sperm occurs, maternally expressed genes play critical roles in processing the paternal genome, replacing protamines with maternal histones (Derijck *et al.*, 2006). In addition, maternally expressed genes, such as *Brg1,* are required for chromatin remodeling of the zygotic genome following fusion of the male and female pronuclei, preparing the genome for transcription (Bultman *et al.*, 2006). Because of their essential function in the oocyte and in the stages following fertilization, loss of function or deletion of maternal effect genes often results in developmental arrest at the one- or two- cell stage (Peng *et al.*, 2012).

The persistence of maternal gene products differs from species to species (Tadros and Lipshitz, 2009). In the mouse, the destabilization and degradation of maternal gene products begins at the one-cell stage (Wang and Dey, 2006). While the mechanisms governing these processes are not well defined, some evidence suggests that small non-coding RNAs may be utilized to mediate degradation (Tang *et al.*, 2007). In addition, the autophagy pathway has also been implicated as a clearing mechanism for maternally deposited proteins (Li *et al.*, 2010). By the two cell stage, only 25% of mRNA and 50% of protein remain. As degradation of maternal genes progresses, the embryo must become reliant on new transcription of the zygotic genome. The major

wave of zygotic genome activation (ZGA) occurs between the two- and four- cell stages (Schultz, 1993) (See Fig 1.4).

While most degradation of maternal proteins occurs early in development, expression of some proteins appears to be maintained well beyond the two-cell stage. For example, maternal deposits of Activating protein 2-gamma (Ap2-γ) and Sox2, both transcription factors, are detectable in embryos until the blastocyst stage (Auman *et al.*, 2002; Avilion *et al.*, 2003). In addition, long-lived maternal proteins may play critical roles in early development past the two-cell stage. Embryos deficient for zygotic *Sox2* (*Sox2*$^{-/-}$) die shortly after implantation into the uterus (Avilion *et al.*, 2003). However, RNAi inhibition of both maternal and zygotic *Sox2* results in embryonic lethality at the two-cell stage (Keramari *et al.*, 2010). Interestingly, similar results have been observed for a number of genes, including Ap2-γ and E-cadherin (Choi *et al.*, 2012; Kanzler *et al.*, 2003). These data indicate a critical role for maternal gene products in preimplantation development.

The use of mouse models to study maternal effects genes is becoming increasingly popular. The Cre-LoxP system allows for gene deletion in a tissue and temporal specific fashion (Nagy, 2000). To date, three oocyte-driven Cre transgenic lines have been developed; *Msx2*-Cre, *Zp3*-Cre, and *Gdf9*-cre (de Vries *et al.*, 2000; Lan *et al.*, 2004). The *Msx2-Cre* transgenic line is capable of driving *Cre* expression in the limbs in addition to the oocyte (Sun *et al.*, 2000). These transgenic lines differ with respect to the time of Cre expression during oocyte development. The *Gdf9-Cre* transgenic line shows *Cre* expression at the primordial follicle stage. The Zp3-Cre transgenic line shows *Cre* expression at the primary follicle stage. Lastly, the Msx2-Cre

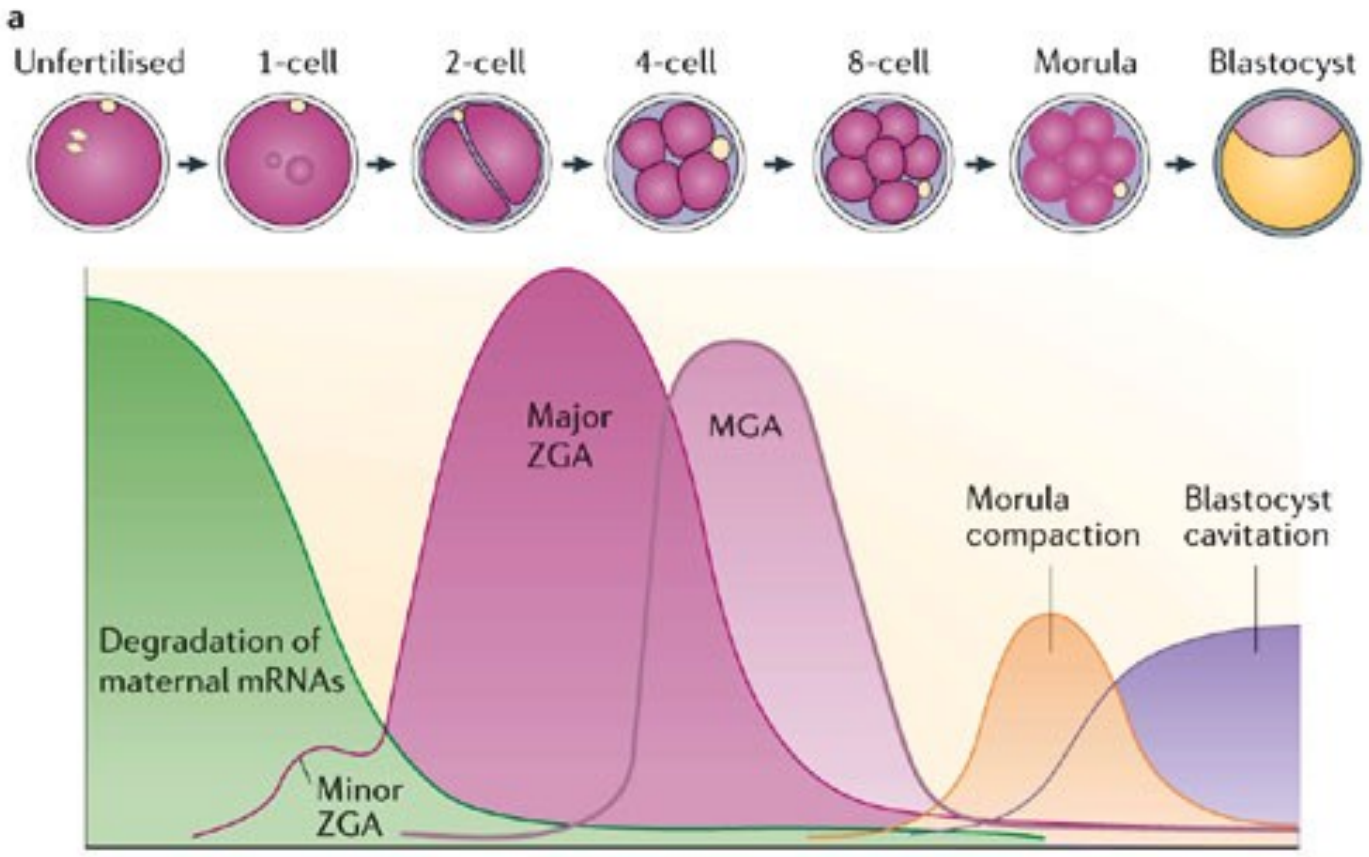

Figure 1.4: Zygotic Genome Activation during preimplantation development. A) Preimplantation development in the mouse from fertilization to formation of the blastocyst. B) Maternal gene products stored in the oocyte persist until the two-cell stage (green curve) when zygotic genome activation (ZGA) occurs (pink curve). Some maternal gene products persist past the two-cell stage. (MGA - mid- preimplantation genome activation) Figure from Wang, H. and Dey, S. K., 2006.

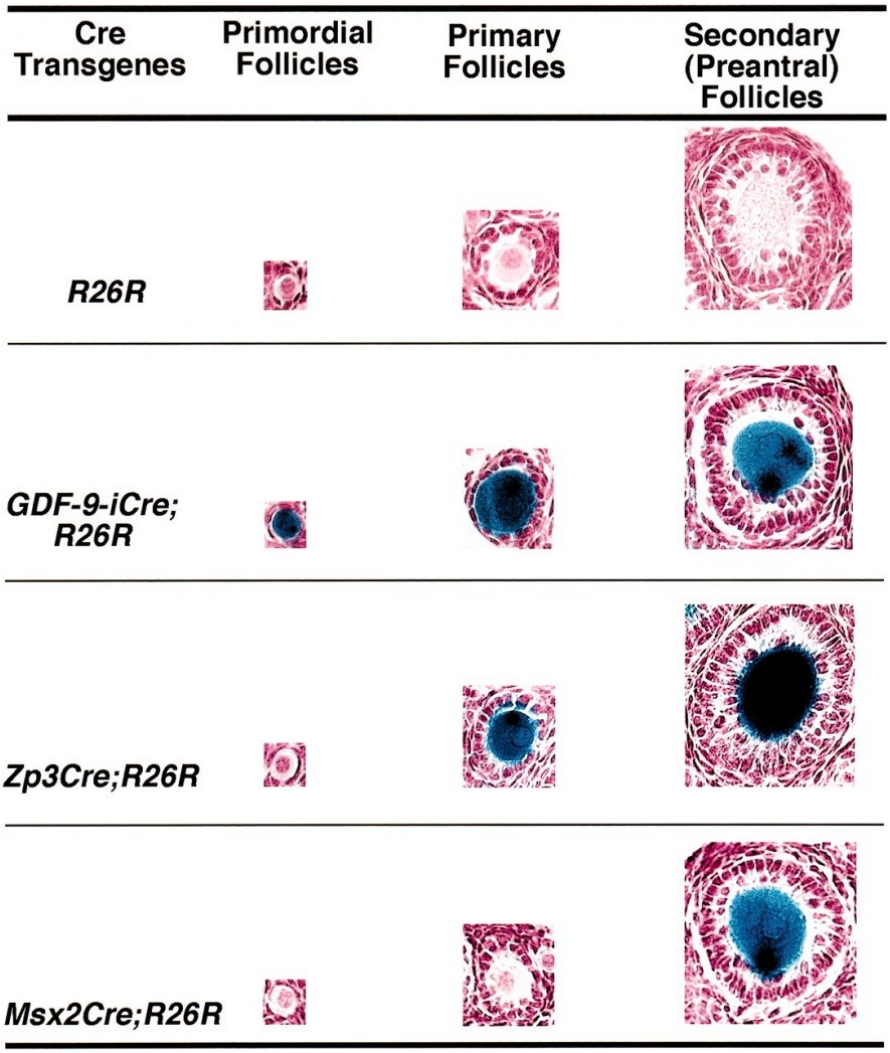

Figure 1.5: **Cre activity of oocyte specific Cre transgenic mouse lines.** Cre expression was analyzed using the ROSA26-reporter line. Figure from Lan *et al*. 2004.

transgenic line shows *Cre* expression at the secondary follicle stage (see Fig 1.5). Thus, the *Gdf9-Cre* is activated the earliest (Lan *et al.*, 2004). These transgenic lines allow the study of gene function during folliculogenesis, fertilization, and early development.

MOUSE PLACENTAL DEVELOPMENT

The first differentiation process in murine development gives rise to two distinct lineages, the inner cell mass (ICM) and the trophectoderm (TE) (Kunath *et al.*, 2004). The ICM gives rise to the three germ layers of the embryo. The TE represents the extra-embryonic lineage and gives rise to the trophoblast cell types that compose the placenta (Kunath *et al.*, 2004). Specification of the trophectoderm begins at the eight-cell stage during an event known as compaction (Pratt *et al.*, 1982). Compaction is characterized by three events. First, individual blastomeres flatten to form a solid mass of cells. Second, cell-cell adhesions between blastomeres increase (Agostoni, 1993). Specifically, adherens junctions, facilitated by E-cadherin, and tight junctions, facilitated by the zona occluden proteins are upregulated (Larue *et al.*, 1994; Sheth *et al.*, 2008). Lastly, at the eight-cell stage, blastomeres acquire an apical-basal polarity (Agostoni, 1993). The atypical protein kinase C (aPKC)/Partioning (Par) system defines this polarity. During compaction, aPKC and Par3 become localized to the apical membrane (Pauken and Capco, 2000; Plusa *et al.*, 2005). In contrast, Par1 and cell-cell adhesion molecules are localized to the basolateral membrane (Vinot *et al.*, 2005). Downregulation of aPKC, by overexpression of a dominant negative aPKC, and Par3, by siRNA, results in adoption of an ICM fate suggesting that the apico-basal polarity is required for specification of the trophectoderm (Plusa *et al.*, 2005). The following

cleavage is asymmetrical producing a 16-celled morula. The morula consists of two populations, inner non-polar cells and outer polarized cells (Rossant and Tam, 2009). These outer cells are fated to become the trophectoderm and begin to upregulate the transcription factor Cdx2 (Beck *et al.*, 1995). At the 32-cell stage, the developing embryo is a blastocyst. The blastocyst consists of the ICM, expressing Oct4, and the trophectoderm, expressing Cdx2 (Beck *et al.*, 1995; Palmieri *et al.*, 1994).

Placental development and implantation of the embryo begins with differentiation of the trophectoderm. Trophectoderm cells that are not in direct contact with the ICM differentiate into primary trophoblast giant cells (Cross *et al.*, 1994). These cells invade the overlying decidua, facilitating implantation of the murine embryo (Zybina *et al.*, 2000). Trophectoderm cells in contact with the ICM proliferate to give rise to the extra-embryonic ectoderm (ExE) and the ectoplacental cone (EPC). The diploid cells of the ExE and EPC are the precursors to the trophoblast cells that compose the placenta (Chavez *et al.*, 1984).

The murine placenta is composed of three distinct zones, the labyrinth zone, the junctional zone, and a monolayer of secondary trophoblast giant cells (Georgiades *et al.*, 2002) (See Fig 1.6). The trophoblast cells that compose the labyrinth zone (LZ), syncytiotrophoblast and cytotrophoblast, are derived from the ExE. The labyrinth zone is the site of feto-maternal exchange of nutrients and gases (Coan *et al.*, 2004). The second zone of the murine placenta is the junctional zone (JZ). The junctional zone is composed of spongiotrophoblast derived from the EPC. The JZ functions in structural support for the underlying labyrinth and hormone production. Secondary trophoblast giant cells are also derived from the EPC (Malassine *et al.*, 2003). Trophoblast giant

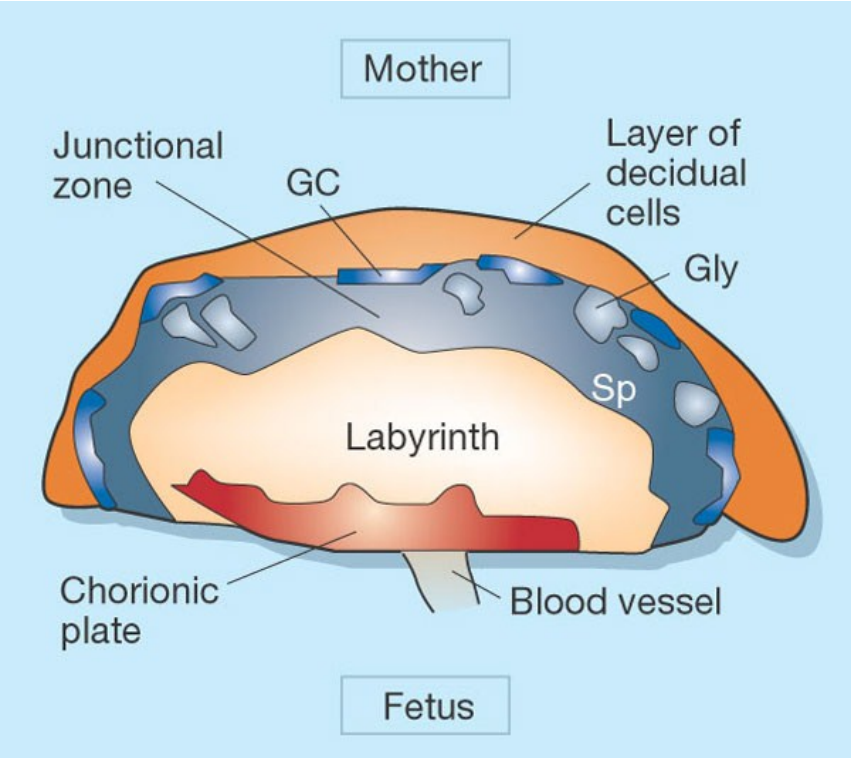

Figure 1.6: **Diagram of the murine placenta**. The fetal placenta is composed of two zones, the labyrinth zone and the junctional zone. GC = trophoblast giant cells, Gly = Trophoblast glycogen cells, Sp = spongiotrophoblast. Figure from Tycko, B. and Efstratiadis, A. 2002

cells endoreplicate without intervening mitoses and produce hormones required for the maintenance of pregnancy (Linzer and Fisher, 1999).

Trophoblast glycogen cells (TGC) are found in the JZ. Trophoblast glycogen cells precursors are detectable in the junctional zone as early as E6.5 (Tesser *et al.*, 2010). However, it is not until E12.5 that trophoblast glycogen cells increase greatly in number within the junctional zone. The origin of these cells in unknown, however both the spongiotrophoblast and TGCs express the marker *Tpbpa*, suggesting a common precursor (Coan *et al.*, 2006). Occasionally, islets of TGCs are found in the LZ. As gestation progresses, TGCs migrate to and invade maternal tissues. This migratory phenotype is thought to be mediated by matrix metalloproteinase-9 (Mmp-9), a protease that degrades the extracellular matrix. Inhibition of proliferation of TGCs is concomitant with the expression of $p57^{kip2}$, a cyclin-dependent kinase inhibitor. Expression of Mmp-9 follows that of $p57^{kip2}$ (Coan *et al.*, 2006).

INTERFERON REGULATORY FACTOR 6

The Interferon Regulatory Factor (IRF) family of transcription factors are well known regulators of immune cell development and immune response (Tamura *et al.*, 2008). Phylogenetic analysis of IRF genes suggest that the family first arose in the last common ancestor of all metazoans. To date, IRF genes have been identified in all basal groups of metazoans (Porifera, Ctenophora, Cnidaria and Bilateria). In lower order metazoans, such as Porifera, Ctenophora and Cnidarians, only two IRF genes have been identified. In Bilaterians, the IRF family is more expansive. Specifically, in vertebrates, the IRF family consists of up to ten members (IRF 1-10). However, in both mouse and human, IRF10 has been lost. In addition to this species specific loss of

IRF10, the IRF family members have been lost in nematodes and insects. Members of the IRF family have not been identified in invertebrates (Huang *et al.*, 2010; Nehyba *et al.*, 2001).

The IRF family shares two conserved functional domains. The first is a highly conserved helix-turn-helix DNA binding domain (DBD) at the N-terminus. The DBD harbors a penta-tryptophan repeat. Studies using protein models indicate that three of these tryptophan residues are critical for contact with DNA. Consistent with the high conservation of the DNA binding domain, all members of the IRF family recognize and bind to a similar core consensus sequence termed the Interferon Stimulated Response Element (5'-A/GNGAAANNGAAACT-3') (Little *et al.*, 2009).

At the C-terminus, the IRFs share a less conserved protein binding domain known as the Interferon Association Domain (IAD). Through this domain, IRFs are capable of homodimerization or heterodimerization with other IRFs and co-factors (see Fig 1.7). The activity of IRF members can be mediated by their protein binding partners, governing their function as repressors or activators and defining specificity via DNA binding sites (Tamura *et al.*, 2008). Characterization of the IAD has led to two specific IRF supergroups (IRF-SG); IRF1-SG and IRF4-SG. The IRF1-SG is comprised of IRF1 and IRF2 and contains a unique IAD (IAD2). The IRF4-SG is divided into three smaller subgroups, the IRF3 group (IRF3, IRF7), the IRF4 group (IRF4, IRF8, IRF9, IRF10) and the IRF5 group (IRF5, IRF6). The IRF4-SG contains an IAD that is related to the MH2 domain of the Smad proteins, termed IAD1. The most ancient IRF family members, identified in sponges, show regions of sequence similarity to the IAD. This

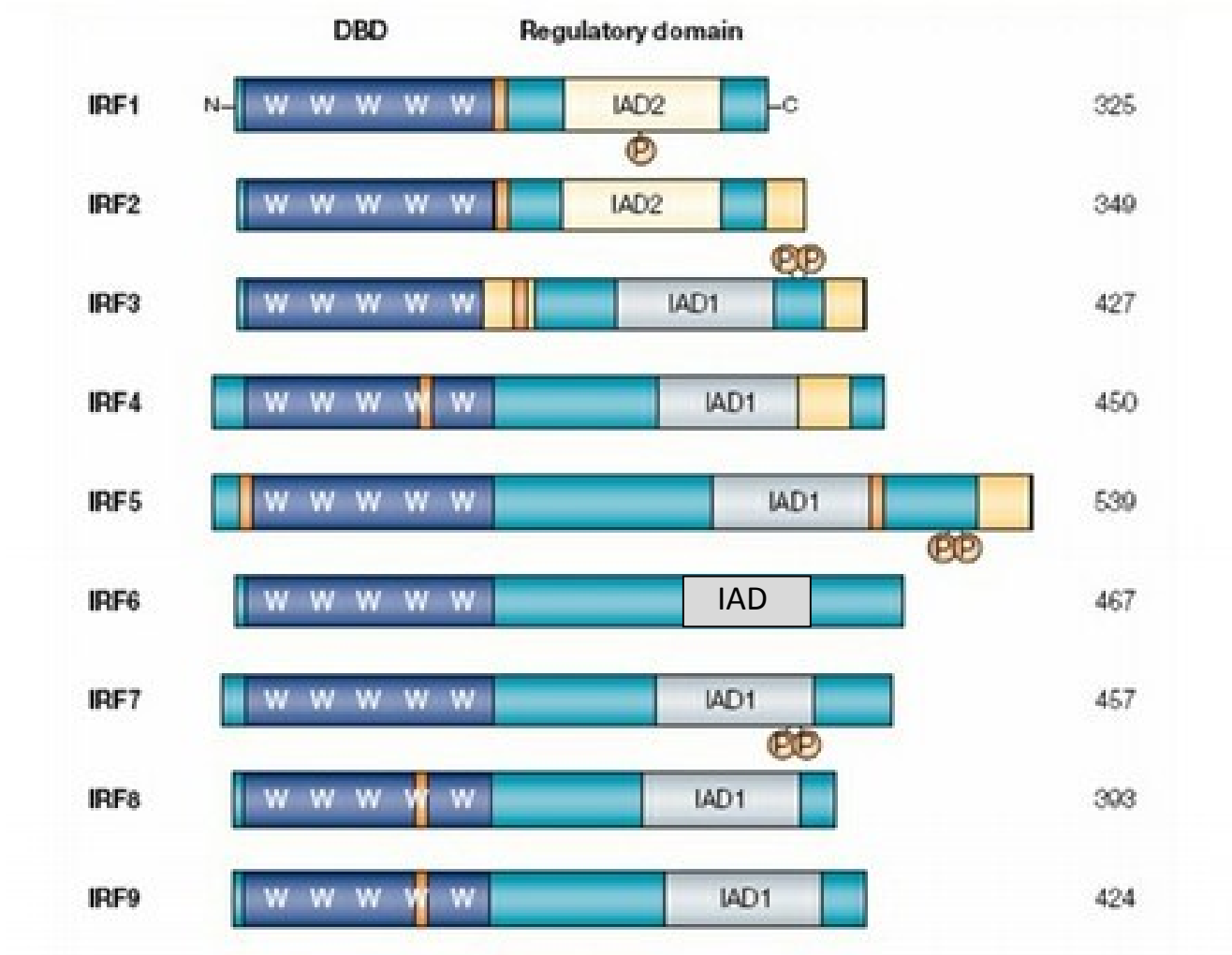

Figure 1.7: **Interferon Regulatory Factor (IRF) family of transcription factors.**

Figure 1.7 (cont'd)

IRFs are characterized by a highly conserved DNA binding domain (DBD) and a much less conserved protein association domain (regulatory domain; IAD – Interferon Association Domain). Figure modified from Lohoff and Mak, 2005.

suggests that the members of the IRF4-SG are more ancient and existed prior to diversification of the family (Nehyba *et al.*, 2009).

Unlike other family members, *IRF6* has no known function in innate immunity. Instead, *Irf6* is critical for proper embryonic development. Mutations in *IRF6* cause two rare, autosomal dominant clefting disorders, Van der Woude syndrome (VWS) and Popliteal Pterygium Syndrome (PPS) (Kondo *et al.*, 2002). VWS is characterized by cleft lip with or without cleft palate (CL/P) and the presence of lower lip pits (Van Der Woude, 1954). Mutations in *IRF6* account for 70% of all VWS cases (de Lima *et al.*, 2009). Patients with PPS present a more severe phenotype, displaying CL/P and lip pits along with webbing behind the knees and between fingers and toes and genital abnormalities (Froster-Iskenius, 1990). Interestingly, there is a phenotype-genotype correlation between mutations in *IRF6* and the occurrence of PPS. Specifically, PPS missense mutations are most commonly localized to residues within the DNA binding domain that directly contact the DNA, indicating the importance of this domain to IRF6 function (Little *et al.*, 2009). Common DNA variation in *IRF6* also increases risk for isolated cleft lip and palate, one of the most common congenital birth defects (Rahimov *et al.*, 2008; Zucchero *et al.*, 2004). To study *Irf6* function in the pathogenesis of cleft lip and palate, knock out mouse models have been generated.

The use of primary antibodies against Irf6 have allowed for the analysis of protein expression in both mouse and human tissues (Botti *et al*., 2011; Ingraham *et al*., 2006). Most extensively, Irf6 protein expression has been characterized in the mouse. Ingraham et al (2006) documented Irf6 expression in mouse tissue using a rabbit polyclonal antibody against Irf6 produced by the Schutte lab (referred to as Irf6-

ResGen). This antibody was made against two peptides within the “linker region” of human IRF6 (see Table 1.1). The linker region lies between the DNA binding domain and the protein association domain and represents the most degenerative region amongst the IRF family. This region was selected to reduce cross-hybridization with other members of the IRF family. The two peptides were co-injected and the resulting antibody was affinity purified. Specificity of this antibody was confirmed by Ingraham et al (2006) via immunofluorescent staining and Western Blot analysis. Specifically, Irf6 signal is lost in skin from embryos homozygous for a null allele of Irf6 (*Irf6*$^{gt/gt}$*)* (Ingraham *et al*., 2006).

Because this resource is no longer available, a second rabbit anti-Irf6 antibody was generated by the Schutte lab (referred to as Irf6-SPEA). This antibody was produced with the approach used to generate the Irf6-ResGen antibody but by a different commercial vendor (see Table 1.1). Another difference is that the antibody was affinity purified for each peptide independently, SPEA and EDEL (named for the first four residues of each peptide). Immunofluorescent staining of palatal epithelium in wildtype embryos using Irf6-SPEA recapitulated the staining that was observed with ResGen-Irf6 (Fakhouri *et al.*, 2012). However, a loss of Irf6 signal has not been observed in *Irf6*$^{gt/gt}$ tissues (Schutte Lab, Unpublished data). Irf6-SPEA has not been used for Western Blot analysis.

To further study Irf6 expression, a commercial antibody was purchased (Sigma-Aldrich, St. Louis, MO, Cat. No. SAB1100039) (referred to as Irf6–Sigma). This antibody was raised in rabbit and made against a peptide in the C-terminus of the human IRF6 protein (see Table 1.1). Immunofluorescent staining in skin from wildtype

Name	Peptide	Peptide source	Validation			
			Wildtype		*Irf6*$^{gt/gt}$	
			IF	WB	IF	WB
Irf6-ResGen	[1]SPEAVWPKTEPLEMEV [2] EDELDQSQHHVPIQDTF	Human /Mouse	**+**	**+**	**-**	**-**
Irf6-SPEA	SPEAVWPKTEPLEMEV	Human /Mouse	**+**[*]	**n/a**	**+**	**n/a**
Irf6-Sigma	RILQTQESWQPMQPT	Human	**+**	**+**	**-**	**-**
Irf6-Akira	SPESVWPKTEPLEMEV	Mouse	**n/a**	**n/a**	**n/a**	**n/a**

Table 1.1: Production and validation of Irf6 antibodies.

Table 1.1 (cont'd)

All four antibodies were produced in rabbit. Immunizing peptide for Irf6-ResGen and Irf6-SPEA do not share completely homology to neither the human nor mouse amino acid sequence. Differing amino acids are underlined. Immunofluoresent (IF) and Western Blot (WB) validation of each antibody was conducted on skin collected from embryonic skin (E17.5).

*Immunofluorescent validation of Irf6-SPEA in wildtype tissue was assessed using palatal epithelium.

murine embryos replicates that of the Irf6-ResGen antibody. In addition, Irf6-Sigma immunofluorescent signal is lost in *Irf6*$^{gt/gt}$ tissues (Smith and Schutte, Unpublished Data). Similar results were observed in Western blot analysis of wildtype and *Irf6*-deficient skin (Kousa and Schutte, Unpublished Data).

Most recently, another rabbit anti-Irf6 antibody was generated by Dr. Akira Kinoshita (referred to Irf6-Akira). Similar to the Irf6-ResGen and Irf6-SPEA antibodies, this antibody was made against a peptide in the linker region of Irf6. However, this peptide was a direct match to the mouse amino acid sequence of Irf6. Irf6 expression analysis in skin using this antibody has yet to be conducted. These antibodies were used to determine expression patterns throughout this project.

Irf6 is highly expressed in the mouse (Kondo *et al.*, 2002). More specifically, *Irf6* is highly expressed in the palatal epithelium, tongue, genitalia, and the epidermis during late stages of embryonic development (Fakhouri *et al.*, 2012; Goudy *et al.*, 2013; Kondo *et al.*, 2002). Mice homozygous for a gene trap allele of *Irf6 (Irf6*$^{gt/gt}$*)* or a dominant negative *Irf6* mutation (*Irf6*$^{R84C/R84C}$) display severe skin, limb, and craniofacial abnormalities, including cleft palate. In addition, these embryos have epithelial adhesions within the oral cavity and esophagus, which may result from the loss of the periderm, a squamous epithelium that coats the embryos during early development. Loss of *Irf6* results in hyperproliferation of the epidermis and failure of differentiation of keratinocytes (Ingraham *et al.*, 2006; Richardson *et al.*, 2006). *In vitro* studies using mouse embryonic keratinocytes confirm the essential role for *Irf6* in promoting keratinocyte differentiation. However, introduction of exogenous *Irf6* is not sufficient to

induce differentiation (Biggs *et al.*, 2012). These data indicate a critical role for *Irf6* in mediating proliferation and differentiation in keratinocytes.

In addition to its well characterized expression in ectoderm, Irf6 expression has been detected in the mesoderm derived muscle of the tongue. Tongue tissue from *Irf6*-deficient embryos is disorganized and shows impaired cytoskeleton organization in the segmental paraxial mesoderm where Irf6 expression was observed. Tongues from *Irf6*-deficient embryos also showed loss of the inter-molar eminence. Irf6 expression was not observed in the inter-molar eminence. These data confirm the function of *Irf6* in regulating differentiation and development in a cell autonomous fashion. However, these data also indicate that *Irf6* is capable of acting in a non-cell autonomous fashion, regulating differentiation and development of tissues it is not expressed in (Goudy *et al.*, 2013).

To date, numerous roles have been identified in development of adult tissues and adult onset disease. In the mouse, *Irf6* is highly expressed in mammary epithelium during mammary gland development (Bailey and Hendrix, 2008; Bailey *et al.*, 2009). Maximal expression is observed during lactation, where mammary epithelial cells are fully differentiated, and markedly reduced following cessation of lactation. In these cells, Irf6 appears to be restricted to the apical membrane and subsequently secreted into breast milk (Bailey *et al.*, 2009). IRF6 expression is reduced or absent in mammary carcinomas. Reintroduction of *IRF6* in breast cancer cell lines results in cell cycle arrest (Bailey *et al.*, 2005). IRF6 is also expressed in adult skin. Furthermore, Irf6 is down-regulated in squamous cell carcinomas (SCC) (Botti *et al.*, 2011). In addition, patients with VWS have increased risk of wound complications following cleft repair surgery,

suggesting a role for Irf6 in wound healing (Jones *et al.*, 2010). These data indicate that IRF6 functions as a tumor suppressor gene and play a critical role in adult tissue development and disease.

Irf6 expression is regulated by an enhancer element 9.7kb upstream of the transcription start site (MCS9.7) (Fakhouri *et al.*, 2012; Rahimov *et al.*, 2008). Analysis of *MCS9.7* activity using an *MCS9.7-LacZ* transgenic mouse line shows that this element is sufficient to recapitulate most, but not all, endogenous Irf6 expression (Fakhouri *et al.*, 2012). The lack of *MCS9.7* activity in all tissues where (Fakhouri *et al.*, 2012) expression is observed suggests that alternate enhancer elements exist to dictate Irf6 expression. To date, this enhancer element has not been identified.

Transcriptional regulation of Irf6 is understudied. *MCS9.7* harbors consensus binding sites for numerous transcription factors, including P63, MAFB, the AP2 family and E-box sites for the basic helix-loop-helix family of transcription factors (Fakhouri *et al.*, 2014; Rahimov *et al.*, 2008; Thomason *et al.*, 2010). One known regulator of IRF6 is p63, a pro-proliferation gene. In keratinocytes, p63 positively regulates *Irf6* expression (Moretti *et al.*, 2010; Thomason *et al.*, 2010). In turn, IRF6 targets p63 for degradation via the proteasome by a mechanism that is not well defined (Moretti *et al.*, 2010). Irf6 expression is also regulated via Notch signaling and *Tgfb3* in keratinocytes (Iwata *et al.*, 2013; Restivo *et al.*, 2011; Richardson *et al.*, 2009). In addition to transcriptional regulation via *MCS9.7*, Irf6 expression appears to be regulated through methylation. In SCC, *Irf6* downregulation is correlated with methylation of a CpG island around the promoter region (Botti *et al.*, 2011).

Irf6 expression can be regulated post-transcriptionally. In mammary epithelial cells, Irf6 exists in a phosphorylated state. Specifically, in quiescent, non-proliferative cells, Irf6 is maintained in its non-phosphorylated state. Upon commencement of proliferation, Irf6 is rapidly phosphorylated. This phosphorylation may act as a signal for translocation into the nucleus and targets Irf6 for degradation (Bailey *et al.*, 2008). As a result, the function of Irf6 in the nucleus is transient and nuclear localization is rarely observed via immunodetection (Bailey *et al.*, 2009; Ingraham *et al.*, 2006).

Irf6 function can be regulated by binding partners. Maspin, a serine protease inhibitor, was identified as an Irf6 binding partner via yeast-two hybrids (Bailey *et al.*, 2005). Maspin has been classified as a tumor suppressor protein as its expression is down-regulated in numerous types of cancer, including breast cancer (Berardi *et al.*, 2013). Dimerization of IRF family members with protein binding partners affects their function as an activator or inhibitor of gene expression (Tamura *et al.*, 2008). To date, Maspin is the only known binding partner for Irf6. Throughout mammary development, both Irf6 and Maspin show dynamic expression profiles suggesting a cooperative role in regulation of mammary epithelium differentiation (Bailey *et al.*, 2009). As stated earlier, reintroduction of Irf6 into breast cancer cell lines results in cessation of proliferation. This effect is augmented upon co-expression with Maspin (Bailey *et al.*, 2008).

In addition to its documented function in mouse and human, more recent reports have implicated *Irf6* in reproductive development in mammals. *Irf6* is expressed in the trophectoderm of ovine embryos and in the uterine epithelium (Fleming *et al.*, 2009). Furthermore, Fleming et al (2009) showed that Irf6 acts as a transcriptional activator in ovine uterine and trophectoderm cell lines (Fleming *et al.*, 2009). In addition, Irf6 was

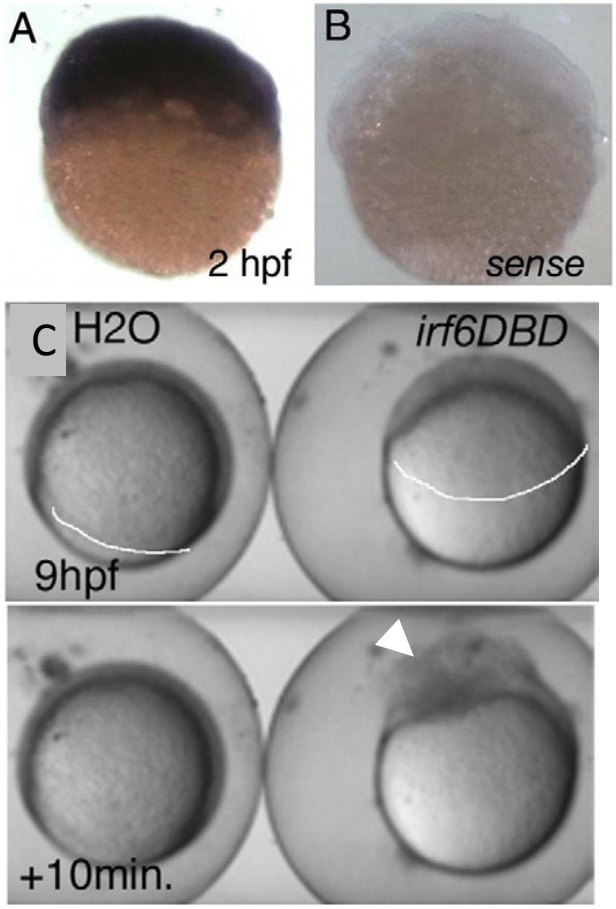

Figure 1.8: **Maternal irf6 is required for zebrafish development.** A) *irf6* is maternally expressed in zebrafish. B) Signal is loss when incubated with the sense probe. C) Zebrafish embyros injected with water (left) or dominant negative *irf6* DNA binding domain (irf6DBD) rupture (see white arrow). Figure modified from Sabel, J. 2009

found to be maternally expressed in mature bovine oocytes at late developmental stages (Regassa *et al.*, 2011). Together these data indicate that Irf6 may play a critical role in pregnancy in mammalian species.

In zebrafish and frog, *irf6* is also maternally expressed (Ben *et al.*, 2005; Sabel *et al.*, 2009) . Maternal irf6 perdures past fertilization in both species and is detected in the superficial epithelial layer of developing zebrafish and Xenopus embryos. In zebrafish, this superficial layer is known as the enveloping layer (EVL). Inhibition of function of maternal and zygotic *irf6* using a dominant negative irf6 construct results in early embryonic lethality in zebrafish embryos. Specifically, embryos injected with dominant-negative *irf6* allele undergo exogastrulation due to failure of differentiation of the EVL (see Fig1.8). Introduction of the *irf6* mRNA resulted in partial rescue of this phenotype. Interestingly, the use of morpholinos to target only zygotic *irf6* mRNA resulted in normal embryonic development. Similar results were observed when Xenopus oocytes were injected with morpholinos inhibiting translation of maternal *irf6* transcript. These data indicate a conserved and essential role for maternally deposited in early embryonic development (Sabel *et al.*, 2009).

SUMMARY

Irf6 is a critical regulator of proliferation and differentiation in epithelial cell types. More recent data suggest that maternal stores of irf6 may play a critical role in oocyte, early embryonic and placental. In humans, common conception and pregnancy complications arise due to impaired oocyte, pre-implantation, and placental development. Inhibition of maternal irf6 in zebrafish embryos results in early embryonic lethality. However, mice deficient for zygotic *Irf6* die shortly after birth. We hypothesize

that this delay in lethality is due to presence of maternal Irf6 in mouse embryos. This dissertation focuses on uncovering the function of Irf6 in reproductive processes, namely determining the role of maternal Irf6 in oocyte and early embryonic development, and placental development, through the use of mouse models.

REFERENCES

REFERENCES

Agostoni E. 1993. Preimplantation development of the mammalian embryo. Annali dell'Istituto superiore di sanita 29: 15-25.

Auman HJ, Nottoli T, Lakiza O, Winger Q, Donaldson S, Williams T. 2002. Transcription factor AP-2gamma is essential in the extra-embryonic lineages for early postimplantation development. Development 129: 2733-2747.

Avilion AA, Nicolis SK, Pevny LH, Perez L, Vivian N, Lovell-Badge R. 2003. Multipotent cell lineages in early mouse development depend on SOX2 function. Genes Dev 17: 126-140.

Bailey CM, Abbott DE, Margaryan NV, Khalkhali-Ellis Z, Hendrix MJ. 2008. Interferon regulatory factor 6 promotes cell cycle arrest and is regulated by the proteasome in a cell cycle-dependent manner. Mol Cell Biol 28: 2235-2243.

Bailey CM, Hendrix MJ. 2008. IRF6 in development and disease: a mediator of quiescence and differentiation. Cell Cycle 7: 1925-1930.

Bailey CM, Khalkhali-Ellis Z, Kondo S, Margaryan NV, Seftor RE, Wheaton WW, Amir S, Pins MR, Schutte BC, Hendrix MJ. 2005. Mammary serine protease inhibitor (Maspin) binds directly to interferon regulatory factor 6: identification of a novel serpin partnership. J Biol Chem 280: 34210-34217.

Bailey CM, Margaryan NV, Abbott DE, Schutte BC, Yang B, Khalkhali-Ellis Z, Hendrix MJ. 2009. Temporal and spatial expression patterns for the tumor suppressor Maspin and its binding partner interferon regulatory factor 6 during breast development. Dev Growth Differ 51: 473-481.

Beck F, Erler T, Russell A, James R. 1995. Expression of Cdx-2 in the mouse embryo and placenta: possible role in patterning of the extra-embryonic membranes. Developmental dynamics : an official publication of the American Association of Anatomists 204: 219-227.

Ben J, Jabs EW, Chong SS. 2005. Genomic, cDNA and embryonic expression analysis of zebrafish IRF6, the gene mutated in the human oral clefting disorders Van der Woude and popliteal pterygium syndromes. Gene Expr Patterns 5: 629-638.

Berardi R, Morgese F, Onofri A, Mazzanti P, Pistelli M, Ballatore Z, Savini A, De Lisa M, Caramanti M, Rinaldi S, Pagliaretta S, Santoni M, Pierantoni C, Cascinu S. 2013. Role of maspin in cancer. Clin Transl Med 2: 8.

Biggs LC, Rhea L, Schutte BC, Dunnwald M. 2012. Interferon regulatory factor 6 is necessary, but not sufficient, for keratinocyte differentiation. J Invest Dermatol 132: 50-58.

Botti E, Spallone G, Moretti F, Marinari B, Pinetti V, Galanti S, De Meo PD, De Nicola F, Ganci F, Castrignano T, Pesole G, Chimenti S, Guerrini L, Fanciulli M, Blandino G, Karin M, Costanzo A. 2011. Developmental factor IRF6 exhibits tumor suppressor activity in squamous cell carcinomas. Proc Natl Acad Sci U S A 108: 13710-13715.

Bultman SJ, Gebuhr TC, Pan H, Svoboda P, Schultz RM, Magnuson T. 2006. Maternal BRG1 regulates zygotic genome activation in the mouse. Genes Dev 20: 1744-1754.

Center For Disease Control and Prevention, American Society for Reproductive Medicine, Society for Assisted Reproductive Technology. 2013. 2011 Assisted Reproductive Technology Fertility Clinic Success Rates Report. In. Atlanta, GA.

Chavez DJ, Enders AC, Schlafke S. 1984. Trophectoderm cell subpopulations in the periimplantation mouse blastocyst. The Journal of experimental zoology 231: 267-271.

Chen Y, Jefferson WN, Newbold RR, Padilla-Banks E, Pepling ME. 2007. Estradiol, progesterone, and genistein inhibit oocyte nest breakdown and primordial follicle assembly in the neonatal mouse ovary in vitro and in vivo. Endocrinology 148: 3580-3590.

Choi I, Carey TS, Wilson CA, Knott JG. 2012. Transcription factor AP-2gamma is a core regulator of tight junction biogenesis and cavity formation during mouse early embryogenesis. Development.

Coan PM, Conroy N, Burton GJ, Ferguson-Smith AC. 2006. Origin and characteristics of glycogen cells in the developing murine placenta. Developmental dynamics : an official publication of the American Association of Anatomists 235: 3280-3294.

Coan PM, Ferguson-Smith AC, Burton GJ. 2004. Developmental dynamics of the definitive mouse placenta assessed by stereology. Biology of reproduction 70: 1806-1813.

Cross JC, Werb Z, Fisher SJ. 1994. Implantation and the placenta: key pieces of the development puzzle. Science 266: 1508-1518.

Dandekar PV, Martin MC, Glass RH. 1988. Polyovular follicles associated with human in vitro fertilization. Fertil Steril 49: 483-486.

de Lima RL, Hoper SA, Ghassibe M, Cooper ME, Rorick NK, Kondo S, Katz L, Marazita ML, Compton J, Bale S, Hehr U, Dixon MJ, Daack-Hirsch S, Boute O, Bayet B, Revencu N, Verellen-Dumoulin C, Vikkula M, Richieri-Costa A, Moretti-Ferreira D, Murray JC, Schutte BC. 2009. Prevalence and nonrandom distribution of exonic mutations in interferon regulatory factor 6 in 307 families with Van der Woude syndrome and 37 families with popliteal pterygium syndrome. Genet Med 11: 241-247.

de Vries WN, Binns LT, Fancher KS, Dean J, Moore R, Kemler R, Knowles BB. 2000. Expression of Cre recombinase in mouse oocytes: a means to study maternal effect genes. Genesis 26: 110-112.

Derijck AA, van der Heijden GW, Giele M, Philippens ME, van Bavel CC, de Boer P. 2006. gammaH2AX signalling during sperm chromatin remodelling in the mouse zygote. DNA Repair (Amst) 5: 959-971.

Fakhouri WD, Rahimov F, Attanasio C, Kouwenhoven EN, Ferreira De Lima RL, Felix TM, Nitschke L, Huver D, Barrons J, Kousa YA, Leslie E, Pennacchio LA, Van Bokhoven H, Visel A, Zhou H, Murray JC, Schutte BC. 2014. An etiologic regulatory mutation in IRF6 with loss- and gain-of-function effects. Hum Mol Genet 23: 2711-2720.

Fakhouri WD, Rhea L, Du T, Sweezer E, Morrison H, Fitzpatrick D, Yang B, Dunnwald M, Schutte BC. 2012. MCS9.7 enhancer activity is highly, but not completely, associated with expression of Irf6 and p63. Dev Dyn 241: 340-349.

Faye-Petersen OM. 2008. The placenta in preterm birth. J Clin Pathol 61: 1261-1275.

Fleming JA, Song G, Choi Y, Spencer TE, Bazer FW. 2009. Interferon regulatory factor 6 (IRF6) is expressed in the ovine uterus and functions as a transcriptional activator. Mol Cell Endocrinol 299: 252-260.

Froster-Iskenius UG. 1990. Popliteal pterygium syndrome. J Med Genet 27: 320-326.

Georgiades P, Ferguson-Smith AC, Burton GJ. 2002. Comparative developmental anatomy of the murine and human definitive placentae. Placenta 23: 3-19.

Goudy S, Angel P, Jacobs B, Hill C, Mainini V, Smith AL, Kousa YA, Caprioli R, Prince LS, Baldwin S, Schutte BC. 2013. Cell-autonomous and non-cell-autonomous roles for IRF6 during development of the tongue. PLoS One 8: e56270.

Greenfeld CR, Babus JK, Furth PA, Marion S, Hoyer PB, Flaws JA. 2007a. BAX is involved in regulating follicular growth, but is dispensable for follicle atresia in adult mouse ovaries. Reproduction 133: 107-116.

Greenfeld CR, Pepling ME, Babus JK, Furth PA, Flaws JA. 2007b. BAX regulates follicular endowment in mice. Reproduction 133: 865-876.

Hahn KL, Johnson J, Beres BJ, Howard S, Wilson-Rawls J. 2005. Lunatic fringe null female mice are infertile due to defects in meiotic maturation. Development 132: 817-828.

Hirshfield AN. 1991. Theca cells may be present at the outset of follicular growth. Biol Reprod 44: 1157-1162.

Huang B, Qi ZT, Xu Z, Nie P. 2010. Global characterization of interferon regulatory factor (IRF) genes in vertebrates: glimpse of the diversification in evolution. BMC Immunol 11: 22.

Hunt PA, Lawson C, Gieske M, Murdoch B, Smith H, Marre A, Hassold T, VandeVoort CA. 2012. Bisphenol A alters early oogenesis and follicle formation in the fetal ovary of the rhesus monkey. Proc Natl Acad Sci U S A 109: 17525-17530.

Hustin J, Jauniaux E, Schaaps JP. 1990. Histological study of the materno-embryonic interface in spontaneous abortion. Placenta 11: 477-486.

Iguchi T, Kamiya K, Uesugi Y, Sayama K, Takasugi N. 1991. In vitro fertilization of oocytes from polyovular follicles in mouse ovaries exposed neonatally to diethylstilbestrol. In Vivo 5: 359-363.

Ingraham CR, Kinoshita A, Kondo S, Yang B, Sajan S, Trout KJ, Malik MI, Dunnwald M, Goudy SL, Lovett M, Murray JC, Schutte BC. 2006. Abnormal skin, limb and craniofacial morphogenesis in mice deficient for interferon regulatory factor 6 (Irf6). Nat Genet 38: 1335-1340.

Iwata J, Suzuki A, Pelikan RC, Ho TV, Sanchez-Lara PA, Urata M, Dixon MJ, Chai Y. 2013. Smad4-Irf6 genetic interaction and TGFbeta-mediated IRF6 signaling cascade are crucial for palatal fusion in mice. Development 140: 1220-1230.

Jefferson W, Newbold R, Padilla-Banks E, Pepling M. 2006. Neonatal genistein treatment alters ovarian differentiation in the mouse: inhibition of oocyte nest breakdown and increased oocyte survival. Biol Reprod 74: 161-168.

Jones JL, Canady JW, Brookes JT, Wehby GL, L'Heureux J, Schutte BC, Murray JC, Dunnwald M. 2010. Wound complications after cleft repair in children with Van der Woude syndrome. J Craniofac Surg 21: 1350-1353.

Kanzler B, Haas-Assenbaum A, Haas I, Morawiec L, Huber E, Boehm T. 2003. Morpholino oligonucleotide-triggered knockdown reveals a role for maternal E-cadherin during early mouse development. Mech Dev 120: 1423-1432.

Keramari M, Razavi J, Ingman KA, Patsch C, Edenhofer F, Ward CM, Kimber SJ. 2010. Sox2 is essential for formation of trophectoderm in the preimplantation embryo. PLoS One 5: e13952.

Kerr JB, Duckett R, Myers M, Britt KL, Mladenovska T, Findlay JK. 2006. Quantification of healthy follicles in the neonatal and adult mouse ovary: evidence for maintenance of primordial follicle supply. Reproduction 132: 95-109.

Kondo S, Schutte BC, Richardson RJ, Bjork BC, Knight AS, Watanabe Y, Howard E, de Lima RL, Daack-Hirsch S, Sander A, McDonald-McGinn DM, Zackai EH, Lammer EJ, Aylsworth AS, Ardinger HH, Lidral AC, Pober BR, Moreno L, Arcos-Burgos M, Valencia C, Houdayer C, Bahuau M, Moretti-Ferreira D, Richieri-Costa A, Dixon MJ, Murray JC. 2002. Mutations in IRF6 cause Van der Woude and popliteal pterygium syndromes. Nat Genet 32: 285-289.

Konishi I, Fujii S, Okamura H, Parmley T, Mori T. 1986. Development of interstitial cells and ovigerous cords in the human fetal ovary: an ultrastructural study. J Anat 148: 121-135.

Kunath T, Strumpf D, Rossant J. 2004. Early trophoblast determination and stem cell maintenance in the mouse--a review. Placenta 25 Suppl A: S32-38.

Lan ZJ, Xu X, Cooney AJ. 2004. Differential oocyte-specific expression of Cre recombinase activity in GDF-9-iCre, Zp3cre, and Msx2Cre transgenic mice. Biol Reprod 71: 1469-1474.

Larue L, Ohsugi M, Hirchenhain J, Kemler R. 1994. E-cadherin null mutant embryos fail to form a trophectoderm epithelium. Proceedings of the National Academy of Sciences of the United States of America 91: 8263-8267.

Li L, Zheng P, Dean J. 2010. Maternal control of early mouse development. Development 137: 859-870.

Lintern-Moore S, Moore GP. 1979. The initiation of follicle and oocyte growth in the mouse ovary. Biol Reprod 20: 773-778.

Linzer DI, Fisher SJ. 1999. The placenta and the prolactin family of hormones: regulation of the physiology of pregnancy. Molecular endocrinology 13: 837-840.

Little HJ, Rorick NK, Su LI, Baldock C, Malhotra S, Jowitt T, Gakhar L, Subramanian R, Schutte BC, Dixon MJ, Shore P. 2009. Missense mutations that cause Van der Woude syndrome and popliteal pterygium syndrome affect the DNA-binding and transcriptional activation functions of IRF6. Hum Mol Genet 18: 535-545.

Lykke JA, Paidas MJ, Langhoff-Roos J. 2009. Recurring complications in second pregnancy. Obstet Gynecol 113: 1217-1224.

Malassine A, Frendo JL, Evain-Brion D. 2003. A comparison of placental development and endocrine functions between the human and mouse model. Human reproduction update 9: 531-539.

Mazaud S, Guyot R, Guigon CJ, Coudouel N, Le Magueresse-Battistoni B, Magre S. 2005. Basal membrane remodeling during follicle histogenesis in the rat ovary: contribution of proteinases of the MMP and PA families. Dev Biol 277: 403-416.

McMullen ML, Cho BN, Yates CJ, Mayo KE. 2001. Gonadal pathologies in transgenic mice expressing the rat inhibin alpha-subunit. Endocrinology 142: 5005-5014.

Mehlmann LM. 2005. Stops and starts in mammalian oocytes: recent advances in understanding the regulation of meiotic arrest and oocyte maturation. Reproduction 130: 791-799.

Moretti F, Marinari B, Lo Iacono N, Botti E, Giunta A, Spallone G, Garaffo G, Vernersson-Lindahl E, Merlo G, Mills AA, Ballaro C, Alema S, Chimenti S, Guerrini L, Costanzo A. 2010. A regulatory feedback loop involving p63 and IRF6 links the pathogenesis of 2 genetically different human ectodermal dysplasias. J Clin Invest 120: 1570-1577.

Myers M, Britt KL, Wreford NG, Ebling FJ, Kerr JB. 2004. Methods for quantifying follicular numbers within the mouse ovary. Reproduction 127: 569-580.

Nagy A. 2000. Cre recombinase: the universal reagent for genome tailoring. Genesis 26: 99-109.

Navot D, Bergh PA, Williams MA, Garrisi GJ, Guzman I, Sandler B, Grunfeld L. 1991. Poor oocyte quality rather than implantation failure as a cause of age-related decline in female fertility. Lancet 337: 1375-1377.

Nehyba J, Hrdlickova R, Bose HR. 2009. Dynamic evolution of immune system regulators: the history of the interferon regulatory factor family. Mol Biol Evol 26: 2539-2550.

Nehyba J, Hrdličková R, Bose HR. 2001. Evolution of the Interferon Regulatory Factor Family. In: eLS: John Wiley & Sons, Ltd.

Ness RB, Sibai BM. 2006. Shared and disparate components of the pathophysiologies of fetal growth restriction and preeclampsia. Am J Obstet Gynecol 195: 40-49.

Palmieri SL, Peter W, Hess H, Scholer HR. 1994. Oct-4 transcription factor is differentially expressed in the mouse embryo during establishment of the first two extraembryonic cell lineages involved in implantation. Developmental biology 166: 259-267.

Pauken CM, Capco DG. 2000. The expression and stage-specific localization of protein kinase C isotypes during mouse preimplantation development. Developmental biology 223: 411-421.

Peng H, Chang B, Lu C, Su J, Wu Y, Lv P, Wang Y, Liu J, Zhang B, Quan F, Guo Z, Zhang Y. 2012. Nlrp2, a maternal effect gene required for early embryonic development in the mouse. PLoS One 7: e30344.

Pepling M. 2013. Oocyte Development before and during Folliculogenesis. In: Oocyte Physiology and Development in Domestic Animals: Wiley-Blackwell. p 1-19.

Pepling ME. 2006. From primordial germ cell to primordial follicle: mammalian female germ cell development. Genesis 44: 622-632.

Pepling ME, Spradling AC. 1998. Female mouse germ cells form synchronously dividing cysts. Development 125: 3323-3328.

Pepling ME, Spradling AC. 2001. Mouse ovarian germ cell cysts undergo programmed breakdown to form primordial follicles. Dev Biol 234: 339-351.

Pesce M, De Felici M. 1994. Apoptosis in mouse primordial germ cells: a study by transmission and scanning electron microscope. Anat Embryol (Berl) 189: 435-440.

Peters H. 1969. The development of the mouse ovary from birth to maturity. Acta Endocrinol (Copenh) 62: 98-116.

Plusa B, Frankenberg S, Chalmers A, Hadjantonakis AK, Moore CA, Papalopulu N, Papaioannou VE, Glover DM, Zernicka-Goetz M. 2005. Downregulation of Par3 and aPKC function directs cells towards the ICM in the preimplantation mouse embryo. Journal of cell science 118: 505-515.

Pratt HP, Ziomek CA, Reeve WJ, Johnson MH. 1982. Compaction of the mouse embryo: an analysis of its components. Journal of embryology and experimental morphology 70: 113-132.

Racki WJ, Richter JD. 2006. CPEB controls oocyte growth and follicle development in the mouse. Development 133: 4527-4537.

Rahimov F, Marazita ML, Visel A, Cooper ME, Hitchler MJ, Rubini M, Domann FE, Govil M, Christensen K, Bille C, Melbye M, Jugessur A, Lie RT, Wilcox AJ, Fitzpatrick DR, Green ED, Mossey PA, Little J, Steegers-Theunissen RP, Pennacchio LA, Schutte BC, Murray JC. 2008. Disruption of an AP-2alpha binding site in an IRF6 enhancer is associated with cleft lip. Nat Genet 40: 1341-1347.

Regassa A, Rings F, Hoelker M, Cinar U, Tholen E, Looft C, Schellander K, Tesfaye D. 2011. Transcriptome dynamics and molecular cross-talk between bovine oocyte and its companion cumulus cells. BMC Genomics 12: 57.

Restivo G, Nguyen BC, Dziunycz P, Ristorcelli E, Ryan RJ, Ozuysal OY, Di Piazza M, Radtke F, Dixon MJ, Hofbauer GF, Lefort K, Dotto GP. 2011. IRF6 is a mediator of Notch pro-differentiation and tumour suppressive function in keratinocytes. EMBO J 30: 4571-4585.

Richardson RJ, Dixon J, Jiang R, Dixon MJ. 2009. Integration of IRF6 and Jagged2 signalling is essential for controlling palatal adhesion and fusion competence. Hum Mol Genet 18: 2632-2642.

Richardson RJ, Dixon J, Malhotra S, Hardman MJ, Knowles L, Boot-Handford RP, Shore P, Whitmarsh A, Dixon MJ. 2006. Irf6 is a key determinant of the keratinocyte proliferation-differentiation switch. Nat Genet 38: 1329-1334.

Rossant J, Cross JC. 2001. Placental development: lessons from mouse mutants. Nat Rev Genet 2: 538-548.

Rossant J, Tam PP. 2009. Blastocyst lineage formation, early embryonic asymmetries and axis patterning in the mouse. Development 136: 701-713.

Sabel JL, d'Alencon C, O'Brien EK, Van Otterloo E, Lutz K, Cuykendall TN, Schutte BC, Houston DW, Cornell RA. 2009. Maternal Interferon Regulatory Factor 6 is required for the differentiation of primary superficial epithelia in Danio and Xenopus embryos. Dev Biol 325: 249-262.

Schultz RM. 1993. Regulation of zygotic gene activation in the mouse. Bioessays 15: 531-538.

Sheth B, Nowak RL, Anderson R, Kwong WY, Papenbrock T, Fleming TP. 2008. Tight junction protein ZO-2 expression and relative function of ZO-1 and ZO-2 during mouse blastocyst formation. Experimental cell research 314: 3356-3368.

Sibai B, Dekker G, Kupferminc M. 2005. Pre-eclampsia. Lancet 365: 785-799.

Su W, Guan X, Zhang D, Sun M, Yang L, Yi F, Hao F, Feng X, Ma T. 2013. Occurrence of multi-oocyte follicles in aquaporin 8-deficient mice. Reprod Biol Endocrinol 11: 88.

Sun X, Lewandoski M, Meyers EN, Liu YH, Maxson RE, Jr., Martin GR. 2000. Conditional inactivation of Fgf4 reveals complexity of signalling during limb bud development. Nat Genet 25: 83-86.

Tadros W, Lipshitz HD. 2009. The maternal-to-zygotic transition: a play in two acts. Development 136: 3033-3042.

Tamura T, Yanai H, Savitsky D, Taniguchi T. 2008. The IRF family transcription factors in immunity and oncogenesis. Annu Rev Immunol 26: 535-584.

Tang F, Kaneda M, O'Carroll D, Hajkova P, Barton SC, Sun YA, Lee C, Tarakhovsky A, Lao K, Surani MA. 2007. Maternal microRNAs are essential for mouse zygotic development. Genes Dev 21: 644-648.

Tesser RB, Scherholz PL, do Nascimento L, Katz SG. 2010. Trophoblast glycogen cells differentiate early in the mouse ectoplacental cone: putative role during placentation. Histochemistry and cell biology 134: 83-92.

Thomason HA, Zhou H, Kouwenhoven EN, Dotto GP, Restivo G, Nguyen BC, Little H, Dixon MJ, van Bokhoven H, Dixon J. 2010. Cooperation between the transcription factors p63 and IRF6 is essential to prevent cleft palate in mice. J Clin Invest 120: 1561-1569.

Van Der Woude A. 1954. Fistula labii inferioris congenita and its association with cleft lip and palate. Am J Hum Genet 6: 244-256.

Verkman AS. 2005. More than just water channels: unexpected cellular roles of aquaporins. J Cell Sci 118: 3225-3232.

Vinot S, Le T, Ohno S, Pawson T, Maro B, Louvet-Vallee S. 2005. Asymmetric distribution of PAR proteins in the mouse embryo begins at the 8-cell stage during compaction. Developmental biology 282: 307-319.

Wang H, Dey SK. 2006. Roadmap to embryo implantation: clues from mouse models. Nat Rev Genet 7: 185-199.

Williams SA, Stanley P. 2008. Mouse fertility is enhanced by oocyte-specific loss of core 1-derived O-glycans. FASEB J 22: 2273-2284.

Xu J, Gridley T. 2013. Notch2 is required in somatic cells for breakdown of ovarian germ-cell nests and formation of primordial follicles. BMC Biol 11: 13.

Yan C, Wang P, DeMayo J, DeMayo FJ, Elvin JA, Carino C, Prasad SV, Skinner SS, Dunbar BS, Dube JL, Celeste AJ, Matzuk MM. 2001. Synergistic roles of bone morphogenetic protein 15 and growth differentiation factor 9 in ovarian function. Mol Endocrinol 15: 854-866.

Zucchero TM, Cooper ME, Maher BS, Daack-Hirsch S, Nepomuceno B, Ribeiro L, Caprau D, Christensen K, Suzuki Y, Machida J, Natsume N, Yoshiura K, Vieira AR, Orioli IM, Castilla EE, Moreno L, Arcos-Burgos M, Lidral AC, Field LL, Liu

YE, Ray A, Goldstein TH, Schultz RE, Shi M, Johnson MK, Kondo S, Schutte BC, Marazita ML, Murray JC. 2004. Interferon regulatory factor 6 (IRF6) gene variants and the risk of isolated cleft lip or palate. N Engl J Med 351: 769-780.

Zybina EV, Zybina TG, Stein GI. 2000. Trophoblast cell invasiveness and capability for the cell and genome reproduction in rat placenta. Early Pregnancy 4: 39-57.

CHAPTER TWO

Generation and Characterization of a Conditional *Irf6* Allele

ABSTRACT

Interferon Regulatory Factor 6 (IRF6) is a member of the Interferon Regulatory Factor family of transcription factors. Mutations in *IRF6* cause Van der Woude syndrome and Popliteal Pterygium syndrome, two autosomal dominant disorders characterized by cleft lip with or without cleft palate. In addition DNA variation in *IRF6* confers significant risk for non-syndromic cleft lip and palate, the most common congenital birth defect. *IRF6* is also implicated in adult onset development and disease processes, such as mammary gland development and squamous cell carcinoma. Mice homozygous for a null allele of *Irf6* die shortly after birth due to severe skin, limb, and craniofacial defects, thus impeding the study of gene function in adult stages. To circumvent this, a conditional allele of *Irf6* was generated. This conditional allele had LoxP sites flanking exons three and four which hold critical regions of the DNA binding domain. To validate the functionality of the conditional allele, we used three "deleter" Cre strains: *Gdf9-Cre*, *CAG-Cre*, and *Ella-Cre*. When Cre expression was driven by the *Gdf9-Cre* or *CAG-Cre* transgenes, 100% recombination was observed as indicated by DNA genotyping and phenotyping. Recombination of the conditional allele of *Irf6* was sufficient to produce a null allele. In contrast, use of the *Ella-Cre* transgenic line resulted in incomplete recombination, despite expression at the one-cell stage. In sum, we generated a novel tool to delete *Irf6* in a tissue specific fashion, allowing for study of gene function past perinatal stages. However, recombination efficiency of this allele was dictated by the *Cre*-driver used.

INTRODUCTION

Interferon Regulatory Factor 6 (IRF6) is a member of the Interferon Regulatory Factor family of transcription factors(Tamura *et al.*, 2008). This nine member family contains a highly conserved DNA binding domain and a less conserved protein association domain (Kondo *et al.*, 2002; Tamura *et al.*, 2008). With the exception of *IRF6*, all other members of the *IRF* family have been implicated in immune response(Tamura *et al.*, 2008). Alternatively, mutations in *IRF6* cause two autosomal dominant clefting disorders, Van der Woude syndrome (VWS; OMIM#119300) and Popliteal Pterygium syndrome (PPS; OMIM#119500) (Kondo *et al.*, 2002; Little *et al.*, 2009). In addition, a DNA variant present in 30% of the population confers significant risk for non-syndromic cleft lip and palate, one of the most common congenital defects (Rahimov *et al.*, 2008; Zucchero *et al.*, 2004).

Irf6 is highly expressed in the mouse during embryonic development. Specifically, *Irf6* is expressed in embryonic skin and numerous other epithelial cell types (Ingraham *et al.*, 2006; Kondo *et al.*, 2002; Richardson *et al.*, 2006). More recent reports have also indicated Irf6 expression and function in mesoderm derived tissues, namely, the tongue (Goudy *et al.*, 2013). Knockout murine models using conventional gene targeting strategies have been generated to study Irf6 function during embryogenesis. Mice homozygous for a null allele of *Irf6* (*Irf6*$^{gt/gt}$) display severe skin, limb, and craniofacial abnormalities (Ingraham *et al.*, 2006; Richardson *et al.*, 2006). Skin from *Irf6*$^{gt/gt}$ embryos at embryonic day 17.5 (E17.5) display an expansion of the epidermis due to increased proliferation. In addition, these embryos fail to develop the most differentiated epidermal layers, the granular and cornified layers (Ingraham *et al.*,

2006; Richardson *et al.*, 2006). *Irf6* is a critical regulator of proliferation and differentiation in keratinocytes. In zebrafish, *irf6* is required for proper differentiation of the enveloping layer (EVL), a simple monolayer epithelium that develops during embryonic development (Sabel *et al.*, 2009). *Irf6* has an evolutionarily conserved role in regulating proliferation and differentiation of epithelial cell types (Biggs *et al.*; Ingraham *et al.*, 2006; Richardson *et al.*, 2006; Sabel *et al.*, 2009).

More recent studies indicate a role for *Irf6* in adult development and disease. In the mouse, Irf6 is expressed throughout development of the mammary gland, reaching maximal expression during lactation (Bailey *et al.*, 2009). Interestingly, *IRF6* expression is reduced or absent in breast carcinomas (Bailey *et al.*, 2005). Re-introduction of *Irf6*, along with its binding partner Maspin, into breast cancer cells resulted in cell cycle arrest (Bailey *et al.*, 2008; Bailey *et al.*, 2005). In addition, IRF6 was down-regulated in invasive squamous cell carcinoma. This down-regulation was strongly associated with methylation of CpG islands near the *IRF6* promoter. These data support a tumor suppressive role for *IRF6* (Botti *et al.*, 2011). Along with this, children with VWS have increased risk of wound complications following surgical repair of orofacial clefts, suggesting a role for *IRF6* in wound healing (Jones *et al.*, 2010). Studies of wound closure in $Irf6^{gt/gt}$ embryos indicate a role for *Irf6* in the regulation of cell migration. In sum, *Irf6* has been implicated in both congenital and adult disease processes of significant clinical impact.

Studies of *Irf6* function post embryogenesis are precluded by current mouse models because the loss of *Irf6* in the mouse results in perinatal lethality (Ingraham *et al.*, 2006; Richardson *et al.*, 2006). However, the advent of conditional mutation

systems, such as the Cre-LoxP system, now permits the study of post-natal functions of such genes (Nagy, 2000). Here, we report the generation and characterization of a conditional mouse model of *Irf6* using the Cre-LoxP system. In addition, we compared the efficiency of classical 'deleter' strains in recombination of our conditional allele and propose a new mating strategy for assessing the functionality of conditional alleles.

MATERIALS AND METHODS

Generation of a conditional allele for Irf6

Mouse BAC clone (RPCI22-516G1) was digested with restriction enzymes. A 1.8 kb *Kpn*I/*Bam*HI fragment for the 5'-arm and a 3.9 kb of *Bam*HI/*Hind*III fragment for the 3'-arm were cloned into pBluescript II SK(-) (Agilent Technologies). Three kilobases (kb) of the *Bam*HI fragment, containing exons three and four, was cloned into the ploxP3-Neo-pA vector (kind gift from Professor Takeshi Yagi, Osaka University). 5.8 kb of the *Xba*I fragment which contains floxed exons and *Pgk-Neo* cassette was subcloned into the *Bam*HI site between 5'- and 3'- arms (see Fig. 2.1A). The resulting targeting construct was digested with *Not*I and electroporated into mouse R1 ES cells. After G418 selection, ES cells were screened by PCR. Primer set of 5'-GAGAAATAGGGCCTTCACGGTG-3' (sense) and 5'-TGTGCCCTCTGATGCTGGAACAG-3' (antisense) for 5'-side, 5'-TCGCCTTCTTGACGAGTTCTTCTG-3' (sense, in *Pgk-Neo* cassette) and 5'-GCTCAACTCCCTTTGTGACTGTCC-3' (antisense) for 3' side were used (see Fig 2.1B). Recombinant ES clones were used for establishment of *Irf6* hypomorphic mouse (*Irf6*^{neo}). To establish floxed exons (*fl*) and null (*nl*) strains, the *Pgk-Neo* cassette and the floxed exons, respectively, were removed in the recombinant ES cells by transfection

with a *Cre* expression vector. Resultant clones were then screened by Southern hybridization. Genomic DNA was disgested with ApaL1 or Nhe1 and hybridized to a 5' or 3' probe, respectively (see Fig 2.1C). The 5' probe corresponded to a region in Intron two. The 3' probe corresponded to a region within exon and intron seven. Hybridization with the 5' probe following restriction enzyme digest resulted in two products, 11.3kb (wildtype allele) and 8.3kb (null). Hybridization with the 3' probe also produced two fragments, 14.3kb (wildtype) and 11.3kb (null). The 5' hybridization probe was amplified with primer set *5'-AGTTGTGACTGACTGTAGGATCAGG-3'* (forward) and *5'-ACCAAAACTTCACCAGGAGTATAGGA-3'* (reverse). The 3' hybridization probe was amplified with primer set of *5'- AGAGTAAAGAATGGTTGTCAGTGGAG-3'* (forward) and *5'- GACACCAGTATTCAAGAGGATTGAG-3'* (reverse) (see Fig 2.1C). To generate a conditional mouse line for *Irf6*, embryonic stem cells carrying the $Irf6^{fl}$ allele were injected into C57Bl/6J blastocyst and inserted into pseudo-pregnant dams. Chimeric males were mated to C57Bl/6J females and germline transmission was determined by Polymerase Chain Reaction (PCR)-based genotyping of progeny.

Mouse and embryo genotyping

To attain genomic DNA, tail tissue was digested in lysis buffer (10 mM Tris-HCl, 150 mM NaCl, 10 mM EDTA, 0.1% SDS) with Proteinase-K (20mg/ml, Roche) at 55°C, overnight, followed by ethanol precipitation of DNA. PCR-based genotyping was used to identify alleles (see below). All PCR was conducted using JumpStart REDTaq Ready Mix (Sigma-Aldrich, St. Louis, MO) and separated and visualized by electrophoresis on 1.5% agarose gels.

Detection of the Irf6^{neo}, Irf6^{fl}, and Irf6^{nl} alleles

Primer set oBS4380 and oBS4381 was used to distinguish between the *Irf6*$^{+}$ and *Irf6*^{neo} alleles. Primer set of oBS3318 and oBS3319 was used to distinguish the *Irf6*$^{+}$allele from the *Irf6*^{fl} allele. Primer set of oBS4380 and oBS3319 was used to detect the *Irf6*^{nl} (see Table 2.1 for primers sequences). PCR was performed as follows: 1) 95°C for two minutes, 2) 95°C for 15 seconds, 3) 55°C for 15 seconds, 4) 72°C for 45 seconds, 5) repeat steps 2-4 35 times, 6) 72°C for five minutes.

Detection of the Irf6^{gt} allele

Primer set of oBS144 and oBS145 was used to identify the *Irf6*^{gt} allele. Primer set of oBS146 and oBS145 was used to identify the wildtype allele (see Table 2.1 for primers sequences). PCR conditions were as follows: 1) 95°C for three minutes, 2) 95°C for 38 seconds, 3) 60°C for 50 seconds, 4) 72°C for 15 seconds, 5) repeat steps 2-4 40 times, 6) 72°C for five minutes. PCR Master Mix was supplemented with 5M Betaine monohydrate to aid in amplification of GC-rich regions.

Detection of Cre transgenes

The *Gdf9-Cre* transgene was detected using primer set of oBS4934 and oBS4935 (see Table 2.1). PCR conditions were as follows: 1) 95°C for five minutes, 2) 95°C for one minute, 3) 58°C for two minutes, 4) 72°C for one minute, 5) repeat steps 2-4 35 times, 6) 72°C for five minutes. Master mix was supplemented with 5 Molar (5M) Betaine monohydrate to aid in amplification of GC-rich regions.

The *EIIa-Cre* transgene was detected using primer set of oBS4885 and oBS4886 (see Table 2.1). PCR conditions were as follows: 1) 94°C for three minutes, 2) 94°C for

Alleles	Primers	Sequence	Product Size
Irf6^{neo}	oBS 4380 oBS 4381	*GCAGAGTGGAGCACACTTCA* *AAGCATGTCTATTTGGGGGTT*	*592*
Irf6^{fl} *and Irf6*$^{+}$	oBS 3318 oBS 3319	*TGGCAAAATCTATTTCGAGTGG* *CACACTGACCTCAATGTCCAA*	*Irf6*$^{+}$ - 300 *Irf6*^{fl} - 500
Irf6^{nl}	oBS 3319 oBS 4380	*CACACTGACCTCAATGTCCAA* *GCAGAGTGGAGCACACTTCA*	449
Irf6^{+}	oBS 146 oBS 145	*GACCAGACCGTGCAGGGGCTGTGG* *GAGAGGCTAGGGTGGAAGGGATTC*	461
Irf6^{gt}	oBS 144 oBS 145	*AAATGGCGTTACTTAAGCTAGCTTGC* *GAGAGGCTAGGGTGGAAGGGATTC*	283
tg$^{Gdf9\text{-}Cre}$	oBS 4934 oBS 4935	*TCTGATGAAGTCAGGAAGAACC* *GAGATGTCCTTCACTCTGATTC*	~500
tg$^{Ella\text{-}Cre}$	oBS4885 oBS4886	*GCGGTCTGGCAGTAAAAACTATC* *GTG AAACAGCATTGCTGTCACTT*	~100

Table 2.1: PCR primers for genotyping.

30econds, 3) 51.7°C for one minute, 4) 72°C for one minute, 5) repeat steps 2-4 35 times, 6) 72°C for five minutes.

The CAG-Cre transgene was detected using primer set of 5' – CCTACAGCTCCTGGGCAACGTGC-3' (forward) and 5'-CTAATCGCCATCTTCCAGCAGG-3' (reverse). PCR conditions were as follows: 1) 94°C for three minutes, 2) 94°C for 30 seconds, 3) 60°C for 30 seconds, 4) 72°C for two minutes, 5) repeat steps 2-4 30 times, 6) 72°C for five minutes.

Mating Strategies

Gdf9-Cre

A male hemizygous for the *Gdf9-iCre* transgene ($tg^{Gdf9\text{-}Cre/+}$) was purchased from Jackson Labs (www.jax.org) and mated to $Irf6^{fl/fl}$ females to generate females carrying both the *Cre* transgene and one copy of the $Irf6^{fl}$ allele ($tg^{Gdf9\text{-}Cre/+}$; $Irf6^{fl/+}$). These females were mated to compound heterozygous males for *Irf6* ($Irf6^{gt/fl}$) Tail snips were collected from pups upon weaning and genotyped. A chi-squared test was used to determine deviations from expected Mendelian ratios.

$Tg^{Gdf9\text{-}Cre/+}$; $Irf6^{fl/+}$ females were then placed into timed matings with males heterozygous for a null allele of *Irf6* ($Irf6^{gt/+}$). The presence of a copulation plug was denoted as embryonic day 0.5 (E0.5) and embryos were collected on E17.5.

EIIa-Cre

A homozygous *EIIa-Cre* male ($tg^{EIIa\text{-}Cre/EIIa\text{-}Cre}$) was purchased from Jackson Labs (www.jax.org) and mated to $Irf6^{gt/+}$ females to produce double heterozygous $tg^{EIIa\text{-}Cre/+}$;$Irf6^{gt/+}$ mice. Timed matings were set up between $tg^{EIIa\text{-}Cre/+}$;$Irf6^{gt/+}$ animals and

Irf6$^{gt/fl}$ animals. The presence of a copulation plug was denoted as E0.5. Embryos were collected at E17.5.

CAG-Cre

Validation of the *Irf6*^{fl} allele using *CAG-Cre* was conducted multiple ways. 1) Females homozygous (*tg*$^{CAG\text{-}Cre/CAG\text{-}Cre}$) or heterozygous (*tg*$^{CAG\text{-}Cre/+}$) for the CAG-Cre transgene were mated to an *Irf6*$^{fl/fl}$ males. 2) *Tg*$^{CAG\text{-}Cre/+}$ males were mated to *Irf6*$^{fl/fl}$ females. Litters were born and tail snips were collected upon weaning and subjected to PCR based genotyping. A chi-squared test was used to verify Mendelian ratios.

Embryo Collection and processing

On E17.5, pregnant females were sacrificed using isoflurane induced comatosis followed by cervical dislocation. Embryos were decapitated. Heads and bodies were fixed overnight in 10% neutral buffered formalin at 4°C. Following fixation, embryos were processed and embedded in paraffin by the Histopathology Laboratory at Michigan State University using standard protocols. All animals were used in accordance with the National Institutes of Health Guide for the Care and Use of Laboratory Animals, and all procedures were approved by the Michigan State University Institutional Animal Use and Care Committee.

Histological analysis

Whole heads from embryos at E17.5 were sectioned sagitally at 7µm. Sections were then stained with hematoxylin and eosin (H&E). Briefly, for depariffinization and rehydration, sections were passed through three changes of xylene followed by washes through reducing grades of ethanol. Slides were then incubated in Gill's Hematoxylin No. III (Sigma-Aldrich, St. Louis, MO) for 1.5 minutes, washed briefly in tap water, and

incubated in a 1% Eosin solution (Eosin Y- VWR, West Chester, PA) for 1.5 minutes. To dehydrate, slides were passed through increasing grades of ethanol. Lastly, slides were mounted using Permount mounting media (VWR, Radnor, PA). Stained sections were imaged using a Nikon 90i upright microscope.

Dye Exclusion Assay

The dye exclusion assay was carried out as described by Ingraham, et al (2006). Briefly, whole embryos were collected at E17.5 and fixed in 100% methanol for five minutes. Following fixation, embryos were rinsed briefly in 1X PBS and stained in 0.1% toluidine blue for one minute. Staining was followed by washing with 1X PBS.

Immunofluorescence

For immunofluorescent detection of markers of the epidermis, sections were deparaffinized and rehydrated in reducing concentrations of ethanol. Sections were subjected to antigen retrieval by boiling in 10mM Sodium citrate (pH6.0) for 30 minutes. Tissues sections were permeabilized using 0.5% Triton X-100 followed by blocking in blocking solution (10% normal goat serum, 0.1% Bovine Serum Albumin in 1X Phosphate Buffered Saline (PBS)) for one hour at room temperature. Sections were then incubated in anti-mouse F'(ab) fragment (Jackson ImmunoResearch Laboratories, West Grove, PA) for five minutes to reduce non-specific binding of anti-mouse secondary. Sections were incubated with 1:100 rabbit anti-Irf6 (Sigma-Aldrich; St. Louis, MO), 1:250 rabbit anti-Keratin 14 (Covance), 1:150 mouse anti-p63 (Santa Cruz), and 1:250 rabbit anti-loricrin (Covance) overnight at 4°C, followed by incubation with either goat anti-mouse AlexaFluor 488 or goat anti-rabbit AlexaFluor 555 (Life Technologies, Grand Island, NY) . Nuclei were counterstained for 10 minutes in a

1:10,000 dilution of 4' 6- diaminidino-2-phenylindole (DAPI; Life Technologies, Grand Island, NY). Slides were then mounted in ProLong GOLDAntifade reagent (Life Technologies, Grand Island, NY). Images were taken using a Nikon Eclipse 90i fluorescent microscope.

RESULTS

Mice carrying the conditional allele of Irf6 are viable

To generate a conditional allele of *Irf6* (*Irf6^{fl}*), we utilized a three *LoxP* site strategy. The first *LoxP* site was inserted upstream of exon three. In addition, a *LoxP*-flanked (floxed) *Pgk-Neo* cassette was inserted into intron four, generating the *Irf6^{neo}* allele (see Fig 2.1A). Embryonic stem cells containing the recombinant clones were acquired by G418 selection followed by PCR to amplify regions within the *Pgk-Neo* cassette and the 3' arm of the targeting vector (see Fig 2.1B). Excision of the floxed *Pgk-Neo* cassette in ES cells (SV129) was conducted by transfection with a Cre-expression vector. PCR- based genotyping was used to distinguish between the *Irf6$^{+/+}$*, *Irf6^{neo}, Irf6^{fl}* and *Irf6^{nl}* allele. Southern blot analysis confirmed correct targeting and subsequent recombination to generate the *Irf6^{nl}* allele (see Fig 2.1 C). Chimeric mice were generated by injection of ES cells containing the *Irf6^{fl}* allele into C57Bl/6J blastocyst. The *Irf6^{fl}* allele contains *LoxP* sites flanking exons three and four (See Fig 2.2). These exons include regions of the DNA binding domain, an element required for normal protein function (Ingraham *et al.*, 2006). Mice homozygous for the *Irf6* conditional allele (*Irf6$^{fl/fl}$*) were viable and born at the expected Mendelian ratio. They showed no developmental or reproductive defects when compared to *Irf6$^{+/+}$* or *Irf6$^{fl/+}$* littermates, indicating that this allele does not affect normal gene function.

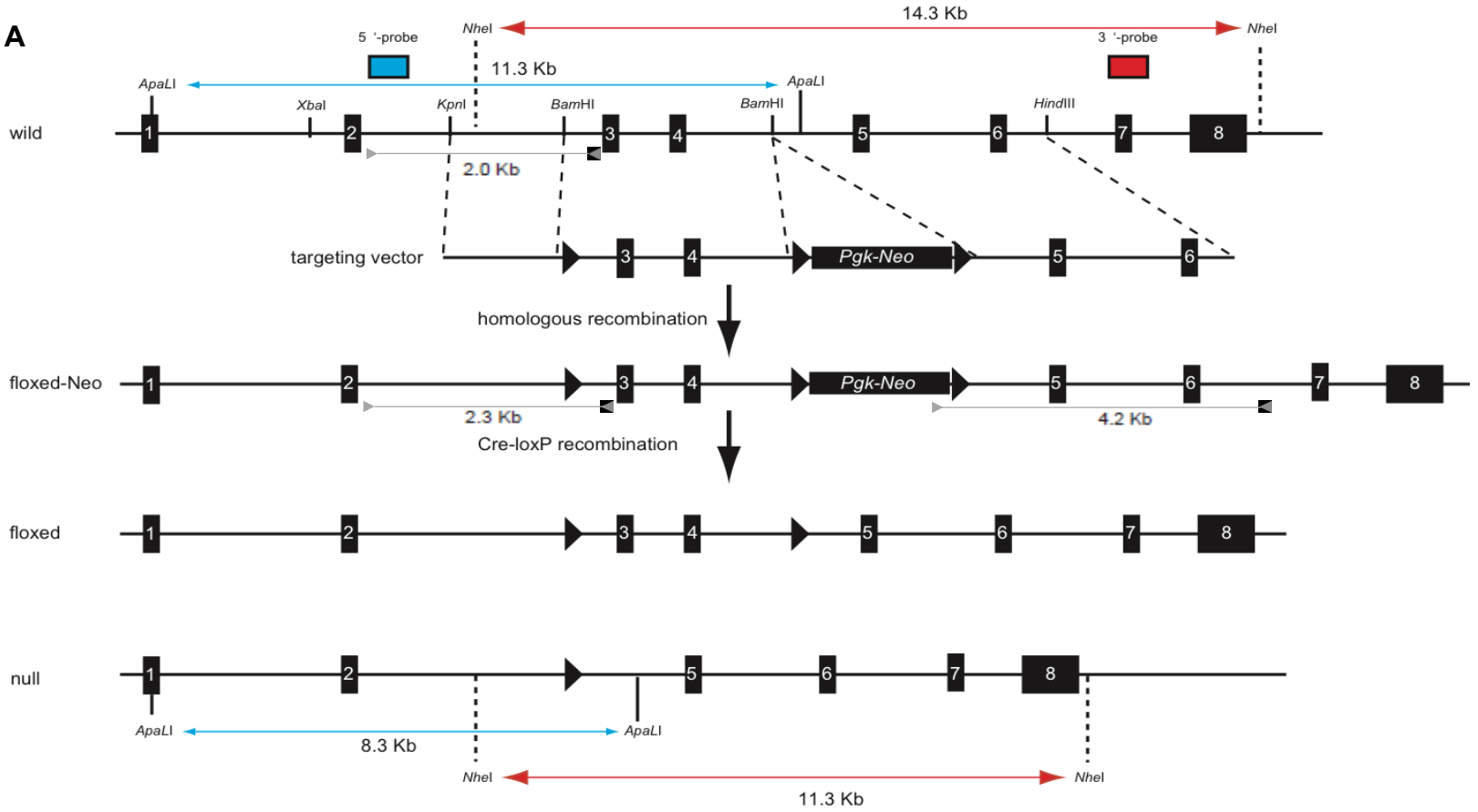

Figure 2.1: Construction of a conditional allele of *Irf6*. A) A targeting vector was generated to contain three LoxP sites (triangles). The targeting vector contained a LoxP flanked PGK-neo cassette inserted 3' of exon four. A third LoxP site was incorporated 5' of exon three. B) Cells carrying the recombinant allele were detected via PCR. Regions amplified are indicated by green tracks. C) Southern blot analysis of ES cells. A 5' probe (indicated by blue tracks) and 3' probe (indicated by red tracks) were used.

Figure 2.1 (cont'd)

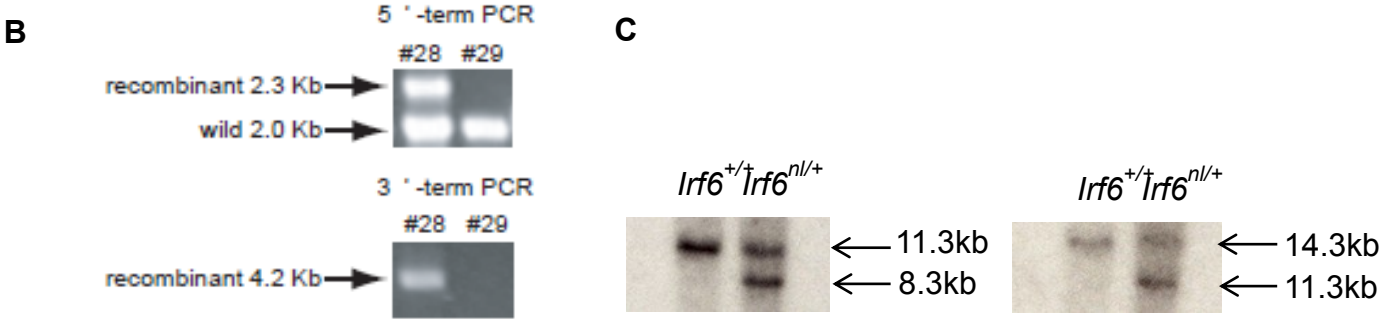

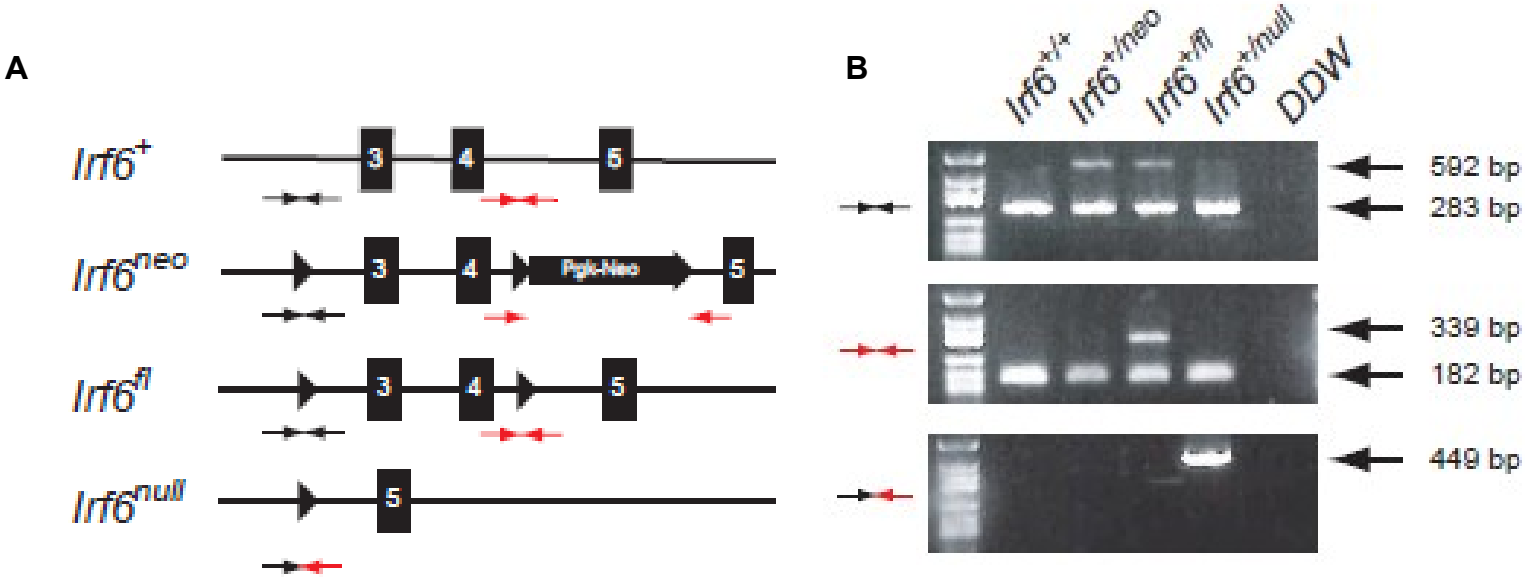

Figure 2.2: **PCR amplification of *Irf6* alleles**. A) Schematic of Irf6 alleles. Black and red arrows indicate primer sets used to amplify specific *Irf6* alleles. B) Gel electrophoresis images for each allele. Black arrows indicate primer set oBS3318 and oBS3319. Red indicates primer set of oBS4380 and oBS4381 (see Table 2.1). Primer set one (black arrows) detects the $Irf6^{+}$ and $Irf6^{neo}$ or $Irf6^{fl}$ alleles.

Recombination of the Irf6^{fl} allele produces a null allele

To test the functionality of the *Irf6^{fl}* allele, we employed the *Gdf9-Cre* transgenic mouse line (*tg$^{Gdf9\text{-}Cre/+}$)*. The *Gdf9* promoter is sufficient to drive expression of *Cre* recombinase in the female germ cell (oocyte) beginning at postnatal day three (Lan *et al.*, 2004). Thus, females were required to carry the Cre transgene in crosses designed to recombine the *Irf6* locus. Recombination of the *Irf6^{fl}* allele was predicted to excise exons three and four, generating a recombined, null allele (*Irf6^{nl})*. When this recombination event is mediated by female mice that carry the *Gdf9-Cre* transgene and are heterozygous for the conditional *Irf6* allele (*tg$^{Gdf9\text{-}Cre/+}$; Irf6$^{fl/+}$*), we expect a recombination event in the oocyte, producing *Irf6^{+}* or *Irf6^{nl}* gametes. To test this hypothesis, *tg$^{Gdf9\text{-}Cre/+}$; Irf6$^{fl/+}$* females were mated to *Irf6$^{gt/fl}$* males. If recombination of the conditional allele were complete, we expect 25% of embryos to phenocopy embryos deficient for *Irf6* (*Irf6$^{gt/gt}$* or knockout). From these matings, six litters were collected at weaning (43 pups). We observed a significant underrepresentation of two genotypes *tg$^{Gdf9\text{-}Cre/+}$; Irf6$^{gt/nl}$* and *tg$^{+/+}$; Irf6$^{gt/nl}$* (X^2- test; p=0.002; See Table 2.2). These data were consistent with the perinatal lethality observed in *Irf6$^{gt/gt}$*.

To confirm if the observed underrepresentation of genotypes was due to peri-natal lethality of mutant pups, we performed timed matings between *tg$^{Gdf9\text{-}Cre/+}$;Irf6$^{fl/+}$* females and *Irf6$^{gt/+}$* males. Pregnant females were sacrificed at E17.5 and three litters were collected (n = 34 embryos). By gross inspection, we observed nine embryos that grossly phenocopied *Irf6$^{gt/gt}$* embryos (see Fig 2.3A-B). These embryos were referred to as conditional knockouts (cKO). In addition to severe skin, limb, and craniofacial

◆ $tg^{Gdf9\text{-}Cre/+}$; $Irf6^{fl/+}$ X ■ $tg^{+/+}$; $Irf6^{gt/fl}$		
Genotype	Expected	Observed
$tg^{Gdf9\text{-}Cre/+}$; $Irf6^{gt/nl}$	5.125	0
$tg^{Gdf9\text{-}Cre/+}$; $Irf6^{fl/nl}$	5.125	7
$tg^{Gdf9\text{-}Cre/+}$; $Irf6^{gt/+}$	5.125	3
$tg^{Gdf9\text{-}Cre/+}$; $Irf6^{fl/+}$	5.125	6
$tg^{+/+}$; $Irf6^{gt/fl}$	5.125	0
$tg^{+/+}$; $Irf6^{fl/nl}$	5.125	8
$tg^{+/+}$; $Irf6^{gt/+}$	5.125	5
$tg^{+/+}$; $Irf6^{fl/+}$	5.125	12
CNG		2 (not included)
TOTAL	41	41

Table 2.2: Gdf9-Cre mediated recombination of *Irf6^{fl}*. Recombination of the *Irf6^{fl}* allele in the female results in production of the *Irf6^{nl}* allele. Data represent offspring from six litters after weaning. There is a significant underrepresentation of mice with *Irf6$^{gt/nl}$* (X^2 *test: p = 0.0018*). CNG – Could Not Genotype.

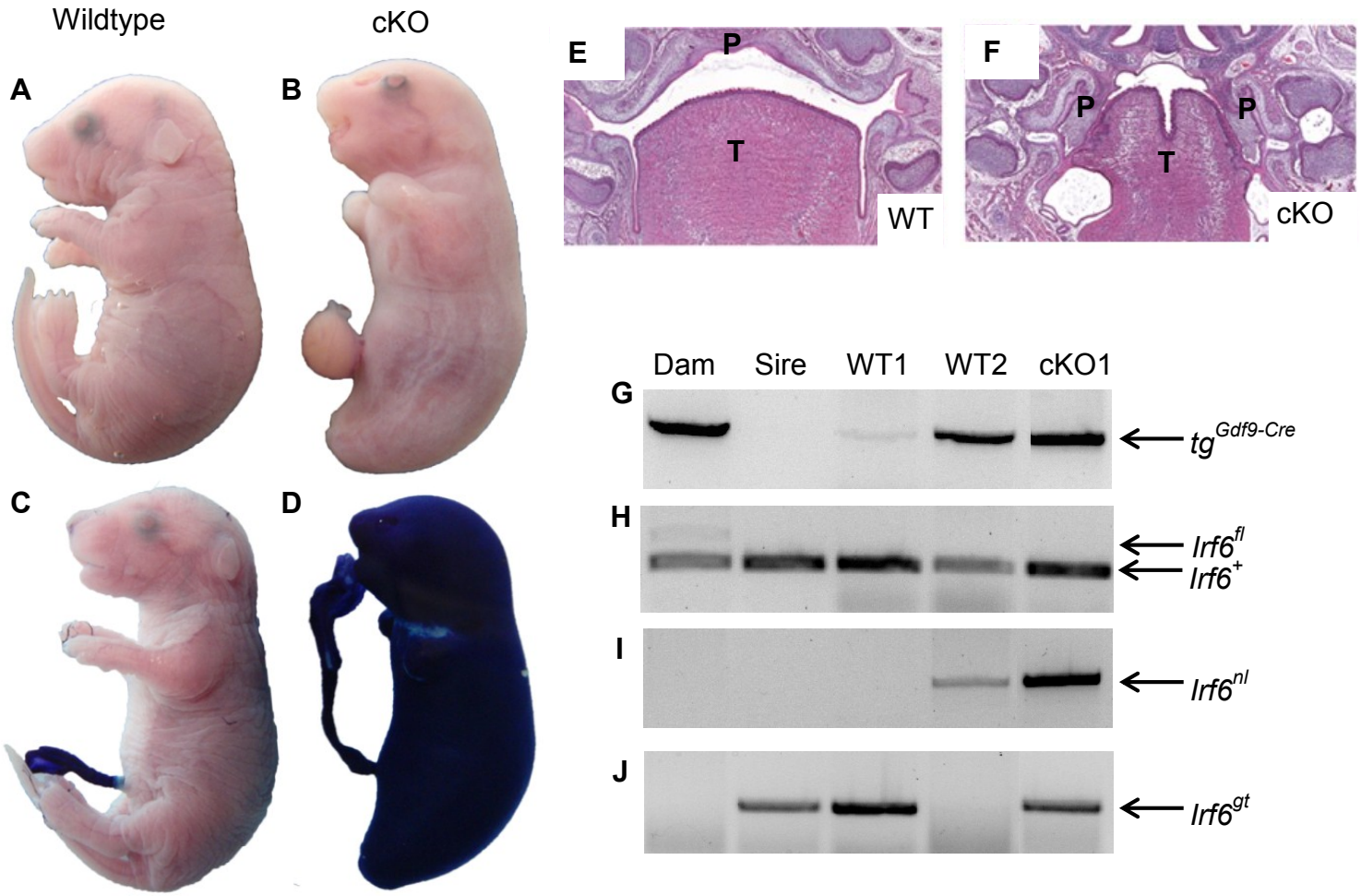

Figure 2.3: Conditional knockout (cKO) embryos phenocopy *Irf6*$^{gt/gt}$ embryos.

Figure 2.3 (cont'd)

A) Wildtype and B) cKO embryos generated from *Gdf9-Cre* mediated recombination of the *Irf6*^{fl} allele. cKO embryos display severe skin, limb, and craniofacial abnormalities and impaired barrier function when compared to wildtype littermates (C, D). Cross sections of wiltype (E) and cKO (F) heads indicate severe oral adhesions in cKO embryos (P – palate; T – tongue). PCR-based genotyping for the *Gdf9-Cre* transgene (G), *Irf6*$^{+}$ and *Irf6*^{fl} (H), *Irf6*^{nl} (I), and *Irf6*^{gt} *(J)*. Complete recombination of the *Irf6*^{fl} is observed irrespective of whether embryos were positive for the *Gdf9-Cre* transgene. cKO embryos were also positive for the *Irf6*^{gt} allele. No embryos were positive for the Irf6^{fl} allele

abnormalities, cKO embryos showed impaired barrier function (see Fig 2.3C-D) and severe oral epithelial adhesions (see Fig 2.3 E-F). Genotypic analysis showed that these embryos completely lacked the *Irf6*^{fl} allele and were positive for the *Irf6*^{nl} and *Irf6*^{gt} alleles (see Fig. 2.3E) Notably, the mutant phenotype was independent of the presence of the *Gdf9-Cre* transgene. Thus, these data indicate that the *Gdf9-Cre* transgene mediated recombination of the *Irf6*^{fl} allele prior to completion of meiosis II in oocytes.

Histological analysis of embryonic skin from wildtype, *Irf6*$^{gt/gt}$ and cKO embryos showed an expanded epidermis (see Fig 2.4A-C). In addition, cKO embryos displayed oral adhesions and a cleft palate, all hallmarks of *Irf6*$^{gt/gt}$ embryos. To confirm the molecular profile, wildtype, *Irf6*$^{gt/gt}$, and cKO embryos were collected at E17.5. Skin sections were analyzed for markers of epidermal growth and differentiation. In wildtype embryos, Irf6 expression was seen throughout the spinous and basal layers of the epidermis. As expected, this expression was lost in *Irf6*$^{gt/gt}$ and cKO embryos (see Fig 2.4D-F). In wildtype skin, Keratin14 (K14) was restricted to the basal layer. K14 was ectopically expressed in *Irf6*$^{gt/gt}$ and cKO embryos, expanding throughout the epidermis (see Fig 2.4G-I). A similar pattern of expression was observed for p63, another marker of the basal layer and a pro-proliferation gene (see Fig 2.4K-L). Lastly, expression of loricrin, a marker of terminally differentiated keratinocytes, was completely lost in cKO embryos. These results are consistent with those observed in *Irf6*-deficient skin (see Fig 2.4M-O).

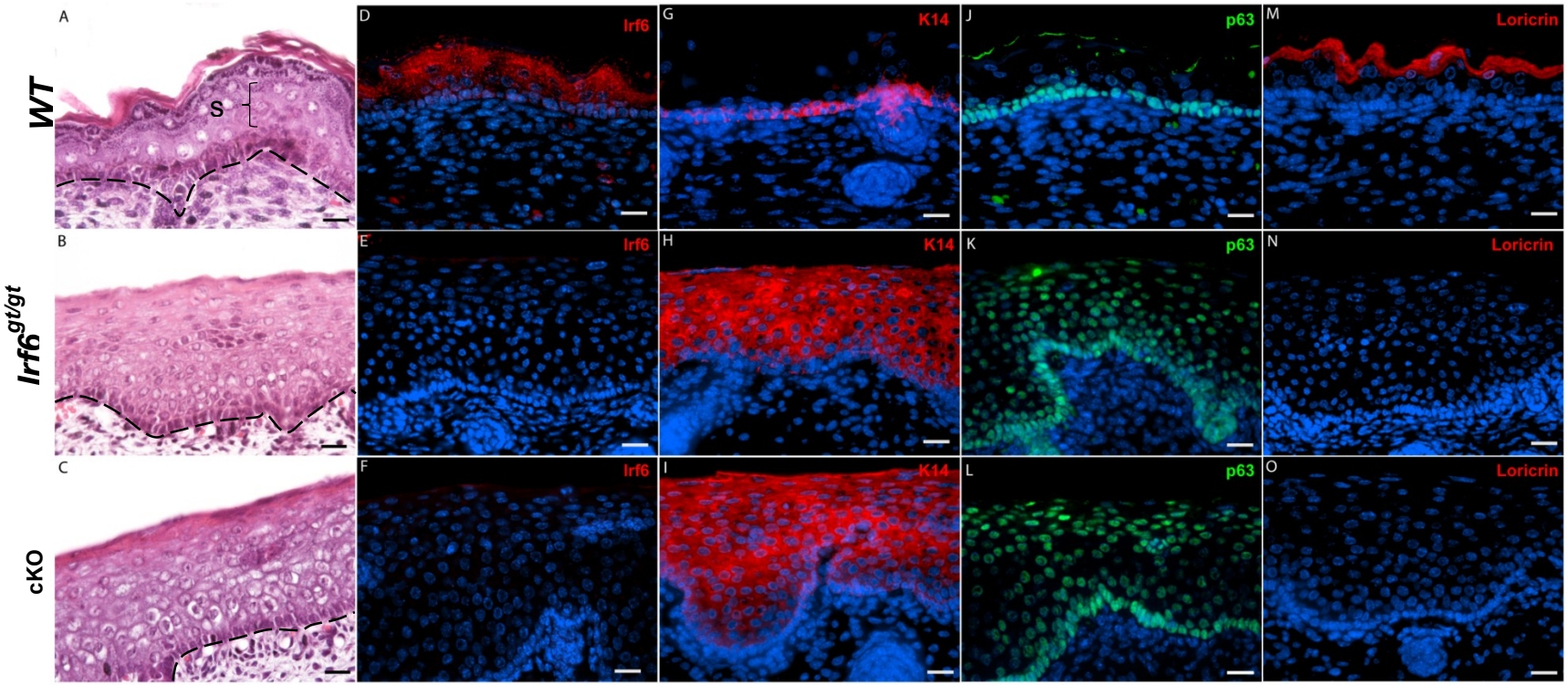

Figure 2.4: **Molecular profile of embryonic skin.** H&E staining of A) Wildtype (WT), B) *Irf6*$^{gt/gt}$ and C) cKO skin. Black dashed line indicates the basal layer of the epidermis. The spinous layer (sp) is indicated in A. Immunofluoresent staining for Irf6 (D-F), K14 (G-I), p63 (J-L), and Loricrin (M-O). Images taken using brightfield fluorescent microscope. Scale bars represent 100μm.

Efficiency of recombination of the Irf6^{fl} allele varies by Cre-driver

To further confirm the functionality of the *Irf6^{fl}* allele, we utilized two other *Cre* transgenic lines. First, we used *CAG-Cre*, where Cre expression is driven by the cytomegalovirus immediate early enhancer-chicken beta-actin promoter in mature oocytes. Sakai et al, (1997) showed the *Cre* mRNA or protein was stored in the oocyte and can facilitate recombination following fertilization. *CAG-Cre* transgene positive (*tg$^{CAG\text{-}Cre/+}$; Irf6$^{+/+}$*) animals were mated to *Irf6$^{fl/fl}$* animals. Thirty embryos were generated from three litters and genotyped upon weaning. Genotypic analysis indicated that ten animals were *tg$^{CAG\text{-}Cre/+}$*. All of these animals showed complete recombination of the *Irf6^{fl}* allele, as evidenced by the presence of only the *Irf6^{nl}* allele (see Table 2.3).

We also used the classic delete strain, *EIIa-Cre*, which targets expression of the recombinase to the stages of embryogenesis preceding implantation. We mated *tg$^{EIIa\text{-}Cre/+}$; Irf6$^{gt/+}$* animals with *Irf6$^{gt/fl}$* animals. This allowed us to produce wildtype and mutant embryos. However, the mutant phenotype could be generated in two ways: 1) *Irf6$^{gt/gt}$* or 2) *tg$^{EIIa\text{-}Cre/+}$; Irf6$^{gt/nl}$*. We produced 124 embryos from 15 matings. Sixty-five (65) of these embryos were *tg$^{EIIa\text{-}Cre/+}$*. Of these embryos, nineteen (19) were also positive for the *Irf6^{fl}* allele but showed no evidence of recombination, completely lacking the *Irf6^{nl}* allele. We observed eight *tg$^{EIIa\text{-}Cre/+}$* embryos that showed incomplete recombination, as indicated by the presence of both the *Irf6^{fl}* and *Irf6^{nl}* alleles (see Fig. 2.5). These embryos were grossly normal. Nine *tg$^{EIIa\text{-}Cre/+}$* embryos showed complete recombination in tail tissues, as indicated by absence of the *Irf6^{fl}* allele and presence of the *Irf6^{nl}* (See Table 2.4). Strikingly, only one embryo phenocopied *Irf6$^{gt/gt}$* embryo

(*tg*$^{Ella\text{-}Cre/+}$; *Irf6*$^{gt/nl}$), despite the fact that three embryos had the correct genotype to generate the mutant phenotype in the event of recombination (*tg*$^{Ella\text{-}Cre/+}$; *Irf6*$^{gt/fl}$).

A)	$tg^{CAG\text{-}Cre/+}$; $Irf6^{+/+}$ x $tg^{+/+}$; $Irf6^{fl/fl}$				
Genotypes	Observed	Expected	P-value	$Irf6^{fl}$	$Irf6^{nl}$
$tg^{CAG\text{-}Cre/+}$; $Irf6^{nl/+}$	11	10.5		-	+
$tg^{+/+}$; $Irf6^{fl/+}$	9	10.5	0.63	+	-
CNG	1	0		n/a	n/a
Total	20	20			
B)	$Tg^{CAG\text{-}Cre/CAG\text{-}Cre}$; $Irf6^{+/+}$ x $tg^{+/+}$; $Irf6^{fl/fl}$				
Genotypes	Observed	Expected	P-value	$Irf6^{fl}$	$Irf6^{nl}$
$tg^{CAG\text{-}Cre/+}$; $Irf6^{nl/+}$	9	9	n/a	-	+
Total	9	9			

Table 2.3: ***CAG-Cre* mediated recombination of *Irf6*^{fl}.** A) Data represent offspring from two litters after weaning. Mice carrying the *CAG-Cre* transgene showed complete recombination of *Irf6*^{fl}. Mice lacking the *CAG-Cre* transgene did not show the *Irf6*^{nl} allele. B) Data represent offspring from one litter following weaning. All animals showed complete recombination of the *Irf6*^{fl} allele. '+' or '-' indicates the presence or absence of an allele determined by PCR based genotyping.

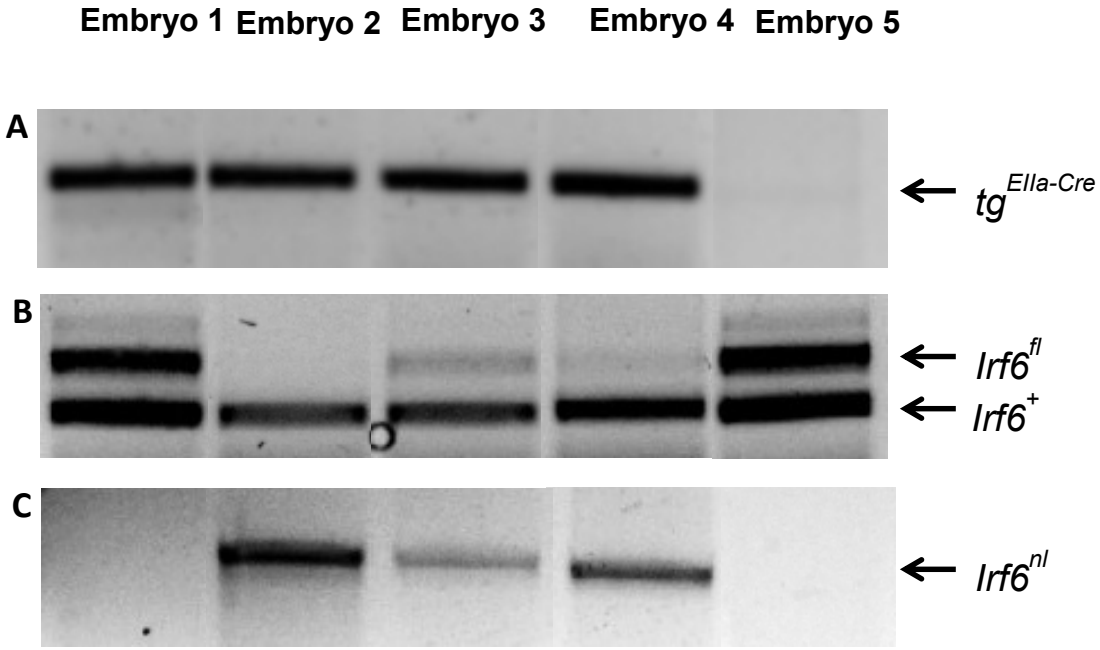

Figure 2.5: **PCR-based genotyping of *EIIa-Cre* transgenic embryos** (A), *Irf6*$^{+}$ and *Irf6*^{fl} (B) and *Irf6*^{nl} (C) from E17.5 embryos. When using the *EIIa-Cre* transgene was used, we observed embryos with no recombination (Embryo 1), complete recombination (Embryo 2), or incomplete recombination (Embryos 3 and 4) of the *Irf6*^{fl} allele. The *Irf6*^{nl} was not detected in the absence of the *EIIa-Cre* transgene (Embryo 5).

$tg^{Ella\text{-}Cre/+}$; $Irf6^{gt/+}$ x $tg^{+/+}$; $Irf6^{gt/fl}$			
Ella-Cre genotype	total	Irf6 genotype	total
$tg^{+/+}$	46	$Irf6^{fl}$	18
		$Irf6^{fl}$ and $Irf6^{nl}$	0
		$Irf6^{nl}$	0
$tg^{Ella/+}$	66	$Irf6^{fl}$	19
		$Irf6^{fl}$ and $Irf6^{nl}$	8
		$Irf6^{nl}$	9

Table 2.4: ***Ella-Cre* mediated recombination of *Irf6*^{fl}**. *A)* Data represent offspring from 15 litters collected at E17.5. Mice lacking the *Ella-Cre* transgene showed no recombination of the Irf6^{fl} allele. Mice carrying the *Ella-Cre* transgene showed mosaic recombination of *Irf6*^{fl}. Some offspring showed no recombination *(Irf6*^{fl} only*)*, presence of both the *Irf6*^{fl} and *Irf6*^{nl} alleles, or complete recombination *(Irf6*^{nl} only*)*.

DISCUSSION

The Cre-LoxP system enables the generation of tissue and temporal gene knockouts as a mechanism to study gene function. This is especially useful for genes, like *Irf6*, where conventional knockout strategies result in embryonic or perinatal lethality, precluding the study of gene function during adult development. Here we report the generation of a conditional allele of *Irf6*, with LoxP sites flanking exons three and four. When paired with the Gdf9-Cre transgene, complete recombination of the conditional allele was observed. In addition, when the recombined allele was paired with a null allele of *Irf6*, the resulting embryos phenocopied the previously reported Irf6$^{gt/gt}$ embryos. Skin from conditional knockout and Irf6$^{gt/gt}$ embryos shared the same histological and molecular profiles, displaying an expanded epidermis and loss of the most differentiated keratinocyte layers. These results confirm that the *Irf6*^{fl} allele is susceptible to *Cre*-mediated recombination and this recombination was sufficient to generate a null allele of *Irf6*.

Recently, roles for Irf6 in adult development and disease processes have been elucidated. Notably, Irf6 was expressed in the mammary epithelium and expression data in mouse and gene manipulation in cell lines indicated a critical role for Irf6 in differentiation and proliferation of mammary epithelium. In addition, Irf6 was implicated as a tumor suppressor in squamous cell carcinomas (Bailey *et al.*, 2008; Bailey *et al.*, 2009). The conditional allele we report here provides a model to query the function of Irf6 in normal mammary development, breast cancer, and squamous cell carcinoma.

Interestingly, we found that not all *Cre*-drivers had the same recombination capacity, despite being expressed at the same time point. We tested two classic

"deleter" strains, *CAG-Cre* and *EIIa-Cre*, both of which are active in the oocyte and at the one-cell stage during the pre-implantation development (Lakso *et al.*, 1996; Sakai and Miyazaki, 1997). *CAG-Cre*, like *Gdf9-Cre*, was active in the oocyte and was able to completely recombine the $Irf6^{fl}$ allele. However, the *eIIa-Cre* showed an incomplete pattern of recombination. This finding was in accordance with results published by Lakso et al (1996), where complete recombination using the *EIIa-cre* allele was only observed in 50% of animals (Lakso *et al.*, 1996) . We note that E*IIa-Cre* was not an effective transgene for assessing the functionality of newly derived conditional alleles. Instead, we propose the usage of oocyte specific Cre-drivers, such as *Gdf9-Cre*, or other more efficient one-cell stage drivers, such as *CAG-Cre*, to validate the functionality of conditional alleles. However, it is important to note that the mating strategy employed for these studies may have promoted the observed recombination inefficiency. It would be beneficial to address recombination with $tg^{EIIa\text{-}Cre/+}$; $Irf6^{fl/+}$ females.

In addition to the inefficiency of *EIIa-Cre*, we also experienced inefficient recombination using tissue specific *Cre* transgenes. *Tgfb3-Cre*, only mediated complete recombination of the $Irf6^{fl}$ allele approximately 8% of the time. Interestingly, this embryo phenocopied $Irf6^{gt/gt}$ embryos (Kousa, Y. et al. Data not published). In addition, the *K14-Cre-ER* (Olson, L. and Dunnwald, M. Data Not Published) and *LysM-Cre* (Dunnwald, M. Data not published) transgenic lines were also utilized and resulted in incomplete recombination of $Irf6^{fl}$ as measured by the presence of Irf6 protein in the skin and in macrophages, respectively. While it is possible that the protein detected represents protein stores preceding recombination, we suggest an alternate explanation. Recent

studies have shown that *Irf6* was methylated at CpG islands in the promoter region. Furthermore, this methylation was associated with down-regulation of *Irf6* expression in squamous cell carcinoma (Botti *et al.*, 2011). Classically, DNA methylation was associated with nucleosome compaction, rendering the DNA inaccessible to transcription factors required to facilitate gene expression. DNA methylation of the promoter region of Irf6 may serve as a signal to condense the *Irf6* locus. As a result, in tissue types where *Irf6* was methylated, we hypothesize that the DNA was inaccessible to Cre recombinase. Long and Rossi (2009) showed that methylation of promoter elements upstream of reporter genes activated by Cre expression (Z/AP and Z/EG strains) inhibited Cre- mediated recombination (Long and Rossi, 2009). Further studies to determine the methylation state of Irf6 in different cell types must be done to confirm this hypothesis.

REFERENCES

REFERENCES

Bailey CM, Abbott DE, Margaryan NV, Khalkhali-Ellis Z, Hendrix MJ. 2008. Interferon regulatory factor 6 promotes cell cycle arrest and is regulated by the proteasome in a cell cycle-dependent manner. Mol Cell Biol 28: 2235-2243.

Bailey CM, Khalkhali-Ellis Z, Kondo S, Margaryan NV, Seftor RE, Wheaton WW, Amir S, Pins MR, Schutte BC, Hendrix MJ. 2005. Mammary serine protease inhibitor (Maspin) binds directly to interferon regulatory factor 6: identification of a novel serpin partnership. J Biol Chem 280: 34210-34217.

Bailey CM, Margaryan NV, Abbott DE, Schutte BC, Yang B, Khalkhali-Ellis Z, Hendrix MJ. 2009. Temporal and spatial expression patterns for the tumor suppressor Maspin and its binding partner interferon regulatory factor 6 during breast development. Dev Growth Differ 51: 473-481.

Biggs LC, Rhea L, Schutte BC, Dunnwald M. Interferon regulatory factor 6 is necessary, but not sufficient, for keratinocyte differentiation. J Invest Dermatol 132: 50-58.

Botti E, Spallone G, Moretti F, Marinari B, Pinetti V, Galanti S, De Meo PD, De Nicola F, Ganci F, Castrignano T, Pesole G, Chimenti S, Guerrini L, Fanciulli M, Blandino G, Karin M, Costanzo A. 2011. Developmental factor IRF6 exhibits tumor suppressor activity in squamous cell carcinomas. Proc Natl Acad Sci U S A 108: 13710-13715.

Goudy S, Angel P, Jacobs B, Hill C, Mainini V, Smith AL, Kousa YA, Caprioli R, Prince LS, Baldwin S, Schutte BC. 2013. Cell-autonomous and non-cell-autonomous roles for IRF6 during development of the tongue. PLoS One 8: e56270.

Ingraham CR, Kinoshita A, Kondo S, Yang B, Sajan S, Trout KJ, Malik MI, Dunnwald M, Goudy SL, Lovett M, Murray JC, Schutte BC. 2006. Abnormal skin, limb and craniofacial morphogenesis in mice deficient for interferon regulatory factor 6 (Irf6). Nat Genet 38: 1335-1340.

Jones JL, Canady JW, Brookes JT, Wehby GL, L'Heureux J, Schutte BC, Murray JC, Dunnwald M. 2010. Wound complications after cleft repair in children with Van der Woude syndrome. J Craniofac Surg 21: 1350-1353.

Kondo S, Schutte BC, Richardson RJ, Bjork BC, Knight AS, Watanabe Y, Howard E, de Lima RL, Daack-Hirsch S, Sander A, McDonald-McGinn DM, Zackai EH, Lammer EJ, Aylsworth AS, Ardinger HH, Lidral AC, Pober BR, Moreno L, Arcos-Burgos M, Valencia C, Houdayer C, Bahuau M, Moretti-Ferreira D, Richieri-Costa A, Dixon MJ, Murray JC. 2002. Mutations in IRF6 cause Van der Woude and popliteal pterygium syndromes. Nat Genet 32: 285-289.

Lakso M, Pichel JG, Gorman JR, Sauer B, Okamoto Y, Lee E, Alt FW, Westphal H. 1996. Efficient in vivo manipulation of mouse genomic sequences at the zygote stage. Proc Natl Acad Sci U S A 93: 5860-5865.

Lan ZJ, Xu X, Cooney AJ. 2004. Differential oocyte-specific expression of Cre recombinase activity in GDF-9-iCre, Zp3cre, and Msx2Cre transgenic mice. Biol Reprod 71: 1469-1474.

Little HJ, Rorick NK, Su LI, Baldock C, Malhotra S, Jowitt T, Gakhar L, Subramanian R, Schutte BC, Dixon MJ, Shore P. 2009. Missense mutations that cause Van der Woude syndrome and popliteal pterygium syndrome affect the DNA-binding and transcriptional activation functions of IRF6. Hum Mol Genet 18: 535-545.

Long MA, Rossi FM. 2009. Silencing inhibits Cre-mediated recombination of the Z/AP and Z/EG reporters in adult cells. PLoS One 4: e5435.

Nagy A. 2000. Cre recombinase: the universal reagent for genome tailoring. Genesis 26: 99-109.

Rahimov F, Marazita ML, Visel A, Cooper ME, Hitchler MJ, Rubini M, Domann FE, Govil M, Christensen K, Bille C, Melbye M, Jugessur A, Lie RT, Wilcox AJ, Fitzpatrick DR, Green ED, Mossey PA, Little J, Steegers-Theunissen RP, Pennacchio LA, Schutte BC, Murray JC. 2008. Disruption of an AP-2alpha binding site in an IRF6 enhancer is associated with cleft lip. Nat Genet 40: 1341-1347.

Richardson RJ, Dixon J, Malhotra S, Hardman MJ, Knowles L, Boot-Handford RP, Shore P, Whitmarsh A, Dixon MJ. 2006. Irf6 is a key determinant of the keratinocyte proliferation-differentiation switch. Nat Genet 38: 1329-1334.

Sabel JL, d'Alencon C, O'Brien EK, Van Otterloo E, Lutz K, Cuykendall TN, Schutte BC, Houston DW, Cornell RA. 2009. Maternal Interferon Regulatory Factor 6 is required for the differentiation of primary superficial epithelia in Danio and Xenopus embryos. Dev Biol 325: 249-262.

Sakai K, Miyazaki J. 1997. A transgenic mouse line that retains Cre recombinase activity in mature oocytes irrespective of the cre transgene transmission. Biochem Biophys Res Commun 237: 318-324.

Tamura T, Yanai H, Savitsky D, Taniguchi T. 2008. The IRF family transcription factors in immunity and oncogenesis. Annu Rev Immunol 26: 535-584.

Zucchero TM, Cooper ME, Maher BS, Daack-Hirsch S, Nepomuceno B, Ribeiro L, Caprau D, Christensen K, Suzuki Y, Machida J, Natsume N, Yoshiura K, Vieira AR, Orioli IM, Castilla EE, Moreno L, Arcos-Burgos M, Lidral AC, Field LL, Liu YE, Ray A, Goldstein TH, Schultz RE, Shi M, Johnson MK, Kondo S, Schutte

BC, Marazita ML, Murray JC. 2004. Interferon regulatory factor 6 (IRF6) gene variants and the risk of isolated cleft lip or palate. N Engl J Med 351: 769-780.

CHAPTER THREE

Oocyte specific deletion of Irf6 leads to increased fertility in the mouse

ABSTRACT

Interferon Regulatory Factor 6 (IRF6) is a member of the IRF family of transcription factors. It is most known for its role in the pathogenesis of cleft lip and palate, a common congenital defect. More recent studies have shown that Irf6 is maternally expressed in the oocytes of zebrafish, frog, and cow. In the zebrafish and frog, this maternally deposited irf6 is essential for early embryonic development and its inhibition results in very early embryonic lethality. Irf6 knockout mice display severe skin, limb and craniofacial defects but survive until shortly after birth. The central hypothesis of this work is that Irf6 is maternally expressed and that this maternal expression is sufficient to surpass early embryonic lethality in the mouse. To test this hypothesis, we conducted immunofluorescent staining in oocytes to confirm the presence of maternal Irf6 in the mouse. To determine the function of maternal Irf6, we generated a mouse model with oocyte specific deletion of *Irf6* using the *Gdf9-Cre* transgene mouse line. Surprisingly, mice born to females with oocyte specific deletion of *Irf6* were viable. In fact, females with oocyte specific deletion showed a 20% increase in litter size and number of eggs ovulated. In addition, these females had an increased incidence of multiple oocyte follicles when compared to their control counterparts. The multiple oocyte follicles did not seem to account for the observed increase in fertility. These data indicate a novel role for *Irf6* in regulating female fertility and follicle development in the mouse.

INTRODUCTION

Litter size in the mouse is a common metric of fertility. One limiting factor of fertility is the number of oocytes ovulated. In the mouse, oocyte development begins during gestation. At mid-gestation, mitotic germ cells populate the gonadal ridge. These mitotic germ cells arrange into germ cell nests, clusters of cells connected by intercellular bridges (Pepling and Spradling, 1998). At E17.5, these germ cells exit mitosis and enter meiosis. Upon entering meiosis, germ cell nests begin to break down. This process is marked by dissolution of intercellular bridges, intercalation of surrounding somatic cells, and widespread oocyte death (Pepling and Spradling, 2001). In fact, approximately two-thirds of the oocyte population will undergo programmed cell death. The endpoint of nest breakdown is the formation of the earliest follicles, the primordial follicles. The follicle represents the functional unit of the ovary and consists of an oocyte surrounded by granulosa cells (Peters, 1969). In wildtype mice, most follicles contain one oocyte. Rarely, a follicle may contain more than one oocyte. These follicles are known as multiple oocyte follicles (MOFs). The number of MOFs in wildtype animals vary by strain (average = 6 MOFs/ovary) (Fekete, 1950).

Numerous mouse models display an increased prevalence of MOFs. The pathogenesis of MOFs can be broken into two categories. The first, and most commonly reported, mechanism underlying MOF formation is impaired germ cell nest breakdown (Jefferson *et al.*, 2006). Estrogen signaling appears to be critical for proper nest breakdown and primordial follicle generation (Chen *et al.*, 2007; Hunt *et al.*, 2012; Jefferson *et al.*, 2006). MOFs are observed in females exposed to genistein, a phytoestrogen, as neonates (Jefferson *et al.*, 2006). Genistein and other estrogen

mimetics result in inhibition of germ cell nest breakdown and reduced oocyte loss (Chen *et al.*, 2007).

Multiple oocyte follicle formation can be due to defects in the oocyte or granulosa cells during the process of germ cell nest breakdown. For example, *Gdf-9* and *Bmp15* are members of the Tgfb3 family and are expressed specifically in the oocyte. Mice homozygous for a null mutation of *Bmp15* and heterozygous for a null mutation of *Gdf9* (*Bmp15*$^{-/-}$; *Gdf9*$^{+/-}$) display MOFs (Yan *et al.*, 2001). In contrast, *Lunatic Fringe*, a regulator of Notch signaling, is expressed specifically in the granulosa cells. MOFs are also observed in mice homozygous for null mutations of *Lunatic Fringe* (Hahn et al., 2005). Likewise, mice with granulosa cell specific deletion of *Notch 2* display MOFs due to impaired persistence of nests and reduced oocyte death (Xu and Gridley, 2013). These data indicate the importance of both *Notch* and *Tgfb3* signaling in primordial follicle formation. Lastly, *Aquaporin-8* – deficient females display MOFs. *Aquaporin-8* expression is restricted to the granulosa cells (Su *et al.*, 2013). These data indicate that germ cell nest breakdown is a coordinated effort between oocyte and granulosa cells and perturbation to this process results in impaired folliculogenesis. Notably, most cases of MOFs are associated with reduced fertility or infertility (Hahn *et al.*, 2005; Xu and Gridley, 2013; Yan *et al.*, 2001).

The second mechanism governing MOF formation is fusion of adjacent follicles. This mechanism is observed in females with oocyte-specific deletion of the *T-synthase* gene (*T-syn*). In this model, *T-syn* deletion is mediated by *ZP3-Cre* at the primary follicle stage, after germ cell nest breakdown. Follicle fusion is observed morphologically through analysis of serial sectioned ovaries. Interestingly, these mice

also display an increase in fertility as measured by litter size and ovulation rates and this increase in fertility is independent of maternal age. However, this increase in fertility does not appear to be due to the increase in MOFs (Williams and Stanley, 2008).

The primordial follicles resulting from nest breakdown represent the entire pool of oocytes a female will have in her lifetime (Peters, 1969). By postnatal day seven, there is estimated to be approximately 2000 primordial follicles (Kerr *et al.*, 2006). During each reproductive cycle, some oocytes will be selected to complete maturation and undergo ovulation (Mehlmann, 2005). The mechanisms governing this selection are ill-defined. However, the quality and number of oocytes a female has is closely linked to fertility. For example, poor oocyte quality is a leading cause of age-related infertility (Navot *et al.*, 1991). Infertility affects 12% of women ages 18-34. Assisted reproductive technologies are available to aid those with reproductive complications. However, these technologies have low success rates (Center For Disease Control and Prevention *et al.*, 2013). The identification of the molecular players required for proper development of the oocyte, the early embryo, and reproductive success will aid in refining current ARTs and provide new therapies.

As the oocyte develops, it becomes transcriptionally silent. As a result, mRNA and protein from genes being expressed in the oocyte are stored for future use. These maternal effect genes play critical roles in oocyte maturation and post-fertilization development (Li *et al.*, 2010). Interferon regulatory factor 6, a member of the interferon regulatory factor family of transcription factors, is a maternally expressed gene. Maternal stores of *irf6* are detectable in zebrafish and frog embryos (Ben *et al.*, 2005; Sabel *et al.*, 2009). In addition, *Irf6* is highly expressed in mature bovine oocytes

(Regassa *et al.*, 2011), suggesting that maternal expression of Irf6 is conserved across species.

In zebrafish and frog, inhibition of maternal irf6 protein using a dominant-negative *irf6* allele results in early embryonic lethality. Specifically, these embryos have a failure of differentiation of the superficial epithelium (Sabel *et al.*, 2009). Interestingly, mice deficient for *Irf6* (zygotic) survive until term, dying shortly after birth with severe skin, limb, and craniofacial defects (Ingraham *et al.*, 2006; Richardson *et al.*, 2006). The primary goal of this research was to determine the role of maternally expressed Irf6 in the mouse. The study of maternally expressed genes in the murine system has been greatly enhanced by the generation of oocyte-specific *Cre* drivers. Here we report the detection of maternally expressed Irf6 in the mouse and the generation of females with oocyte specific deletion of Irf6 using a conditional allele of Irf6 (*Irf6^{fl}*) in combination with the Gdf9-Cre transgenic line. *Gdf9-Cre* drives *Cre* expression in primordial follicles, making it the oocyte specific line with the earliest Cre activity (Lan *et al.*, 2004).

MATERIALS AND METHODS

Mouse and embryo genotyping

To attain genomic DNA, tail biopsies were digested in lysis buffer (10 mM Tris-HCl, 150 mM NaCl, 10 mM EDTA, 0.1% SDS) with Proteinase-K (20mg/ml, Roche) at 55°C, overnight, followed by ethanol precipitation of DNA. PCR-based genotyping was used to identify alleles (see below). All PCR was conducted using JumpStart REDTaq Ready Mix (Sigma-Aldrich, St. Louis, MO) and separated by electrophoresis on 1.5% agarose gels and visualized with ethidium bromide.

Detection of the Irf6^{fl} and Irf6^{nl} alleles

Primer set of oBS3318 and oBS3319 was used to distinguish the *Irf6*$^{+}$allele from the *Irf6*^{fl} allele. Primer set of oBS4380 and oBS3319 was used to detect the *Irf6*^{nl} (see Table 3.1 for primers sequences). PCR was performed as follows: 1) 95°C for two minutes, 2) 95°C for 15 seconds, 3) 55°C for 15 seconds, 4) 72°C for 45 seconds, 5) repeat steps 2-4 35 times, 6) 72°C for five minutes.

Detection of the Irf6^{gt} allele

Primer set of oBS144 and oBS145 was used to identify the *Irf6*^{gt} allele. Primer set of oBS146 and oBS145 was used to identify the wildtype allele (see Table 3.1 for primers sequences). PCR conditions were as follows: 1) 95°C for three minutes, 2) 95°C for 38 seconds, 3) 60°C for 50 seconds, 4) 72°C for 15 seconds, 5) repeat steps 2-4 40 times, 6) 72°C for five minutes. PCR Master Mix was supplemented with 5M Betaine monohydrate to aid in amplification of GC-rich regions.

Detection of Gdf9-Cre transgene

The *Gdf9-Cre* transgene was detected using primer set of oBS4934 and oBS4935 (see Table 3.1). PCR conditions were as follows: 1) 95°C for five minutes, 2) 95°C for one minute, 3) 58°C for two minutes, 4) 72°C for one minute, 5) repeat steps 2-4 35 times, 6) 72°C for five minutes. Master mix was supplements with 5M Betaine monohydrate to aid in amplification of GC-rich regions.

Oocyte specific deletion of Irf6

A male hemizygous for the *Gdf9-iCre* transgene (*tg*$^{+/Gdf9\text{-}Cre}$) was purchased from Jackson Labs (www.jax.org) and mated to females that were compound heterozygotes

at the *Irf6* locus, carrying a null allele and the conditional allele (*Irf6$^{gt/fl}$*). To maximize production of females with oocyte specific deletion of *Irf6*, we employed two mating strategies using offspring from the mating described above (see Fig 3.2). For the first, *Irf6$^{gt/+}$; tg$^{+/Gdf9\text{-}Cre}$* animals were mated to *Irf6$^{fl/fl}$* animals. For the second scheme, *Irf6$^{fl/+}$; tg$^{+/Gdf9\text{-}Cre}$* males were mated to *Irf6$^{gt/fl}$* females. This allowed for the generation of females with oocyte specific deletion of Irf6 via two genotypes; *Irf6$^{gt/fl}$; tg$^{+/Gdf9\text{-}Cre}$* and *Irf6$^{fl/fi}$; tg$^{+/Gdf9\text{-}Cre}$*. These females were referred to as experimental females. Control females had the same genotype at the *Irf6* locus but lacked the *Gdf9-Cre* transgene (*Irf6$^{gt/fl}$; tg$^{+/+}$* or *Irf6$^{fl/fl}$; tg$^{+/+}$*).

Maternal and Zygotic Irf6 deletion

To generate embryos deficient for both maternal and zygotic Irf6, experimental females were placed into timed matings with *Irf6$^{gt/+}$* males. The presence of a copulation plug was denoted as E0.5. Females were euthanized using isoflurane induced comatosis followed by cervical dislocation. Embryos were collected at E17.5. Tail snips were collected from pups upon weaning and genotyped. A chi-squared test was used to determine deviations from expected Mendelian ratios.

Tissue Collection and processing

For collection of adult ovaries, Irf6$^{+/+}$, experimental and control females between the ages of three to nine months were euthanized as described above. Whole ovaries were collected and fixed overnight in 10% neutral buffered formalin at 4°C. Following fixation, ovaries were processed and embedded in paraffin by the Histopathology Laboratory at Michigan State University using standard protocols.

For collection of neonatal ovaries, pups were euthanized by isoflurane induced comatosis followed by decapitation. Ovaries were collected under a dissecting microscope and fixed in 10% neutral buffered formalin for four hours at room temperature. Fixed ovaries were then embedded in HistoGel Specimen Processing Gel before processing. Samples were processed by the MSU Histopathology laboratory as described above. All animals were used in accordance with the National Institutes of Health Guide for the Care and Use of Laboratory Animals, and all procedures were approved by the MSU IACUC.

Ovary Histology

Whole adult ovaries were sectioned at 7µm. Sections were then stained with hematoxylin and eosin. Briefly, for depariffinization and rehydration, sections were passed through three changes of xylene followed by washes through reducing grades of ethanol. Slides were then incubated in Gill's Hematoxylin No. III (Sigma-Aldrich, St. Louis, MO) for 1.5 minutes, washed briefly in tap water, and incubated in a 1% Eosin solution (Eosin Y- VWR, West Chester, PA) for 1.5 minutes. To dehydrate, slides were passed through increasing grades of ethanol. Lastly, slides were mounted using Permount mounting media (VWR, Radnor, PA). Stained sections were imaged using a Nikon 90i upright microscope.

Immunofluorescence

For immunofluorescent detection, rabbit anti-Irf6 antibody (gift from Dr. Akira Kinoshita, Nagasaki University – Irf6-Akira) and rabbit anti- Caspase 3 were used. Sections were deparaffinized and rehydrated in reducing concentrations of ethanol. Sections were subjected to antigen retrieval by boiling in 10mM Sodium citrate (pH6.0)

for 30 minutes. Tissues sections were then permeabilized using 0.5% Triton X-100 followed by blocking in blocking solution (10% normal goat serum, 0.1% Bovine Serum Albumin in 1X PBS) for one hour at room temperature. Rabbit anti-Irf6 was used at a 1:100 concentration and rabbit anti-Caspase 3 was used at a 1:300 concentration. Samples were incubated overnight at 4°C, followed by incubation with goat anti-rabbit AlexaFluor 488 (Life Technologies, Grand Island, NY) at a 1:250 concentration. Nuclei were counterstained for 10 minutes in DAPI (1:10,000; Life Technologies, Grand Island, NY). Slides were then mounted in ProLong GOLD Antifade reagent (Life Technologies, Grand Island, NY).). Images were taken using an Olympus FV1000 Confocal Laser Scanning Microscope or a Nikon Eclipse 90i fluorescent microscope.

Collection of eggs after superovulation

Females between six to twelve weeks of age were administered exogenous gonadotropins to induce ovulation as outlined by Jacksons Laboratory (www.jax.org). Briefly, females were given an intra-peritoneal (IP) injection of 5 International Units (IU) of pregnant mare's serum gonadotropin (PMSG – Sigma-Aldrich, St. Louis, MO) between 1:00pm and 4:00pm on Day 1. Forty two to fifty hours following PMSG administration, mice received an IP injection of 5 IU of human chorionic gonadotropin (HCG – Sigma-Aldrich, St. Louis, MO). Females were immediately placed with a vasectomized or proven male. Oocytes were removed from oviducts approximately 16 hours following HCG administration and washed briefly in M2 media. Oocytes were then incubated in M2 media supplemented the hyaluronidase (300ug/ml – Sigma-Aldrich, St. Louis, MO) to remove granulosa cells. Finally, oocytes were washed with M2 media to remove hyaluronidase.

Western Blot

For Western blot analysis, oocytes were collected from control and experimental mice following superovulation as described above. Oocytes removed from granulosa cells were stored in RIPA buffer supplemented with protease inhibitors. Samples were denatured by incubating at 95°C for 10 minutes and loading dye was added. Lysates were separate on 4-20% gradient gel (Bio-rad). Proteins were transferred to a membrane with 1X Tris-Glycine Transfer Buffer. The membrane was blocked with 5% Bovine Serum Albumin blocking buffer for one hour at room temperature, followed by incubation in rabbit anti- Irf6 antibody (1:2,000, Irf6-Akira) overnight at 4°C. Following incubation in secondary antibody, the membrane was stripped using Restore Plus Western Blot Stripping Buffer (Thermo Scientific, Rockford, IL). Rabbit anti – β-actin primary antibody (1:10,000, kind gift from Dr. Karen Friderici) was used as a loading control. Membranes blotted with primary antibody were then incubated with goat anti-rabbit immunoglobulin G conjugated to horseradish peroxidase (1:5,000, kind gift from Dr. George Smith). Chemiluminescent detection of substrates was done using Pierce ECL Western Blotting Substrate (Thermo Scientific, Rockford, IL). Blots were imaged using the myECL Imager. Band density was determined using Image J Data Analysis Software. Irf6 band density was normalized to actin. A student's T-test was used for statistical analysis.

mRNA collection and real-time PCR

For analysis of mRNA, two experimental and two control females were superovulated as described above. Twenty oocytes were collected per female and pooled. RNA was extracted from each pool using the PicoPure RNA Isolation Kit (Life

Technologies, Grand Island, NY). Synthesis of cDNA was conducted using the SuperScript III First strand Synthesis SuperMix (Life Technologies, Grand Island, NY). One microliter of cDNA was used for real-time PCR analysis.

For quantitative analysis of *Irf6* mRNA, primer set of 5'-AGTGTGGCCCAAAACAGAAC-3' and 5'-GGGTTGCTCACCGTCATAGT-3' was used. For *Irf6*, real time-PCR was carried out using the SYBR Green PCR Master Mix (Life Technologies, Grand Island, NY). As a housekeeping gene, a TaqMan probe against *Ubtf* (kind gift from Dr. Jason Knott) was used. For *Ubtf*, real-time PCR was carried out using the TaqMan Real Time PCR Master Mix (Life Technologies, Grand Island, NY). Data analysis was conducted using the ΔΔCt method. A student's T-test was used to determine statistical significance.

Assessment of Fertility

To determine reproductive capacity, three-month old experimental and control females were placed with proven, wildtype males. These matings persisted for six months and females remained in contact with the male for the duration of the experiments. Pregnancy was monitored daily. Upon birth, the number of pups per litter was counted and fetal weights were taken. A student's T-test was used determine statistically significant differences between experimental and control litter sizes.

Assessment of Natural Ovulation

To assess natural ovulation rates, a vasectomized male was purchased from Jackson Laboratory (www.jax.org). Control and experimental females between six to twelve weeks in age were selected. These females were placed with the vasectomized male. Females were monitored daily and sacrificed upon the presence of a copulation

plug. Oocytes were collected from oviducts and cleared from granulosa cells using M2 media supplemented with hyaluronidase as described above. The number oocytes ovulated per female was recorded. A student's T-test was used to determine statistically significant differences between control and experimental females.

Follicle Counts

Follicle counts were conducted on ovaries from three experimental and three control females. Whole ovaries were sectioned at 7μm. Every other slide was stained with H&E and every tenth section was selected for counting. Follicles were counted if an oocyte was present. Follicles were classified based on criteria described by Myers et al (2004). Briefly, primordial follicles were characterized as an oocyte surrounded by one layer of squamous granulosa cells. Primary follicles were classified as an oocyte with one layer of cuboidal granulosa cells. Secondary follicles had multiple layers of granulosa cells. Early antral follicles were those with multiple layers of granulosa cells with small intervening spaces of antrum. Late antral follicles had multiple layers of granulosa cells and interconnected antrum spaces. Lastly, pre-ovulatory follicles were characterized as follicles with an antrum completely surrounding the oocyte.

Multiple oocyte follicles

Multiple oocyte follicles were characterized as two or more oocytes encompassed within the same follicle. Multiple oocyte follicles were counted on every tenth section across the whole ovary. Follicles were tracked across a distance of 42 microns to determine if more than one oocyte was present in a given follicle. Classification of MOF development followed the same criteria outlined for single oocyte follicles.

RESULTS

Irf6 is maternally expressed in the mouse

Irf6 is expressed in oocytes of zebrafish, frog and cow (Ben *et al.*, 2005; Regassa *et al.*, 2011; Sabel *et al.*, 2009). To determine if maternally expressed Irf6 was conserved in mouse, we assessed Irf6 expression in the murine adult ovaries. Cross-section of ovaries allowed for analysis of oocytes at all developmental stages. Irf6 was diffuse throughout the cytoplasm in oocytes at all developmental stages (see Fig 3.1). This expression was consistent with that observed in bovine oocytes. In addition, we observed Irf6 expression in the somatic granulosa cells surrounding the oocyte. This staining also appeared to be cytoplasmic in nature (see Fig 3.1). Notably, expression of Irf6 in granulosa cells was not observed in the bovine system (Regassa *et al.*, 2011). Nonetheless, these data confirm that maternal expression of Irf6 is conserved in the mouse.

Generation of animals with oocyte specific deletion of Irf6

To study the function of maternally expressed Irf6, we employed a conditional knockout strategy utilizing the *Gdf9-Cre* transgene. Females with oocyte specific deletion of *Irf6* (experimental females) were generated and could have two possible genotypes; $Irf6^{gt/fl}; tg^{+/Gdf9\text{-}Cre}$ and $Irf6^{fl/fl}; tg^{+/Gdf9\text{-}Cre}$ (see Fig 3.2). Experimental females were born at normal Mendelian ratios (data not shown) and displayed no developmental defects. However, it is worth noting that 8 of 41 (20%) mice from matings to generate experimental females displayed a repeated epilation phenotype characterized by cycles of hair loss and regrowth (see Fig. A.1). This phenotype was not sex specific, affecting both males and females. Interestingly, this phenotype was not restricted to animals with

the “experimental genotypes.” In fact, the phenotype was present in animals that carried two alleles of *Irf6* that were genetically modified, affecting experimental and

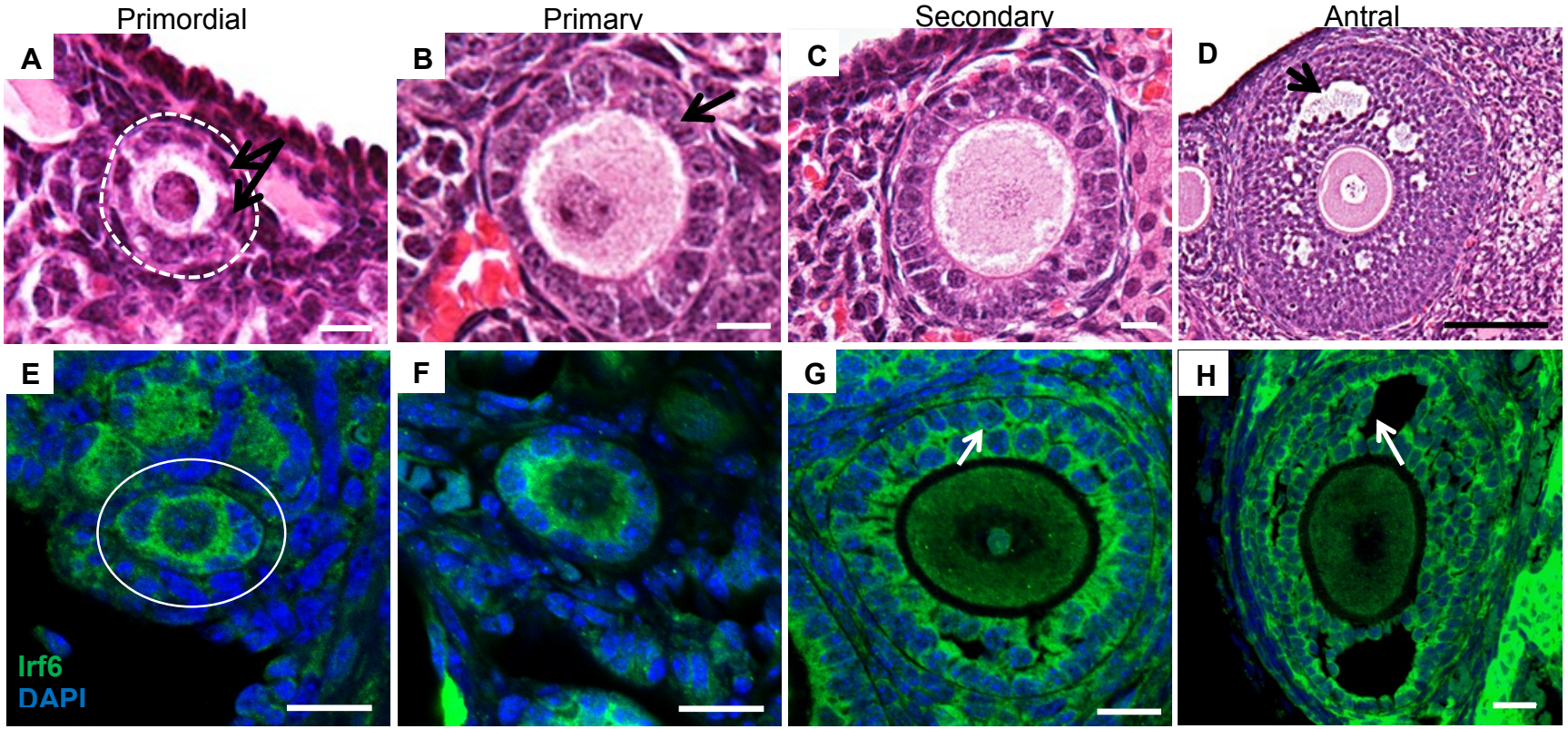

Figure 3.1: Maternally expressed Irf6 in the mouse.

Figure 3.1 (cont'd)

A-D) H&E images from cross – sections of murine ovaries showing primordial (A), primary (B), secondary (C), and antral (D) follicles. Black arrows (A-B) indicate squamous granulosa cells surrounding oocytes at the primordial follicle stage (A) or cuboidal granulosa cells of primary follicles (B). Black arrow in (D) indicates spaces of antrum. E-F) Irf6 (green) was expressed in oocytes at all developmental stages. Irf6 was also detected in granulosa cells at all stages (white arrows in G-H). Nuclei were stained with DAPI (blue). Images were acquired using the Olympus FV1000 Confocal Laser Scanning Microscope. Scale bars represent 10μm (A-C), 50μm (E-F) and 100μm (D, G-H).

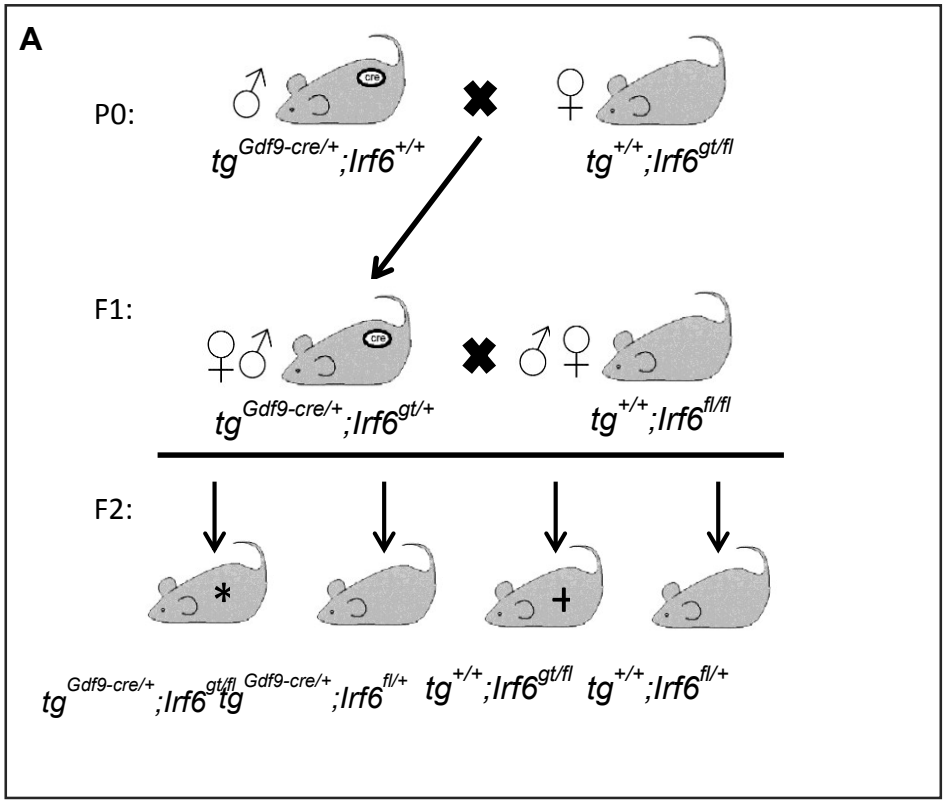

Figure 3.2: Generation of females with oocyte specific deletion of Irf6. A) Mating scheme one: *tg*$^{Gdf9\text{-}cre/+}$;*Irf6*$^{gt/+}$ animals were selected and bred to *tg*$^{+/+}$;*Irf6*$^{fl/fl}$ animals for generation of females with oocyte specific deletion of *Irf6* and control littermates. B) Mating scheme two: *tg*$^{Gdf9\text{-}cre/+}$;*Irf6*$^{fl/+}$ males were bred to *tg*$^{+/+}$;*Irf6*$^{gt/fl}$ females to produce an F2 generation. Females with oocyte specific deletion of *Irf6* (experimental females) are indicated with *****. Control littermates are indicated with **+**.

Figure 3.2 (cont'd)

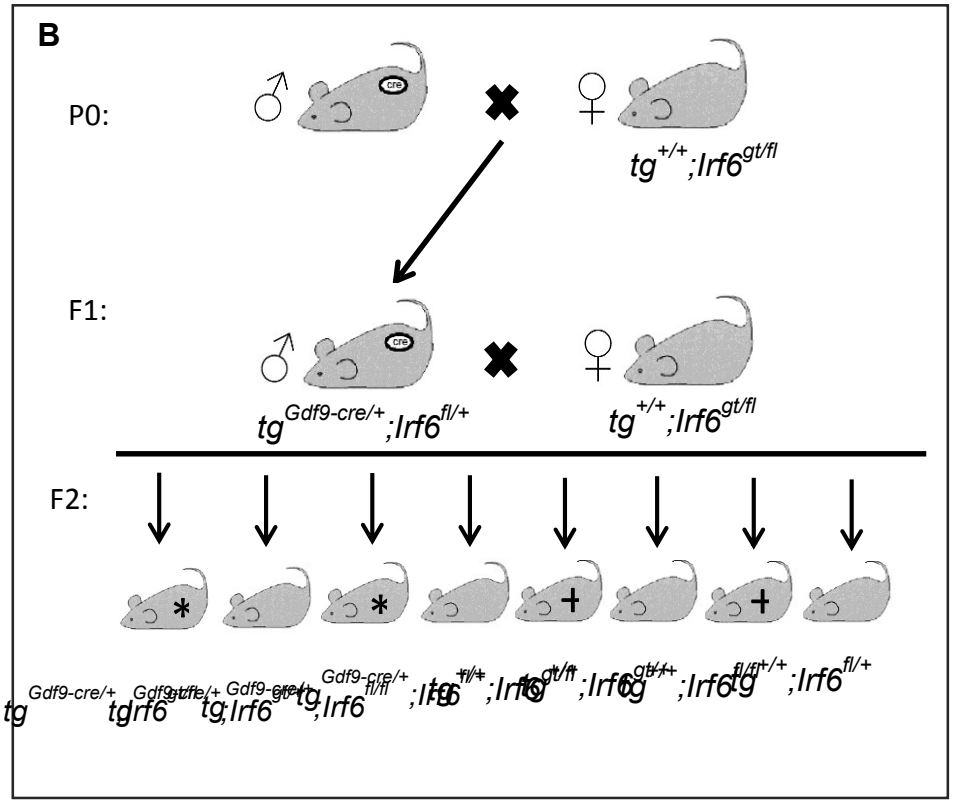

control females (see Table A.1). This phenotype did not appear to alter fitness of affected mice. While this phenotype is interesting, it extends beyond the scope of this work and was not characterized further.

Irf6 is genetically excised but protein levels are not altered

Gdf9-Cre drives Cre expression starting three days post birth (Lan *et al.*, 2004). To confirm genetic deletion of *Irf6* in females carrying both the *Gdf9-Cre* transgene and the conditional allele of *Irf6*, $tg^{Gdf9\text{-}Cre/+;}$ $Irf6^{fl/+}$ females were mated to $Irf6^{gt/fl}$ males. We hypothesized that the *Gdf9-Cre* would mediate recombination in the oocyte of these females, resulting in the production of the $Irf6^{nl}$ allele. Progeny from these matings were genotyped upon weaning. We observed a significant non-representation of two genotypes, $tg^{Gdf9\text{-}Cre/+;}$ $Irf6^{gt/nl}$ and $tg^{+/+;}$ $Irf6^{gt/nl}$ *(see Table 3.2)*. In addition, $tg^{Gdf9\text{-}Cre/+;}$ $Irf6^{fl/+}$ females mated to $Irf6^{gt/+}$ males and embryos were collected at E17.5. We observed embryos that phenocopied $Irf6^{gt/gt}$ animals, displaying severe skin, limb and craniofacial abnormalities (as described in Chapter 2). Genotyping data indicated that these embryos had one of two genotypes: 1) $tg^{Gdf9\text{-}Cre/+;}$ $Irf6^{gt/nl}$ or 2) $tg^{+/+;}$ $Irf6^{gt/nl}$, indicating that the $Irf6^{fl}$ allele was being recombined leading to the generation of a null allele of *Irf6* ($Irf6^{nl}$). The mutant phenotype was observed independent of the transgene being present, indicating that this recombination event occurred before the completion of meiosis I in the oocyte.

To confirm loss of protein, ovaries from experimental females were immuno-stained for Irf6. Interestingly, Irf6 expression in oocytes was not lost in experimental females (see Fig 3.3 A-B). Western blot analysis on oocytes collected from control and experimental females (n=20 oocytes/well) was conducted. Consistent with the

♀ $tg^{Gdf9\text{-}cre/+}$;$Irf6^{fl/+}$ X ♂ $tg^{+/+}$;$Irf6^{gt/fl}$		
Genotype	Expected	Observed
$tg^{Gdf9\text{-}cre/+}$; $Irf6^{gt/nl}$	5.125	0
$tg^{Gdf9\text{-}cre/+}$;$Irf6^{fl/nl}$	5.125	7
$tg^{Gdf9\text{-}cre/+}$; $Irf6^{gt/+}$	5.125	3
$tg^{Gdf9\text{-}cre/+}$; $Irf6^{fl/+}$	5.125	6
$tg^{+/+}$; $Irf6^{gt/fl}$	5.125	0
$tg^{+/+}$; $Irf6^{fl/nl}$	5.125	8
$tg^{+/+}$; $Irf6^{gt/+}$	5.125	5
$tg^{+/+}$; $Irf6^{fl/+}$	5.125	12
CNG		2 (not included)
TOTAL	41	41

Table 3.2: Gdf9-Cre mediated recombination of *Irf6^{fl}*. Recombination of the *Irf6^{fl}* allele in the female results in production of the *Irf6^{nl}* allele. Data represents offspring from six litters after weaning. There is a significant underrepresentation of mice with *Irf6$^{gt/nl}$* (X^2 *test: p = 0.0018*). CNG – Could Not Genotype.

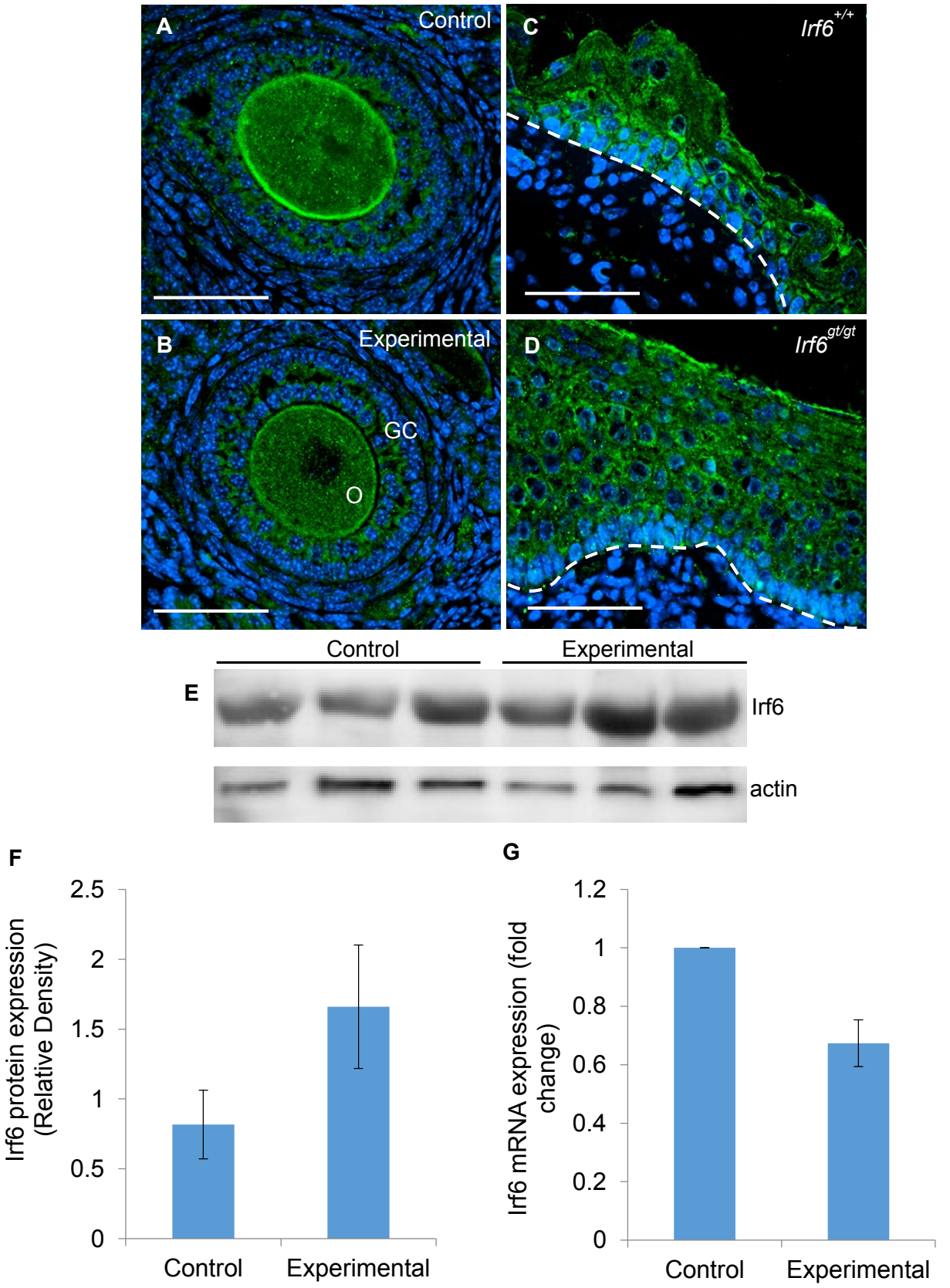

Figure 3.3: **Irf6 expression in experimental females**.

Figure 3.3 (cont'd)

A-B) Ovaries from experimental and control females were cross-sectioned and immuno-stained for Irf6. Irf6 expression (green) was detected in both control (A) and experimental (B) oocytes. Scale bars - 50μM C-D) Skin collected from embryos at E17.5 was cross-sectioned and stained for Irf6. Irf6 expression (green) was observed in skin from both *Irf6*$^{+/+}$ and *Irf6*$^{gt/gt}$. E-F) Western blot analysis of Irf6 protein. Oocytes were collected from three control and three experimental females. Blots were probed for Irf6 and actin (loading control; E). Irf6 expression was normalized to actin. F) While oocytes from experimental animals showed an increase in Irf6 expression, this increase was not significant (0.82±0.25 vs. 1.65±0.44 ; p = 0.09). G) Irf6 mRNA expression was reduced by approximately 30% in oocytes collected from experimental animals compared to control. This reduction was statistically significant using a one-tailed t-test (p = 0.05).

immunofluorescent results, we observed Irf6 protein expression in ovulated oocytes from experimental females (see Fig 3.3 E). However, the Irf6 protein levels were not significantly different (see Fig 3.3 F). As a positive control, skin from wildtype and *Irf6*$^{gt/gt}$ embryos was cross-sectioned and immuno-stained for Irf6. As expected, Irf6 expression was observed in the basal layer of the epidermis and throughout the spinous layer. However, immunofluorescent signal was also detectable in the expanded epidermis of mutant animals. These results indicate non-specific binding of the Irf6 antibody in Irf6 deficient tissue (see Fig 3.3 C-D).

To determine if *Irf6* mRNA was still being produced, oocytes were collected from experimental and control females and RNA was extracted. In conjunction with the presence of Irf6 protein, *Irf6* mRNA was still detected in oocytes from experimental females. Specifically, experimental females showed approximately a 30% reduction in *Irf6* mRNA levels when compared to controls ($p = 0.05$). These results are consistent with perdurance of *Irf6* gene products.

Oocyte specific excision of Irf6 results in increased fertility

In zebrafish, inhibition of maternal irf6 results in early embryonic lethality. Early embryonic loss in the mouse would manifest itself as infertility. To determine the effect of genetic excision of *Irf6* on early embryonic development in the mouse, fertility studies were conducted. Three month old control (n = 12 dams) and experimental (n = 10 dams) females were placed in harem matings with proven, wildtype males. Surprisingly, experimental females had larger litter sizes than their control counterparts (9.94 ± 0.31 vs. 8.05 ± 0.37; $p = 0.001$; see Fig 3.4A). The observed increase in litter size was independent of maternal age as experimental females had larger litter sizes

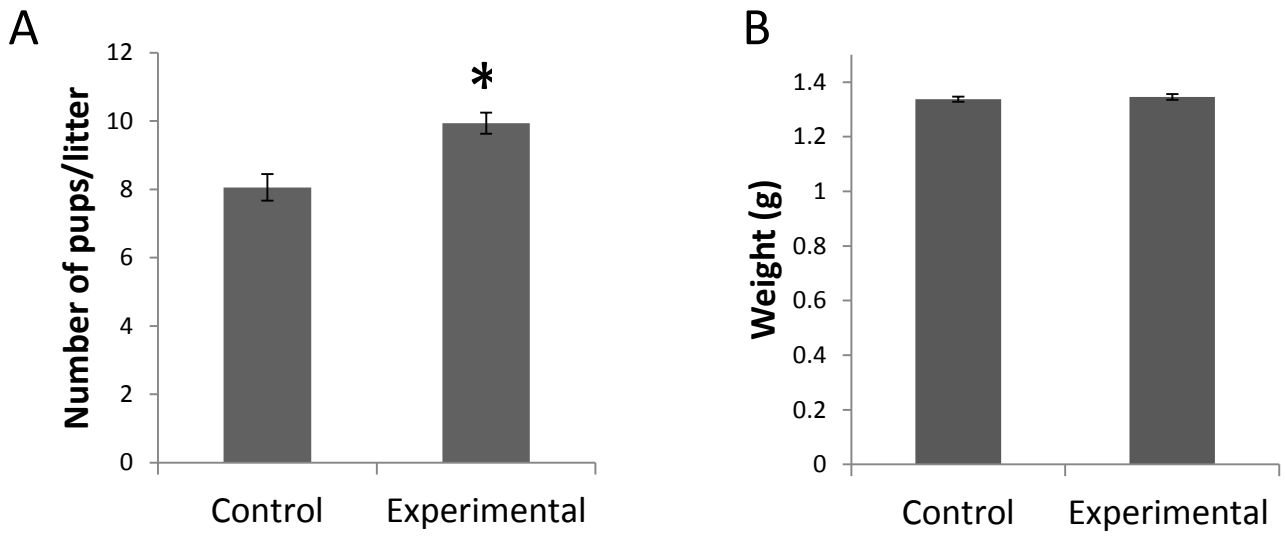

Figure 3.4: Oocyte specific excision of Irf6 leads to increased fertility. A) Experimental females show a 19% increase in litter size (*p = 0.001). Data represents 77 litters from 12 control females and 61 litters from 10 experimental females. B) Increased litter size does not affect fetal weights (control pups – N = 200, experimental pups – N=150). C. Increase in litter size in experimental females is independent of maternal age. Experimental (N = 5) and control (N = 7) were placed in mating with wildtype males for ~6 months. Lines represent logarithmic trendlines.

Figure 3.4 (cont'd)

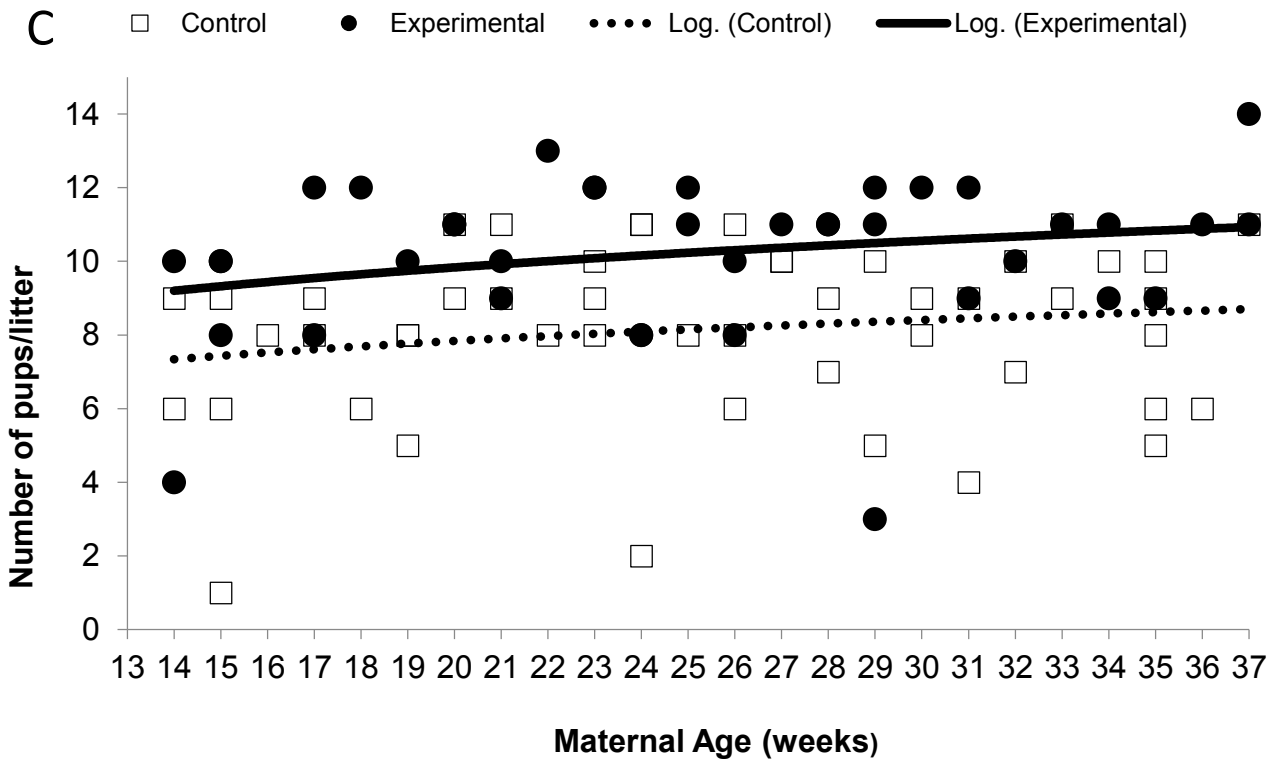

throughout the six month period of mating (See Fig 3.4B). In addition, increased litter size did not affect fetal health as measured by birth weight (see Fig 3.4C). To measure ovulation in females with oocyte specific excision of Irf6, females were placed with vasectomized males and oocytes were collected upon the presence of a copulation plug. Experimental females naturally ovulated more eggs than their control counterparts (9.4 ± 0.66 vs. 6.5 ± 0.5; p = 0.03). This finding is consistent with the observed increase in litter size in experimental females (see Fig. 3.5).

Oocyte specific excision of Irf6 does not affect follicle numbers

In *Irf6*-deficient skin, proliferation was increased and apoptosis was decreased (Ingraham *et al.*, 2006; Richardson *et al.*, 2006). We hypothesized that these mechanisms could function in the oocyte, resulting in altered follicle numbers. To test this hypothesis, we assessed ovarian morphology and follicle numbers. Females with oocyte specific excision of Irf6 displayed normal ovarian morphology. Follicles at all different developmental stages and areas of corpus luteum were apparent in both control and experimental ovaries. To assess follicle numbers, ovaries were collected from seven month old females. Follicles were classified into five developmental stages as described above (see Materials and Methods). There was no difference in the number of follicles at any developmental stage between control and experimental females (see Fig. 3.6).

Oocyte specific excision of Irf6 results in multiple oocyte follicles

While the number of follicles was unchanged, multiple oocyte follicles were observed in ovaries from experimental females (see Fig. 3.7A,B). Multiple oocyte follicles were characterized as any follicle containing more than one oocyte. Experimental females had significantly more MOFs than their control counterparts (14.8

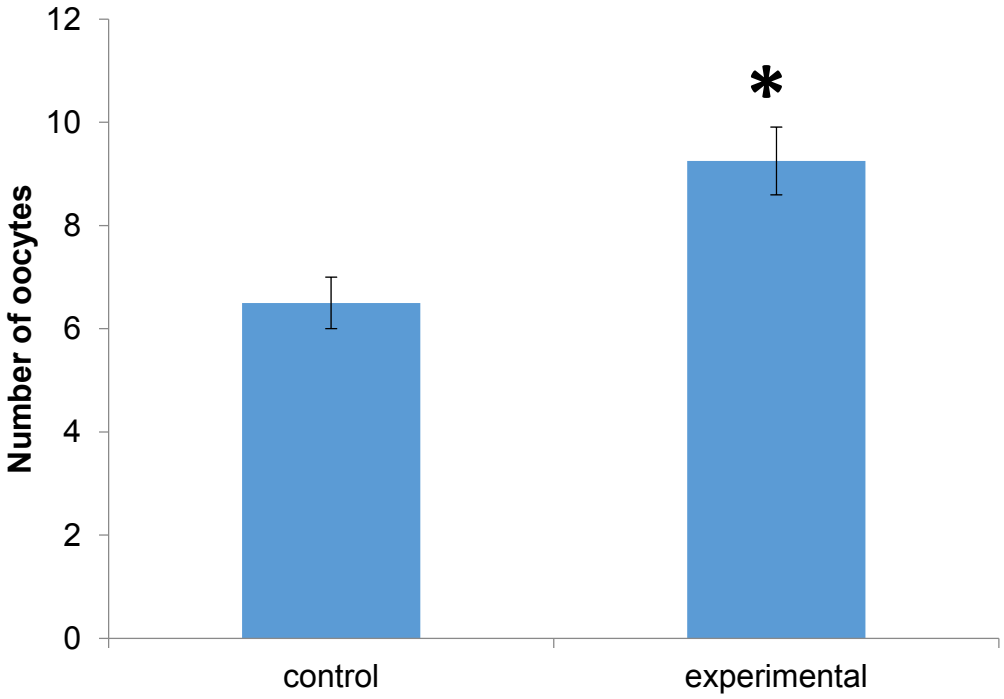

Figure 3.5: Experimental females ovulate more eggs than control females. Females were placed with a vasectomized male and oocytes were collected upon natural ovulation. Data collected from two control and five experimental females. * p = 0.03

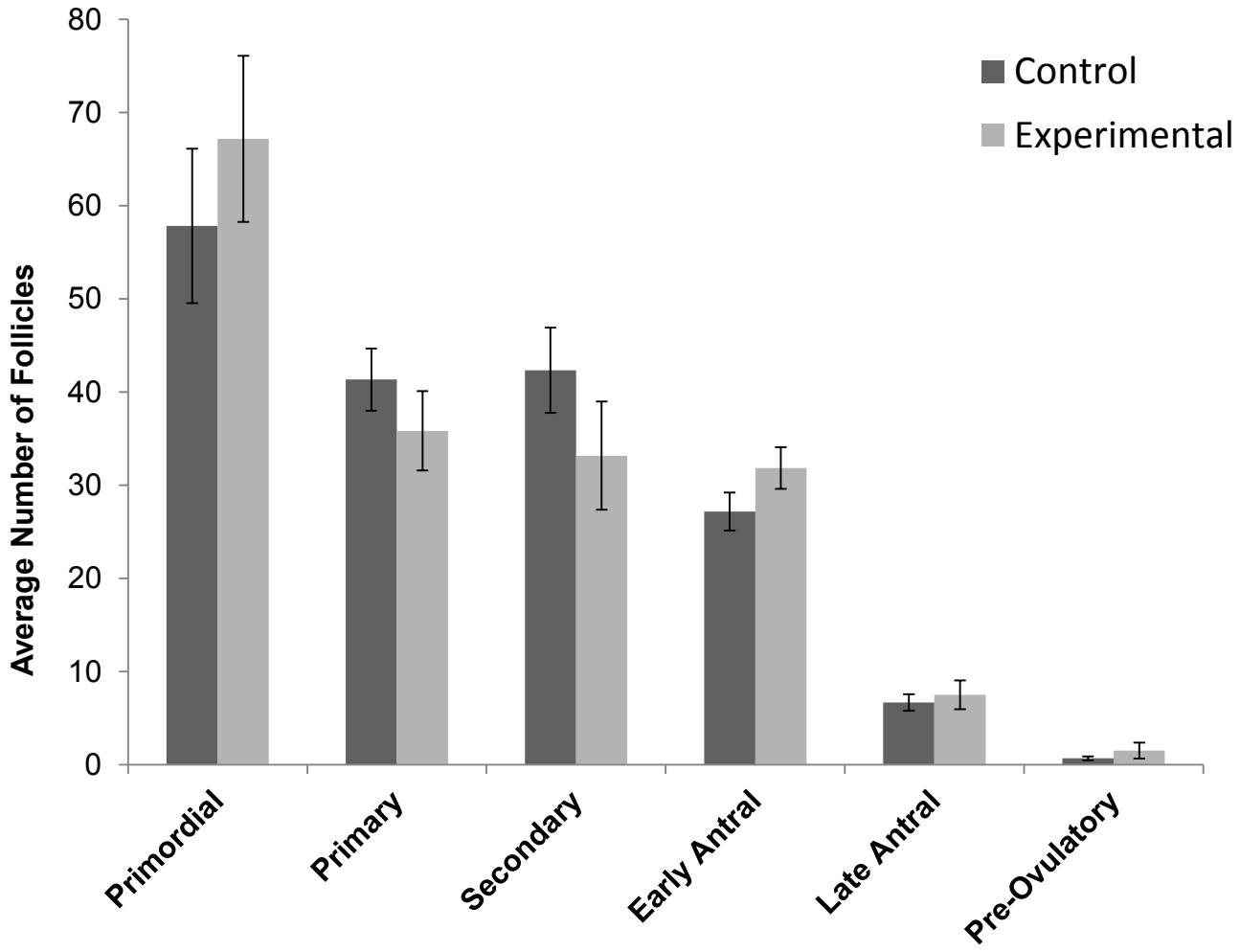

Figure 3.6: Follicle numbers do not differ between groups. Ovaries from three experimental (N = 6) and three control (N= 6) females were cross-section and follicles were counted. There was no difference in the number of follicles between experimental and control females.

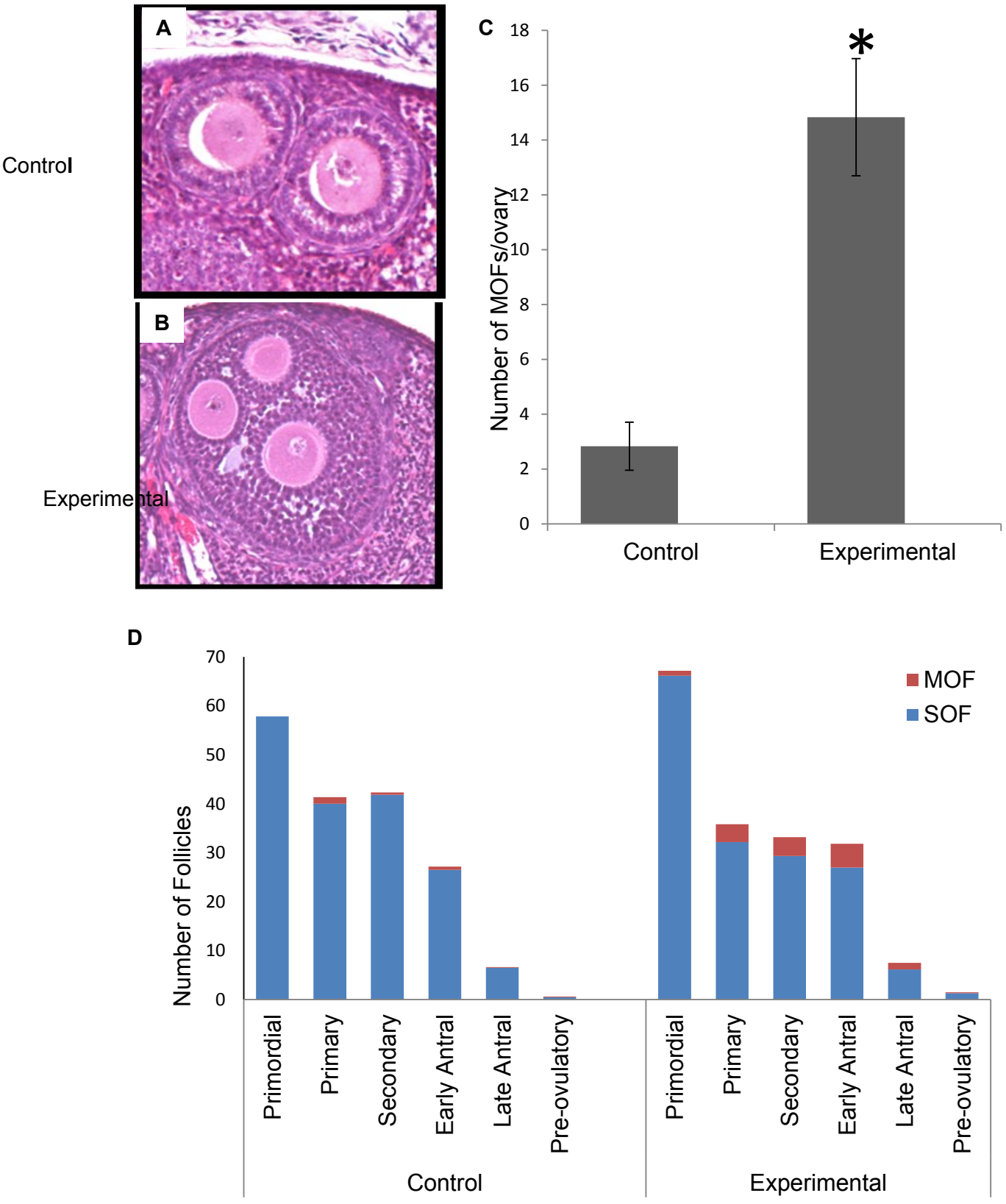

Figure 3.7: Increase in multiple oocyte follicles.

Figure 3.7 (cont'd)

A ,B) Ovary sections stained with H&E. A) Follicles from control females develop as independent units. B) Multiple oocyte follicles were observed in experimental females. C) The number of MOFs were counted. Data represent counts from three control (N=6) and three experimental (N=6) females. There was a significant increase in the number of MOFs in experimental females (*p = 0.001). D) MOFs account for a larger proportion of follicles in experimental females. (SOF – Single oocyte follicles)

± 2.13 vs. 2.83 ± 0.87; p = 0.001; See Fig. 3.7C). In control females, MOFs accounted for 1.6% of all total follicles. Most commonly, these MOFs contained 2 oocytes (94%). Only one MOF in ovaries from control animals contained more than three oocytes. In experimental females, MOFs accounted for 8.3% of all follicles. Similar to control females, most MOFs contained only two oocytes (88%). However, MOFs containing up to five oocytes was observed.

MOFs do not account for increase in fertility

While there was no difference in follicle numbers, MOFs accounted for a larger percentage of follicles in experimental females (see Fig. 3.7D). We sought to determine whether or not MOFs could account for the increase in fertility. To do so, the number of oocytes per female was extrapolated and compared. Due to the MOFs, females with oocyte specific excision of *Irf6* had a greater number of oocytes. However, this increase was not significant (see Fig 3.8). These data suggest that MOFs do not contribute to the observed increase in fertility.

Irf6 is expressed during germ cell nest breakdown

The most common underlying cause of the MOFs is impaired germ cell nest breakdown (Jefferson *et al.*, 2006). In the mouse, germ cell nest breakdown occurs just following birth and is completed by approximately post natal day 6. To determine if *Irf6* is involved in germ cell nest breakdown and primordial follicle formation, ovaries were collected from neonatal females at PND1 and PND6 and immuno-stained for Irf6. At PND1, Irf6 was detected specifically in oocytes of germ cell nests. Here, expression of Irf6 appeared to be restricted to oocytes and was not observed in the surrounding pre-granulosa cells (see Fig. 3.9A). At PND6, Irf6 was observed in primordial follicles and in

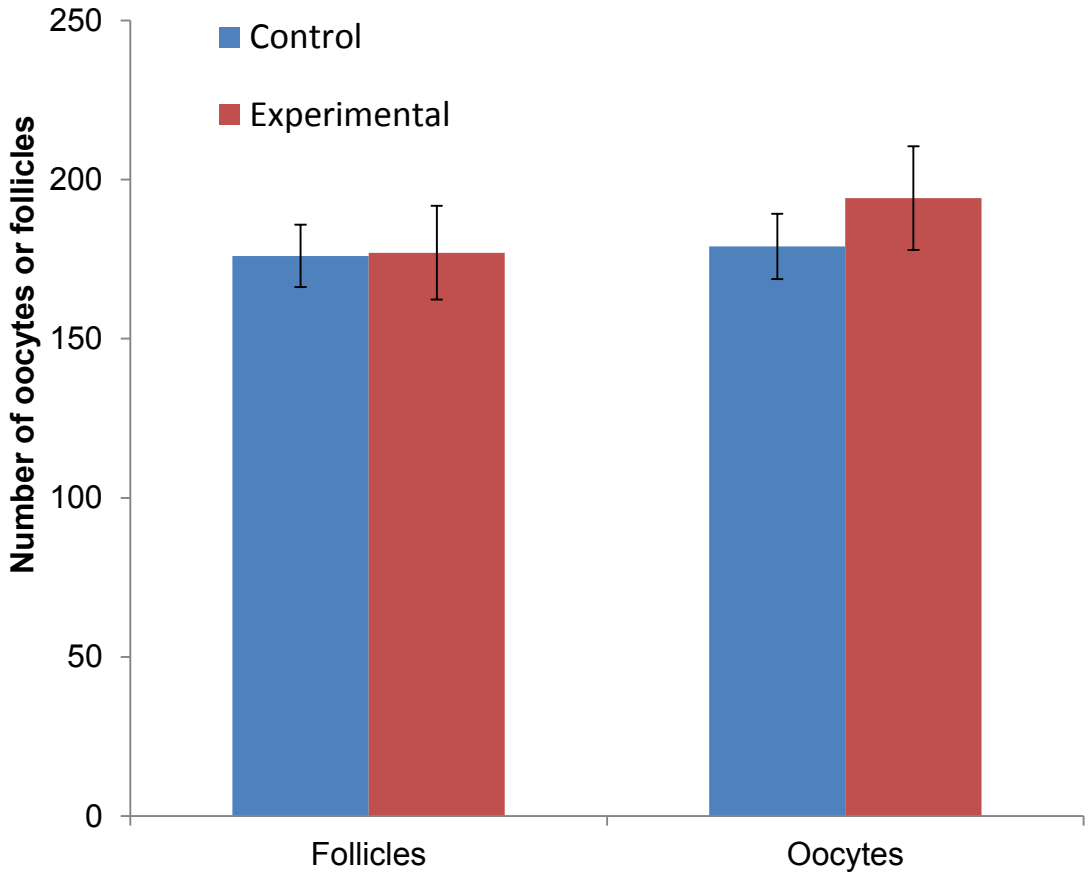

Figure 3.8: **MOFs do not account for increased fertilty**. Follicles were counted. Total follicle numbers include single and multiple oocyte follicles. The number of oocytes was extrapolated based on the number of oocytes in MOFs. Expermental females have more oocytes but this increase is not significant.

newly formed primary follicles. At this stage, Irf6 was also expressed in the granulosa cells surrounding oocytes (see Fig. 3.9B). This expression pattern was consistent with that observed in the adult ovary and suggests that Irf6 expression in the granulosa cells is developmentally regulated.

Numerous mouse models indicate that impaired germ cell nest breakdown concomitant with decreased oocyte loss (Xu and Gridley, 2013). There is a decrease in apoptosis in keratinocytes from *Irf6*-deficient mice (Ingraham *et al.*, 2006; Richardson *et al.*, 2006). Apoptosis plays a critical role in germ cell nest breakdown as 2/3 of the oocyte population die during this process (Pepling and Spradling, 2001). We hypothesized that *Irf6* regulates cell death during germ cell nest breakdown and follicle formation. To test this hypothesis, neonatal ovaries from control and experimental animals were stained for activated *Caspase 3*, a marker of cell death. There was no observable difference in caspase 3 expression at PND 6. Caspase 3 was expressed diffusely throughout the cytoplasm of oocytes. Interestingly, Caspase 3 expression was observed in all oocytes in both control and experimental females (see Fig. 3.9D,E). These results suggest that Irf6 does not regulate oocyte cell death via Caspase 3 during germ cell nest breakdown.

A second mechanism underlying the formation of MOFs is fusion of adjacent follicles. This mechanism was observed in females with oocyte specific deletion of T-syn, mediated by Zp3-Cre (Williams and Stanley, 2008). The Zp3-Cre transgene drives *Cre* expression starting at the primary follicle stage, following germ cell nest breakdown (de Vries *et al.*, 2000). We conducted extensive histological analysis of ovaries from experimental females. Fusion events between follicles in experimental females were

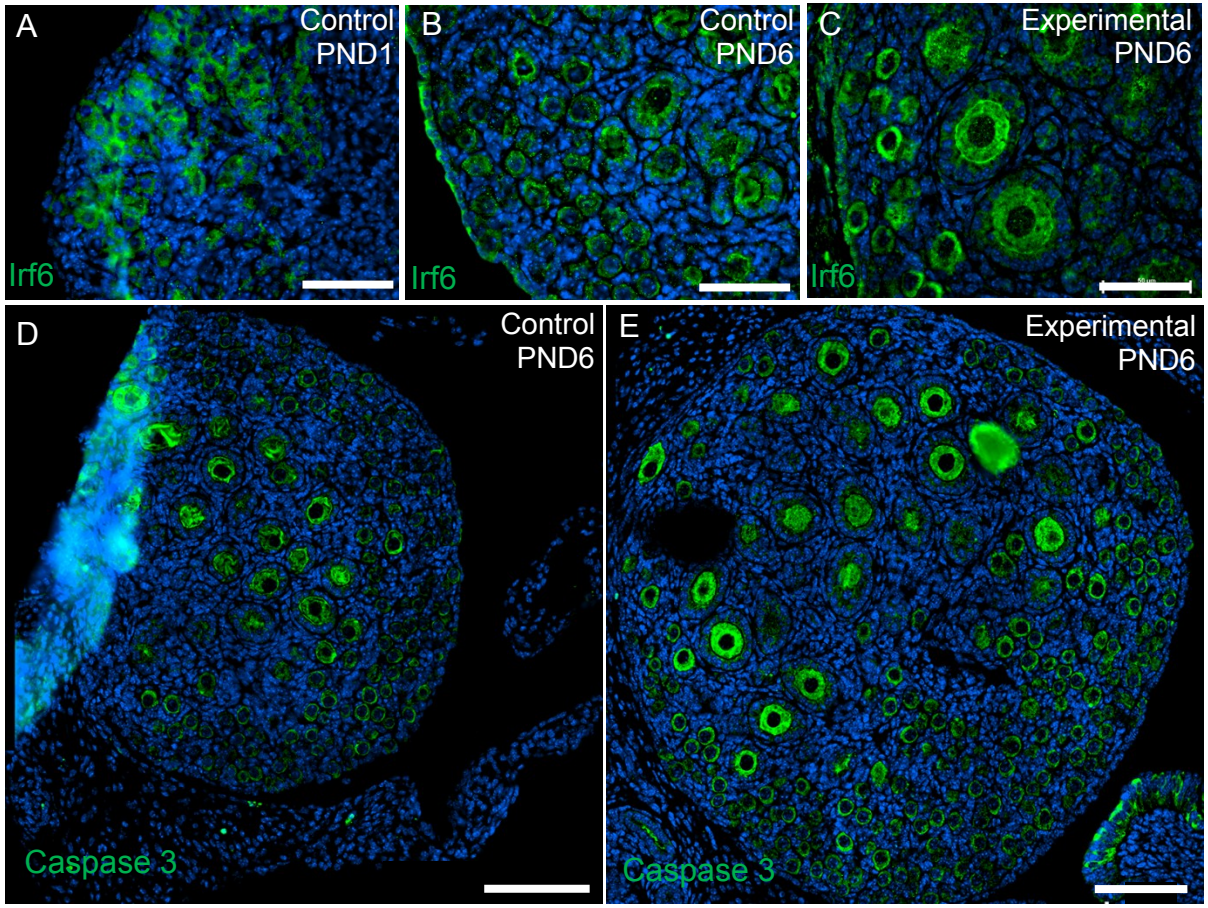

Figure 3.9: Irf6 is expressed during germ cell nest breakdown.

Figure 3.9 (cont'd)

A-C) Irf6 expression in neonatal ovaries. At PND1 (A), Irf6 is localized to germ cell nests. At PND 6 (B), Irf6 was expressed in newly formed primordial and primary follicles (white arrowheads). Interestingly, Irf6 expression was not lost in ovaries from experimental females at PND 6 (C). D-E) Caspase 3 appeared to be expressed in all follicles in control (D) and experimental (E) ovaries at PND6.

not observed. As a result, we conclude that follicle fusion is not the mechanism underlying MOF formation in ovaries from mice with oocyte specific deletion of Irf6.

Generation of Maternal and Zygotic Irf6 Knockout:

Our results suggest that maternally expressed Irf6 plays a role in oocyte development. However, embryos from experimental females developed normally, despite successful recombination of the $Irf6^{fl}$ allele. In zebrafish and frog embryos, injection of a dominant negative allele of *irf6* inhibits both maternal and zygotic irf6 protein, resulting in early embryonic lethality (Sabel *et al.*, 2009). Numerous maternal effect genes display more severe phenotypes when both the maternal gene products and the zygotic genes are deleted (Choi *et al.*, 2012; Kanzler *et al.*, 2003; Keramari *et al.*, 2010). This is due to the ability of the zygotic gene to compensate for loss of maternal gene products following zygotic genome activation. With this in mind, we sought to test the effect of loss of both maternal and zygotic *Irf6*. Experimental females were mated to $Irf6^{gt/+}$ males. All oocytes should be deficient for maternally deposited Irf6. In addition, one-half of all progeny would also be deficient for zygotic *Irf6.* Embryos were collected at E17.5 and genotyped. Genotypic analysis confirmed recombination as indicated by the absence of the $Irf6^{fl}$ allele and presence of the $Irf6^{nl}$ allele. Embryos were present in Mendelian proportions (see Table 3.3). Again, embryos with genotypes of $tg^{Gdf9\text{-}Cre/+;}$ $Irf6^{gt/nl}$ and $tg^{+/+;}$ $Irf6^{gt/nl}$ phenocopied $Irf6^{gt/gt}$ embryos, supporting the claim that recombination of the $Irf6^{fl}$ occurred prior to completion of meiosis in the oocyte. Moreover, we did not observe a more severe or additional phenotypes. These data indicate that recombination of *Irf6* during oogenesis does not result in early embryonic lethality, even when zygotic *Irf6* is also lost.

A	$Irf6^{gt/fl}; tg^{Gdf9\text{-}Cre/+}$ x $Irf6^{gt/+}; tg^{+/+}$	
Genotype	Expected	Actual
$Irf6^{gt/+}; tg^{Gdf9\text{-}Cre/+}$	5.25	6
$Irf6^{nl/+}; tg^{Gdf9\text{-}Cre/+}$	5.25	3
$*Irf6^{gt/gt}; tg^{Gdf9\text{-}Cre/+}$	5.25	6
$*Irf6^{gt/nl}; tg^{Gdf9\text{-}Cre/+}$	5.25	8
$Irf6^{gt/+}; tg^{+/+}$	5.25	8
$Irf6^{nl/+}; tg^{+/+}$	5.25	1
$*Irf6^{gt/gt}; tg^{+/+}$	5.25	4
$*Irf6^{gt/nl}; tg^{+/+}$	5.25	5
CNG	n/a	1
Total	41	41
P-value		0.33

B	$Irf6^{fl/fl}; tg^{Gdf9\text{-}Cre/+}$ x $Irf6^{gt/+}; tg^{+/+}$	
Genotype	Expected	Actual
$Irf6^{nl/+}; tg^{Gdf9\text{-}Cre/+}$	6	7
$*Irf6^{gt/nl}; tg^{Gdf9\text{-}Cre/+}$	6	6
$Irf6^{nl/+}; tg^{+/+}$	6	5
$*Irf6^{gt/nl}; tg^{+/+}$	6	4
CNG	n/a	2
Total	24	24
P-value		0.80

Table 3.3: Maternal and zygotic Irf6 knockout. $Irf6^{gt/+}; tg^{+/+}$ males were mated to $Irf6^{gt/fl}; tg^{Gdf9\text{-}Cre/+}$ *(A)* or $Irf6^{fl/fl}; tg^{Gdf9\text{-}Cre/+}$ (B). From these matings, all embryos were deficient for maternal Irf6. One-half were also deficient for zygotic Irf6. All genotypes were represented in proper Mendelian ratios. Genotypes producing the *Irf6* – null phenotype are indicated with asterisks*. (CNG – Could not genotype).

DISCUSSION:

Recent studies identified a role for *Irf6* in reproductive biology. Specifically, *Irf6* is expressed maternally in zebrafish, frog, and cow (Regassa *et al.*, 2011; Sabel *et al.*, 2009). Here we explored the expression and function of maternal Irf6 in the murine system. Irf6 was detected in murine oocytes at all developmental stages, indicating that maternal expression of Irf6 is also conserved in the mouse. Irf6 was also observed in the surrounding somatic granulosa cells. This is a novel finding as Irf6 was not detected in the granulosa cells of bovine follicles. Granulosa cells are epithelial in nature and function to support maturation and ovulation of the oocyte by the passage of metabolites and small molecules through gap junctions (Buccione *et al.*, 1990). As Irf6 is a critical regulator of differentiation in keratinocytes and other epithelial cell types (Bailey *et al.*, 2009; Ingraham *et al.*, 2006; Richardson *et al.*, 2009; Sabel *et al.*, 2009), it is possible that *Irf6* plays a cell autonomous role in granulosa cell proliferation and differentiation. An alternate hypothesis is that *Irf6* regulates expression of signaling molecules required for oogenesis in granulosa cells. This hypothesis would implicate a non-cell autonomous role for Irf6 in granulosa cells. A *non*-cell autonomous role for *Irf6* has been reported during tongue development (Goudy *et al.*, 2013). To determine the function of *Irf6* in granulosa cells, Cre drivers specific to the somatic cells of the ovary, such as *Amhr2-Cre* ((Xu and Gridley, 2013) or *Cyp19-Cre (Huang et al., 2013)*, should be used to generate a mouse model.

We generated mice with oocyte-specific deletion of *Irf6* to study the function of maternal Irf6 in early development. Genetic experiments confirmed recombination at the *Irf6* locus. In these experiments, $Irf6^{fl/+}$; $tg^{+/Gdf9\text{-}Cre/+}$ females were mated to $Irf6^{gt/+}$ males.

Progeny from these matings phenocopied *Irf6*$^{gt/gt}$ embryos. This was due to recombination of the *Irf6*^{fl} allele in the oocyte. This recombination event was highly efficient and was sufficient to produce a null allele (see Chapter 2). Furthermore, phenotypic and genotypic analysis of progeny from matings between *Irf6*$^{fl/+}$*; tg*$^{+/Gdf9\text{-}Cre/+}$ males and *Irf6*$^{gt/+}$ females indicate that no recombination occurred. These data are consistent with oocyte specific nature of the *Gdf9-Cre* transgene and support the claim that *Irf6* deletion occurred during oogenesis, prior to the completion of meiosis I. However, the exact timing of *Irf6* excision during oogenesis could not be determined.

Surprisingly, Irf6 mRNA and protein expression was observed in oocytes from both control and experimental females as assessed by qPCR, immunofluorescence and Western Blot analysis. A unique feature of the oocyte is storage of maternal mRNAs and proteins to aid in oocyte maturation and post-fertilization development. We observed Irf6 expression at postnatal day one in germ cell nests. This expression precedes *Gdf9-Cre* activation. While our genetic data indicated successful recombination of the *Irf6* conditional allele prior to the completion of meiosis I, the exact timing of this recombination event has yet to be determined. Transcriptional silencing occurs at the antral stages of follicle development. Meiosis I is completed just before ovulation (Pepling, 2013). Therefore, a possible explanation for the observed Irf6 in oocytes from experimental females is that *Irf6* mRNA and protein are stored early in oocyte development and perdure until late stages of development. The storage and persistence of Irf6 mRNA is consistent with observations in zebrafish where maternal irf6 protein is detectable even past activation of the zygotic genome (Sabel *et al.,* 2009).

It is also worth noting that the primers used for qPCR analysis of *Irf6* expression map to exons five and six. Recombination of the conditional allele of *Irf6* results in excision of only exons three and four. This excision is predicted to generate a frameshift and premature stop codon. However, it is possible that this transcript is stored in the oocyte and being detected via qPCR. To confirm the presence of stored full length and recombined Irf6 transcript, primers crossing the exon 2 – exon 5 junction should be tested.

The antibody used for immunofluorescent detection and Western blot analysis of Irf6 in oocytes was not previously validated. To do so, we used skin from E17.5 embryos as a positive control to test the specificity of the antibody used. Irf6 expression and function in skin is well characterized. In wildtype skin, the immunofluorescent signal observed was comparable to that observed by *Ingraham et al* (2006). However, this signal was not lost in the epidermis of $Irf6^{gt/gt}$. These data suggest non-specific binding of this antibody in the absence of Irf6. While it is possible that the staining observed in oocytes from experimental animals represents non-specific binding of the Irf6- Akira, further optimization of experimental conditions are required to properly validate this antibody.

Females with oocyte-specific excision of *Irf6* showed a significant increase in fertility. This increase in fertility was not in tandem with an increase in follicle number in experimental females. However, females with oocyte specific excision of *Irf6* did ovulate at a higher rate. There are few examples of mouse models with increased fertility. Mice over-expressing *Bcl-2*, an anti-apoptosis gene, display increased litter size as a result of decreased oocyte apoptosis (Hsu *et al.*, 1996). We observed

comparable numbers of follicles at all developmental stages in both control and experimental females, suggesting normal apoptosis. Mice with granulosa cell specific deletion of *Tuberous sclerosis complex 1 (Tsc1*) also show increased ovulation and larger litter size. These results are hypothesized to be due to increased activity of mTORC1 (Huang *et al.*, 2013). The activity of mTORC1 in females with oocyte-specific deletion of *Irf6* has not been investigated. Notably, the process of ovulation is reliant on a series of endocrine signals, as well as oocyte specific factors. It is possible that loss of Irf6 in the oocyte increases sensitivity to the endocrine and molecular signals promoting ovulation.

An alternative hypothesis is that *Irf6* regulates cell death in oocytes. This hypothesis is supported by the decrease in apoptosis observed in skin from *Irf6*$^{gt/gt}$ embryos (Ingraham *et al.*, 2006; Richardson *et al.*, 2006). Moreover, mice over-expressing *Bcl-2*, an anti-apoptosis gene, in the somatic cells of the ovary display increased litter size as a result of decreased apoptosis of granulosa cells. These mice also develop benign cystic ovarian teratomas (Hsu *et al.*, 1996), a feature we did not observe in our population. Each cycle, a pool of oocytes enters into maturation. However, a large proportion of these oocytes undergo programmed cell death (Mehlmann, 2005). If loss of *Irf6* resulted in decreased apoptosis, an increase in late stage follicles would be apparent. We did not observe an increase in the number of antral or pre-antral follicles in experimental females. This data suggests that decreased apoptosis does not account for the increase in fertility.

In addition to an increase in fertility, MOFs were also observed in the experimental females. Most reports of MOFs are associated with reduced fertility or

infertility (Hahn *et al.*, 2005; Xu and Gridley, 2013; Yan *et al.*, 2001). In humans, MOFs are observed and can be fertilized however, the ability of oocytes from MOFs to produce live births has not been determined (Dandekar *et al.*, 1988). Multiple oocyte follicles in females with oocyte specific excision of *Irf6* did increase the total number of oocytes. But, this increase was not significant when compared to control females. From these data, we concluded that the observed increase in fertility is independent of an increase in MOFs.

We observed that Irf6 was expressed in germ cell nests of the neonatal ovary. *Gdf9-Cre* expression was not observed at PND1 but was observed at PND3 (Lan *et al.*, 2004). Moreover, germ cell nest breakdown persists until approximately PND6. *Gdf9* and *Bmp-15,* another oocyte-specific factor, are critical for proper germ cell nest breakdown and primordial follicle formation. Mice with mutations in both genes display multiple oocyte follicles (Yan *et al.*, 2001). Both *Gdf9* and *Bmp-15* are members of the *Tgfβ* family. In medial edge epithelium of the palatal shelves*, Irf6* expression is regulated by *Tgfβ3* (Iwata *et al.*, 2013). The Notch signaling pathway is also critical for germ cell nest breakdown as mice deficient for *Lunatic Fringe*, a regulator of Notch signaling, also result in the formation of MOFs (Hahn *et al.*, 2005). Notch signaling induces *Irf6* expression during keratinocyte differentiation (Restivo *et al.*, 2011). It is possible that *Tgfβ* signaling and Notch signaling pathways act on *Irf6* to direct proper germ cell nest breakdown and primordial follicle formation.

There have been reports of only two mouse models displaying both increased fertility and the presence of MOFs. Females with oocyte-specific deletion of *t-syn,* an enzyme that catalyzes the transfer of core 1-derived O-glycans, display a sustained

increase in fertility similar to that observed in females with oocyte specific excision of *Irf6*. This increase was attributed to a delay in folliculogenesis resulting in an accumulation of follicles (Williams and Stanley, 2008). This was not apparent in females with oocyte specific excision of *Irf6* as the number of follicles was comparable between control and experimental animals. In addition, females with oocyte-specific deletion of *t-syn* display an increase in the number of MOFs. In this mouse model, the Zp3-Cre transgenic line was used to facilitate recombination of the *t-syn* gene. Zp3-Cre drives Cre expression at the primary follicle stage, following primordial follicle formation. The MOFs observed in this model are due to fusion events between adjacent follicles (Williams and Stanley, 2008). There was no evidence of follicle fusion in ovaries from females with oocyte specific excision of *Irf6*, further supporting a role for *Irf6* in germ cell nest breakdown and primordial follicle formation.

Within the ovary, Aqp 8 is expressed specifically in the granulosa cells. Mice with deletion of *Aquaporin 8 (Aqp 8$^{-/-}$)* also have increased ovulation naturally and in response to exogenous hormone treatment. It is unknown whether the increase in ovulation is persistent with maternal age as observed in females with oocyte specific excision of *Irf6.* However, the increase in ovulation was attributed to a reduction in apoptosis of granulosa cells resulting in an increase in the number of mature follicles *(Su et al., 2010)*. These mice also displayed an increased numbers of MOFs, likely due to defects in primordial follicle formation (Su *et al.*, 2013). Interestingly, the number of MOFs in this model decreases with age. *Aqp-8* reduces the water permeability of granulosa cells (Su *et al.*, 2010). Reduction of water permeability as a result of deletion of other aquaporin family members can lead to decreased apoptosis and impaired cell

migration (Hara-Chikuma and Verkman, 2008). Reduced apoptosis and impaired cell migration is observed in keratinocytes from *Irf6*-deficient murine embryos (Biggs *et al.*, 2014; Ingraham *et al.*, 2006).

Embryos generated from oocytes where Irf6 was excised were viable. This is in contrast to the early embryonic lethality observed in zebrafish and frog. Occasionally, the effect of maternally expressed genes is masked by activation of the zygotic gene. Embryos generated from oocytes with excision of *Irf6* and deficient for zygotic *Irf6* did not show early embryonic lethality or a more severe phenotype than embryos deficient for only zygotic *Irf6*. However, it is possible that the stores of protein observed in oocytes from experimental females are activated following fertilization, thus still providing normal gene function during early embryonic development. To address this, different conditional knockout strategies must be employed. One strategy is the use of the *VASA*-Cre transgenic mouse line. *VASA-Cre* drives *Cre* expression in germ cells beginning at E15.5 (Gallardo *et al.*, 2007).

In summary, we have defined expression and identified function of Irf6 in the oocyte. Our data suggests that Irf6 regulates female fertility and follicle development. Oocyte specific excision of Irf6 resulted in increased fertility, as measured by increased litter size and ovulation, and generation of MOFs. These two phenotypes appeared to be independent of one another as MOFs did not appear to contribute to the increase in ovulation. Thus, we have uncovered a novel role for Irf6 in female fertility. The mechanism underlying these phenotypes remains to be elucidated.

APPENDIX

APPENDIX

Supplementary Figures

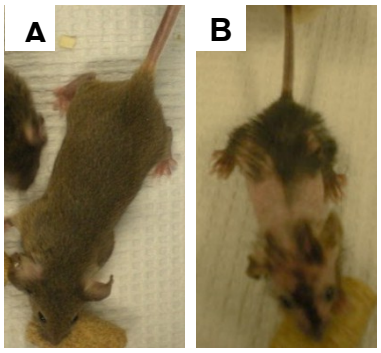

Figure A.1: **Repeated epilation phenotype.** Approximately 20% of progeny from matings to generate females with oocyte specific deletion of *Irf6* display a repeated hair loss phenotype (B). (A) = unaffected sibling.

Genotype	Observed	# "Er-Like"
$Irf6^{gt/fl}$; $tg^{Gdf9\text{-}Cre/+}$	7	2
$Irf6^{fl/fl}$; $tg^{Gdf9\text{-}Cre/+}$	2	2
$Irf6^{gt/+}$; $tg^{Gdf9\text{-}Cre/+}$	3	
$Irf6^{fl/+}$; $tg^{Gdf9\text{-}Cre/+}$	5	
$Irf6^{gt/fl}$; $tg^{+/+}$	6	1
$Irf6^{fl/fl}$; $tg^{+/+}$	1	
$Irf6^{gt/+}$; $tg^{+/+}$	3	1
$Irf6^{fl/+}$; $tg^{+/+}$	12	
CNG	2	2
TOTAL	41	8

Table A.1: **Repeated epilation phenotype.** Approximately 20% of progeny from F1 matings display a repeated epilation phenotype. This phenotype was not sex – specific or dependent of the Gdf9-cre transgene. All affected animals had two non-wildtype alleles of *Irf6*.

REFERENCES

REFERENCES

Bailey CM, Margaryan NV, Abbott DE, Schutte BC, Yang B, Khalkhali-Ellis Z, Hendrix MJ. 2009. Temporal and spatial expression patterns for the tumor suppressor Maspin and its binding partner interferon regulatory factor 6 during breast development. Dev Growth Differ 51: 473-481.

Ben J, Jabs EW, Chong SS. 2005. Genomic, cDNA and embryonic expression analysis of zebrafish IRF6, the gene mutated in the human oral clefting disorders Van der Woude and popliteal pterygium syndromes. Gene Expr Patterns 5: 629-638.

Biggs LC, Naridze RL, DeMali KA, Lusche DF, Kuhl S, Soll DR, Schutte BC, Dunnwald M. 2014. Interferon regulatory factor 6 regulates keratinocyte migration. J Cell Sci 127: 2840-2848.

Buccione R, Schroeder AC, Eppig JJ. 1990. Interactions between somatic cells and germ cells throughout mammalian oogenesis. Biol Reprod 43: 543-547.

Center For Disease Control and Prevention, American Society for Reproductive Medicine, Society for Assisted Reproductive Technology. 2013. 2011 Assisted Reproductive Technology Fertility Clinic Success Rates Report. In. Atlanta, GA.

Chen Y, Jefferson WN, Newbold RR, Padilla-Banks E, Pepling ME. 2007. Estradiol, progesterone, and genistein inhibit oocyte nest breakdown and primordial follicle assembly in the neonatal mouse ovary in vitro and in vivo. Endocrinology 148: 3580-3590.

Choi I, Carey TS, Wilson CA, Knott JG. 2012. Transcription factor AP-2gamma is a core regulator of tight junction biogenesis and cavity formation during mouse early embryogenesis. Development.

Dandekar PV, Martin MC, Glass RH. 1988. Polyovular follicles associated with human in vitro fertilization. Fertil Steril 49: 483-486.

de Vries WN, Binns LT, Fancher KS, Dean J, Moore R, Kemler R, Knowles BB. 2000. Expression of Cre recombinase in mouse oocytes: a means to study maternal effect genes. Genesis 26: 110-112.

Fekete E. 1950. Polyovular follicles in the C58 strain of mice. Anat Rec 108: 699-707.

Gallardo T, Shirley L, John GB, Castrillon DH. 2007. Generation of a germ cell-specific mouse transgenic Cre line, Vasa-Cre. Genesis 45: 413-417.

Goudy S, Angel P, Jacobs B, Hill C, Mainini V, Smith AL, Kousa YA, Caprioli R, Prince LS, Baldwin S, Schutte BC. 2013. Cell-autonomous and non-cell-autonomous roles for IRF6 during development of the tongue. PLoS One 8: e56270.

Hahn KL, Johnson J, Beres BJ, Howard S, Wilson-Rawls J. 2005. Lunatic fringe null female mice are infertile due to defects in meiotic maturation. Development 132: 817-828.

Hara-Chikuma M, Verkman AS. 2008. Roles of aquaporin-3 in the epidermis. J Invest Dermatol 128: 2145-2151.

Hsu SY, Lai RJ, Finegold M, Hsueh AJ. 1996. Targeted overexpression of Bcl-2 in ovaries of transgenic mice leads to decreased follicle apoptosis, enhanced folliculogenesis, and increased germ cell tumorigenesis. Endocrinology 137: 4837-4843.

Huang L, Wang ZB, Jiang ZZ, Hu MW, Lin F, Zhang QH, Luo YB, Hou Y, Zhao Y, Fan HY, Schatten H, Sun QY. 2013. Specific disruption of Tsc1 in ovarian granulosa cells promotes ovulation and causes progressive accumulation of corpora lutea. PLoS One 8: e54052.

Hunt PA, Lawson C, Gieske M, Murdoch B, Smith H, Marre A, Hassold T, VandeVoort CA. 2012. Bisphenol A alters early oogenesis and follicle formation in the fetal ovary of the rhesus monkey. Proc Natl Acad Sci U S A 109: 17525-17530.

Ingraham CR, Kinoshita A, Kondo S, Yang B, Sajan S, Trout KJ, Malik MI, Dunnwald M, Goudy SL, Lovett M, Murray JC, Schutte BC. 2006. Abnormal skin, limb and craniofacial morphogenesis in mice deficient for interferon regulatory factor 6 (Irf6). Nat Genet 38: 1335-1340.

Iwata J, Suzuki A, Pelikan RC, Ho TV, Sanchez-Lara PA, Urata M, Dixon MJ, Chai Y. 2013. Smad4-Irf6 genetic interaction and TGFbeta-mediated IRF6 signaling cascade are crucial for palatal fusion in mice. Development 140: 1220-1230.

Jefferson W, Newbold R, Padilla-Banks E, Pepling M. 2006. Neonatal genistein treatment alters ovarian differentiation in the mouse: inhibition of oocyte nest breakdown and increased oocyte survival. Biol Reprod 74: 161-168.

Kanzler B, Haas-Assenbaum A, Haas I, Morawiec L, Huber E, Boehm T. 2003. Morpholino oligonucleotide-triggered knockdown reveals a role for maternal E-cadherin during early mouse development. Mech Dev 120: 1423-1432.

Keramari M, Razavi J, Ingman KA, Patsch C, Edenhofer F, Ward CM, Kimber SJ. 2010. Sox2 is essential for formation of trophectoderm in the preimplantation embryo. PLoS One 5: e13952.

Kerr JB, Duckett R, Myers M, Britt KL, Mladenovska T, Findlay JK. 2006. Quantification of healthy follicles in the neonatal and adult mouse ovary: evidence for maintenance of primordial follicle supply. Reproduction 132: 95-109.

Lan ZJ, Xu X, Cooney AJ. 2004. Differential oocyte-specific expression of Cre recombinase activity in GDF-9-iCre, Zp3cre, and Msx2Cre transgenic mice. Biol Reprod 71: 1469-1474.

Li L, Zheng P, Dean J. 2010. Maternal control of early mouse development. Development 137: 859-870.

Mehlmann LM. 2005. Stops and starts in mammalian oocytes: recent advances in understanding the regulation of meiotic arrest and oocyte maturation. Reproduction 130: 791-799.

Navot D, Bergh PA, Williams MA, Garrisi GJ, Guzman I, Sandler B, Grunfeld L. 1991. Poor oocyte quality rather than implantation failure as a cause of age-related decline in female fertility. Lancet 337: 1375-1377.

Pepling M. 2013. Oocyte Development before and during Folliculogenesis. In: Oocyte Physiology and Development in Domestic Animals: Wiley-Blackwell. p 1-19.

Pepling ME, Spradling AC. 1998. Female mouse germ cells form synchronously dividing cysts. Development 125: 3323-3328.

Pepling ME, Spradling AC. 2001. Mouse ovarian germ cell cysts undergo programmed breakdown to form primordial follicles. Dev Biol 234: 339-351.

Peters H. 1969. The development of the mouse ovary from birth to maturity. Acta Endocrinol (Copenh) 62: 98-116.

Regassa A, Rings F, Hoelker M, Cinar U, Tholen E, Looft C, Schellander K, Tesfaye D. 2011. Transcriptome dynamics and molecular cross-talk between bovine oocyte and its companion cumulus cells. BMC Genomics 12: 57.

Restivo G, Nguyen BC, Dziunycz P, Ristorcelli E, Ryan RJ, Ozuysal OY, Di Piazza M, Radtke F, Dixon MJ, Hofbauer GF, Lefort K, Dotto GP. 2011. IRF6 is a mediator of Notch pro-differentiation and tumour suppressive function in keratinocytes. EMBO J 30: 4571-4585.

Richardson RJ, Dixon J, Jiang R, Dixon MJ. 2009. Integration of IRF6 and Jagged2 signalling is essential for controlling palatal adhesion and fusion competence. Hum Mol Genet 18: 2632-2642.

Richardson RJ, Dixon J, Malhotra S, Hardman MJ, Knowles L, Boot-Handford RP, Shore P, Whitmarsh A, Dixon MJ. 2006. Irf6 is a key determinant of the keratinocyte proliferation-differentiation switch. Nat Genet 38: 1329-1334.

Sabel JL, d'Alencon C, O'Brien EK, Van Otterloo E, Lutz K, Cuykendall TN, Schutte BC, Houston DW, Cornell RA. 2009. Maternal Interferon Regulatory Factor 6 is

required for the differentiation of primary superficial epithelia in Danio and Xenopus embryos. Dev Biol 325: 249-262.

Su W, Guan X, Zhang D, Sun M, Yang L, Yi F, Hao F, Feng X, Ma T. 2013. Occurrence of multi-oocyte follicles in aquaporin 8-deficient mice. Reprod Biol Endocrinol 11: 88.

Su W, Qiao Y, Yi F, Guan X, Zhang D, Zhang S, Hao F, Xiao Y, Zhang H, Guo L, Yang L, Feng X, Ma T. 2010. Increased female fertility in aquaporin 8-deficient mice. IUBMB Life 62: 852-857.

Williams SA, Stanley P. 2008. Mouse fertility is enhanced by oocyte-specific loss of core 1-derived O-glycans. FASEB J 22: 2273-2284.

Xu J, Gridley T. 2013. Notch2 is required in somatic cells for breakdown of ovarian germ-cell nests and formation of primordial follicles. BMC Biol 11: 13.

Yan C, Wang P, DeMayo J, DeMayo FJ, Elvin JA, Carino C, Prasad SV, Skinner SS, Dunbar BS, Dube JL, Celeste AJ, Matzuk MM. 2001. Synergistic roles of bone morphogenetic protein 15 and growth differentiation factor 9 in ovarian function. Mol Endocrinol 15: 854-866.

CHAPTER FOUR

Irf6 is expressed in the murine placenta but dispensible

ABSTRACT

Interferon Regulatory Factor 6 is a member of the IRF family of transcription factors. It is highly expressed in murine skin where it acts as a critical regulator of keratinocyte differentiation and proliferation. Mice homozygous for a null mutation of Irf6 die shortly after birth due to severe skin, limb, and craniofacial abnormalities. In addition to its expression in skin, Irf6 is highly expressed in numerous epithelial cell types across species. One such tissue is the enveloping layer (EVL) of zebrafish embryos. Inhibition of irf6 in the (EVL) results in early embryonic lethality. The EVL in zebrafish can be likened to the trophectoderm in mammals, as they are both simple monolayer epitheliums that encompass the embryo during early development. In mammals, the trophectoderm gives rise to the trophoblast cell types that compose the murine placenta. Irf6 mRNA was detected in the mouse placenta and in the trophectoderm of ovine embryos. The aim of this research was to determine the role of Irf6 in placental development. To do so, we assessed the spatiotemporal expression of Irf6 in the placenta and utilized a mouse knockout model to conduct morphometric and molecular analyses. Irf6 was detected in the murine placenta during mid-gestation but not in late gestation. However, loss of Irf6 did not affect placental morphology. In conclusion, although Irf6 is expressed in trophectoderm and placenta in mouse, we did not detect an essential role for Irf6 in placental development.

INTRODUCTION

The placenta is a transient developmental organ that is essential to the survival of the mammalian embryo. It serves as the main site of nutrient and gas exchange between the developing fetus and the mother. In addition, the placenta serves as an endrocrine factory, producing a number of hormones required for the maintenance of pregnancy (Rossant and Cross, 2001). Defects in placental development underlie some of the most common pregnancy complications observed in humans. These include pre-eclampsia, intra-uterine growth restriction, and preterm birth (Faye-Petersen, 2008; Ness and Sibai, 2006; Sibai *et al.*, 2005). The prevalence of such complications, specifically pre-eclampsia and preterm birth, are increasing in the U.S, requiring greater efforts to understand pathogenesis and develop interventions (Ananth *et al.*, 2013; Muglia and Katz, 2010). There are a number of similarities between mouse and human placental development, structure, and function, allowing for the use of the mouse as a model system to study placental pathologies.

Development of the mammalian placenta begins with formation of the trophectoderm at the blastocyst stage. The blastocyst is composed of two cell populations, the inner cell mass (ICM) and the trophectoderm (TE). The ICM gives rise to the three germ layers that form the embryo. The TE is a simple monolayer epithelium that encompasses the underlying ICM (Kunath *et al.*, 2004). In the mouse, TE cells that are not in direct contact with the ICM, differentiate to form primary trophoblast giant cells (TGCs). Primary TGCs invade into the overlying uterine tissue, facilitating embryo implantation (Zybina *et al.*, 2000). Polar TE cells, those in direct contact with the ICM, proliferate to give rise to the extra-embryonic ectoderm and the ectoplacental cone

(EPC). The trophoblast cell types that populate the murine placenta arise from these two lineages (Chavez *et al.*, 1984).

The fully formed mouse placenta is composed of three distinct zones. The first zone is a monolayer of secondary trophoblast glycogen cells, lying in direct contact with the maternal uterine tissue, the decidua (Georgiades *et al.*, 2002). These cells arise from endoreplication of EPC precursors and serve as sites of hormone production (Linzer and Fisher, 1999; Malassine *et al.*, 2003). The second layer, the junctional zone (JZ), is composed of spongiotrophoblast and trophoblast glycogen cells. The JZ provides structural support and endocrine function for the placenta (Malassine *et al.*, 2003). The final zone of the mouse placenta is the labyrinth zone (LZ). The LZ is composed of syncytiotrophoblast and cytotrophoblast which line fetal chorionic villi. These villi are bathed in maternal blood and are the site of feto-maternal exchange of nutrients and gases (Cross, 2006).

Within the junctional zone, there are two trophoblast populations, spongiotrophoblast and trophoblast glycogen cells. Spongiotrophoblast cells express a number of pregnancy specific hormones (Malassine *et al.*, 2003). The role of trophoblast glycogen cells is less well defined. Glycogen cells become apparent at approximately embryonic day 12.5 (E12.5) within the JZ (Coan *et al.*, 2006; Tesser *et al.*, 2010). They are highly vacuolated, glycogen-filled cells, features that make them detectable by routine histology. As development progresses, trophoblast glycogen cells migrate from the JZ into the overlying maternal decidua (Coan *et al.*, 2006).

Interferon Regulatory Factor 6 (IRF6) is a member of the Interferon Regulatory Factor family of transcription factors (Ingraham *et al.*, 2006; Richardson *et al.*, 2006).

Mice homozygous for a null allele of *Irf6* (*Irf6*$^{gt/gt}$) display severe skin, limb, and craniofacial abnormalities (Ingraham *et al.*, 2006). These animals die shortly after birth. Skin from *Irf6*$^{gt/gt}$ show an expanded epidermis that is due to an increase in proliferation and failure of differentiation of keratinocytes (Ingraham *et al.*, 2006). In addition to its role in skin, Irf6 has been implicated in development of other epithelial cell types. It is expressed in mammary epithelium during mammary gland development (Bailey *et al.*, 2009). Irf6 is also expressed in the periderm, an embryonic squamous epithelium (de la Garza *et al.*, 2013; Richardson *et al.*, 2009). In Irf6-deficient embryos, the periderm is lost leading to severe epithelial adhesions in the oral cavity (Ingraham *et al.*, 2006; Richardson *et al.*, 2006). These data indicate a conserved role for Irf6 in regulating the proliferation and differentiation of epithelial cell types.

In zebrafish and frog (*Xenopus laevis*), *irf6* is expressed in the superficial epithelium (Ben *et al.*, 2005; Sabel *et al.*, 2009). In the zebrafish, this superficial epithelium is known as the enveloping layer (EVL). Inhibition of *irf6* results in early embryonic lethality due to failure of proper EVL differentiation (Sabel *et al.*, 2009). The EVL can be likened to the trophectoderm in mammals. Both the EVL and TE are the first epithelial layers to develop. They are both simple monolayer epitheliums that encompass the developing embryo (Fan *et al.*, 2007). Fleming et al (2009) showed that Irf6 is expressed in the trophectoderm of sheep embryos. In addition, Irf6 acts as a transcriptional activator in trophectoderm cell lines (Fleming *et al.*, 2009).

Irf6 has an evolutionarily conserved role in epithelial proliferation and differentiation. The trophoblast lineage is epithelial in nature and composes the murine placenta. The purpose of this study was to assess the role of Irf6 in placental

development using a mouse model. To do this, we employed an Irf6- knockout mouse to study gene function.

MATERIALS AND METHODS

Mouse Breeding and Genotyping

To generate *Irf6*-deficient embryos (*Irf6*$^{gt/gt}$), animals heterozygous for a null allele of Irf6 (*Irf6*$^{gt/+}$) were crossed. *Irf6*$^{gt/+}$ animals were placed into timed matings on the evening of estrus. Mice were separated the following morning and the presence of a copulation plug was denoted as embryonic day 0.5 (E0.5). Embryos were collected on E14.5 and E17.5. Tails snips from live mice and embryos were collected and used for PCR-based genotyping. All animals were used in accordance with the National Institutes of Health Guide for the Care and use of laboratory animals, and all protocols were approved by the MSU IACUC.

Upon collection, tail snips were incubated in lysis buffer (10 mM Tris-HCl, 150 mM NaCl, 10 mM EDTA, 0.1% SDS, supplemented with 100 mg of proteinase K) overnight at 55°C. DNA was extracted by ethanol purification. PCR was conducted using the REDTaq ReadyMix PCR reaction mix (Sigma-Aldrich, St. Louis, MO). For detection of the wildtype allele, primers set of 5'-*GAGAGGCTAGGGTGGAAGGGATTC-3' (oBS145)* and 5'-*GACCAGACCGTGCAGGGGCTGTG-3' (oBS146)* was used. For detection of the *Irf6*^{gt} allele, primer set *of 5'-AAATGGCGTTACTTAAGCTAGCTTG-3*' (oBS144) and oBS145 was used. PCR conditions were as follows: 1) 95°C for three minutes, 2) 95°C for 38 seconds, 3) 60°C for 50 seconds, 4) 72°C for 15 seconds, 5) repeat steps 2-4 40 times, 6) 72°C for five minutes. PCR products were separated and visualized by gel electrophoresis on 1.5% agarose gels.

Tissue Collection and Processing

To obtain blastocysts, *Irf6*$^{+/+}$ females were superovulated by intra-peritoneal injection of 5 International Units (IU) of Pregnant Mare Serum Gonadotropin (PMSG – Sigma-Aldrich, St. Louis, MO) on Day 0. An intra-peritonal injection of Human Chorionic Gonadotropin (HCG – Sigma-Aldrich, St. Louis, MO) at a concentration of 5IU was given approximately 48 hours later. Superovulated females were placed with proven males and euthanized 21-24 hours post HCG injection. One-cell embryos were recovered from the oviduct and incubated with M2 media supplemented with hyaluronidase (300µg/ml – Sigma-Aldrich, St. Louis, MO) to remove granulosa cells. Embryos were rinsed in M2 media, plated in microdrop cultures with KSOM media and cultured *in vitro*. Three days following plating, blastocysts were collected and fixed in 10% neutral buffered formalin for 20 minutes at room temperature. Blastocysts were subjected to immunofluorescent staining as described below.

To collect placentas, embryos were harvested at E14.5 and E17.5. At either time point, females were euthanized via isoflurane induced comatosis followed by cervical dislocation. The abdominal cavity was exposed and all embryos were extracted. At the time of harvest, wet weight of each embryo and the corresponding placenta were taken. The placentas were then fixed in 10% neutral buffered formalin (VWR, Radnor, PA) overnight. Following fixation, tissues were stored in a 50% ethanol solution until further processing. Tissues were processed and embedded in paraffin using standard protocols by the Histopathology Laboratory at Michigan State University. Embedded whole placentas were sagittally sectioned at 7µm.

Immunofluorescence

For placenta, a polyclonal rabbit anti-Irf6 was used for detection of Irf6 (Ingraham *et al.*, 2006). Mid-sagittal sections were selected. To deparaffinize and rehydrate sections, slides were passed through three changes of Xylene, followed reducing concentrations of ethanol. Antigen retrieval was conducted by boiling in 10mM Sodium Citrate pH6.0 for ten-twenty minutes. Sections were permeabilized in 0.5% Triton X-100 and blocked for one hour in blocking solution (10% normal goat serum, 0.1% Bovine Serum Albumin in 1X Phosphate Buffered Saline (PBS)) at room temperature. Sections were then incubated in primary antibody diluted in blocking solution; rabbit anti-Irf6 antibody (1:100) overnight at 4°C. Following incubation, slides were washed three times in 1X PBS and incubated in secondary antibody (goat anti-rabbit Alexa Fluor 488-Life Technologies) for one hour at room temperature. To detect nuclei, slides were incubated in DAPI (1:10,000 in distilled water) for 10 minutes. Slides were imaged using the Nikon i90 upright fluorescent microscope.

For blastocyst, a polyclonal rabbit anti-Irf6 (Sigma-Aldrich, St. Louis, MO.) antibody was used at a concentration of 1:100. Formalin fixed blastocysts were washed in 1X PBS and permeabilized in 0.05% Triton X-100 for thirty minutes. Embryos were then blocked with blocking solution (0.01% Bovine Serum Albumin, 0.0001% Tween-20 in 1X PBS) for one hour at room temperature followed incubation in primary antibody overnight at 4°C. In addition to Irf6, blastocysts were dual stained for mouse anti-Cdx2 (kind gift from Dr. Jason Knott) at a 1:2 dilution. Blastocysts were then washed and incubated in secondary antibody at a concentration of 1:100 (goat anti-rabbit Alexa Fluor 555 and goat anti-mouse Alexa Fluor 488; Life Technologies, Carlsbad, CA)

Histology and Morphometrics

To assess differences in placental composition between *Irf6*$^{+/+}$ and *Irf6*$^{gt/gt}$ placenta, mid-sagittal placental sections were selected. Mid-sagittal was identified by total area, with the largest area representing the central most region of the placenta. In addition, the central maternal artery, an artery that inserts central into the placenta, was used as a mid-sagittal landmark. Once the mid-sagittal section was identified, two additional sections 70μm before and after were selected for measurements.

Slides were stained with Hematoxylin and Eosin (H&E). Briefly, slides were dehydrated in three changes of Xylene followed by reducing concentrations of ethanol. Slides were incubated in hematoxylin (Gill's No. III Hematoxylin, Sigma-Aldrich, St. Louis, MO) for 1.5 minutes, rinsed quickly in tap water, and incubate in 1% Eosin (Eosin Y, VWR) for 1.5 minutes. For dehydration, slides were passed through increasing grades of ethanol, then Xylene. Slides were mounted in Permount mounting medium (VWR).

For morphometric analysis, H&E-stained placental sections were stitched at 10X magnification using the Nikon i90 upright microscope. Prior to analysis, the review was blinded to the genotype of all tissues. Whole area, junctional zone and labyrinth zone measurements were taken using the NIS elements software. For data analysis, zone measurements across all three sections were averaged. A student's T-test was used to analyze differences.

Histological Analysis of Glycogen clusters

To assess localization of TGCs, three mid-sagittal sections per placenta, each 70μm apart, were selected and stained with Periodic Acid Schiff (PAS; Sigma Aldrich, St. Louis, MO). PAS was used to detect glycogen in fixed tissues. Briefly, sections were

deparaffinized and dehydrated as described above. Slides were incubated in 1% Periodic Acid for five minutes at room temperature. Slides were washed briefly followed by incubation in Schiff's reagent for 15 minutes at room temperature. Nuclei were stained using Gill's No. III Hematoxylin for 1.5 minutes. Slides were washed in tap water, dehydrated by passing through increasing grades of ethanol followed by xylene, and mounted with Permount mounting medium.

As a negative control, serial sections were incubated in 0.5% α-amylase for 20 minutes at room temperature before PAS staining. Images of whole sections were stitched at 10X. Prior to analysis, the review was blinded to the genotype of all tissues. Positively stained trophoblast glycogen clusters in the labyrinth zone were counted on the microscope using 40X magnification. Trophoblast glycogen cluster count was averaged across the three sections. A student's T-test was used to assess differences between *Irf6*$^{+/+}$ and *Irf6*$^{gt/gt}$ placenta.

Quantification of Total Glycogen Content

Quantification of glycogen content in placenta was conducted based on methods used by Rampon, et al (2008). To precipitate glycogen, whole placenta were collected and weighed. Whole placentas were digested in a 30% Potassium Hydroxide solution saturated with sodium sulfate. Samples were boiled at 100°C for 20-30 minutes until tissue was completely digested. Samples were vortexed then cooled on ice. One volume of 95% ethanol was added to precipitate glycogen. Samples were cooled on ice and centrifuged for 30 minutes at 840 x g. Pellets were dried and resuspended in 1ml of distilled water. Standards were made using glycogen diluted to 0, 25, 50 and 75µg/ml. To quantify glycogen, one mL of 5% phenol was added to each sample.

Sulfuric acid was added rapidly and directly to the surface of each sample. Samples were then incubated on ice for 30 minutes. Samples were run in triplicate and read at OD490 using a Beckman DU-640B spectrophotometer. Data expressed as milligrams of glycogen per gram of placenta.

RESULTS

Irf6 is expressed in the trophectoderm and placenta

Placental sections and blastocysts were immuno-stained for Irf6 using a rabbit polyclonal antibody. Irf6 expression was detected in the trophectoderm of mouse embryos. This expression appeared to be nuclear (See Fig. 4.1). Irf6 expression was detected at E14.5 in wildtype placenta (see Fig 4.2A). Specifically, Irf6 expression was observed in the trophoblast giant cells (see Fig 4.2C). This localization was completely cytoplasmic and punctate. In addition, Irf6 expression was observed throughout the junctional zone. Within the spongiotrophoblast, Irf6 expression was also cytoplasmic and punctate (see Fig. 4.2D). In the trophoblast glycogen cells within the junctional zone, Irf6 appeared to be localized just around the nucleus (see Fig4.2E. Occasionally, Irf6 expression was detected in the labyrinth zone. This was due to the localization of trophoblast glycogen clusters in the labyrinth zone. In wildtype placenta, Irf6 was no longer detectable by E17.5. Irf6 expression was also detected in the uterine epithelium, maternal tissue attached to the placenta. Here, Irf6 was localized to the apical membrane (See Fig 4.2F). These data are consistent with a role for Irf6 in trophectoderm and placental development.

IRF6 expression was also observed in fixed human placental tissue. Specifically, IRF6 expression was detected in the chorionic villi, a structure analogous to the villi

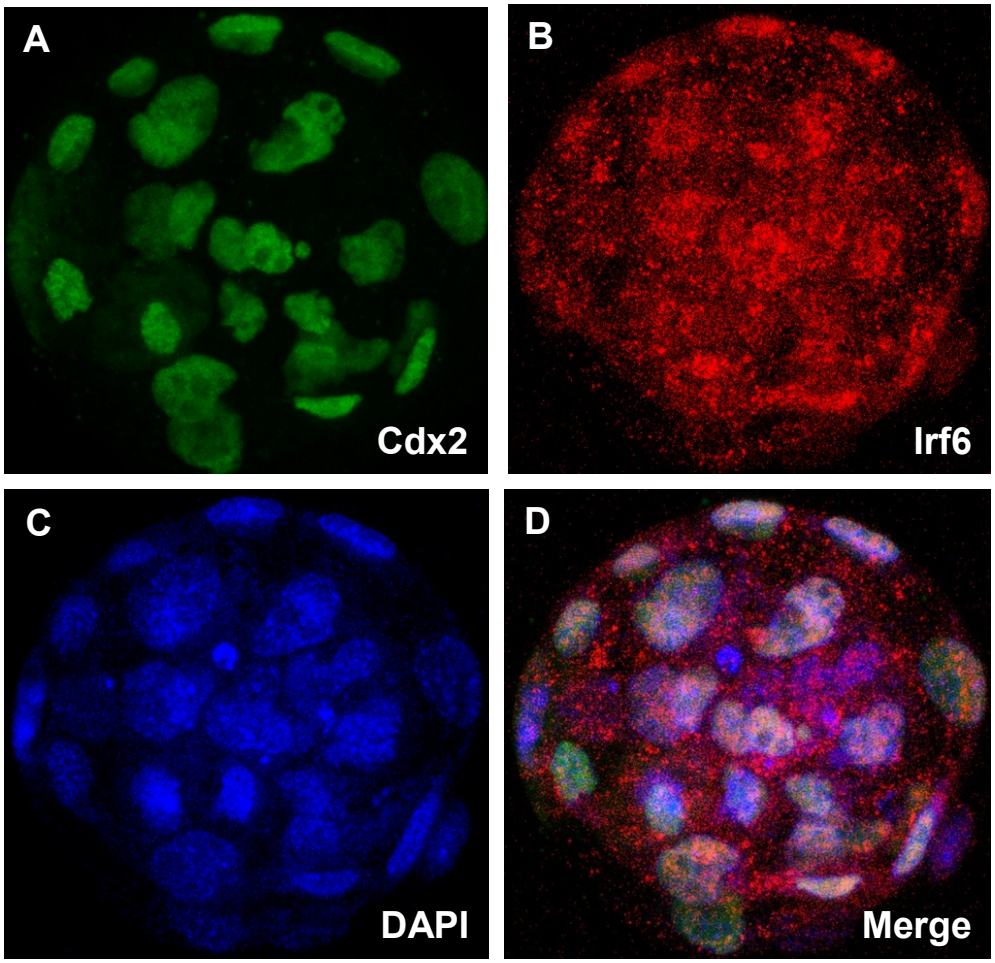

Figure 4.1: **Irf6 expression in the trophectoderm**. Blastocysts were stained for Cdx2 (A), a marker of the trophectoderm, and Irf6 (B). DAPI (C) represents nuclei. D) Merge of all three images.

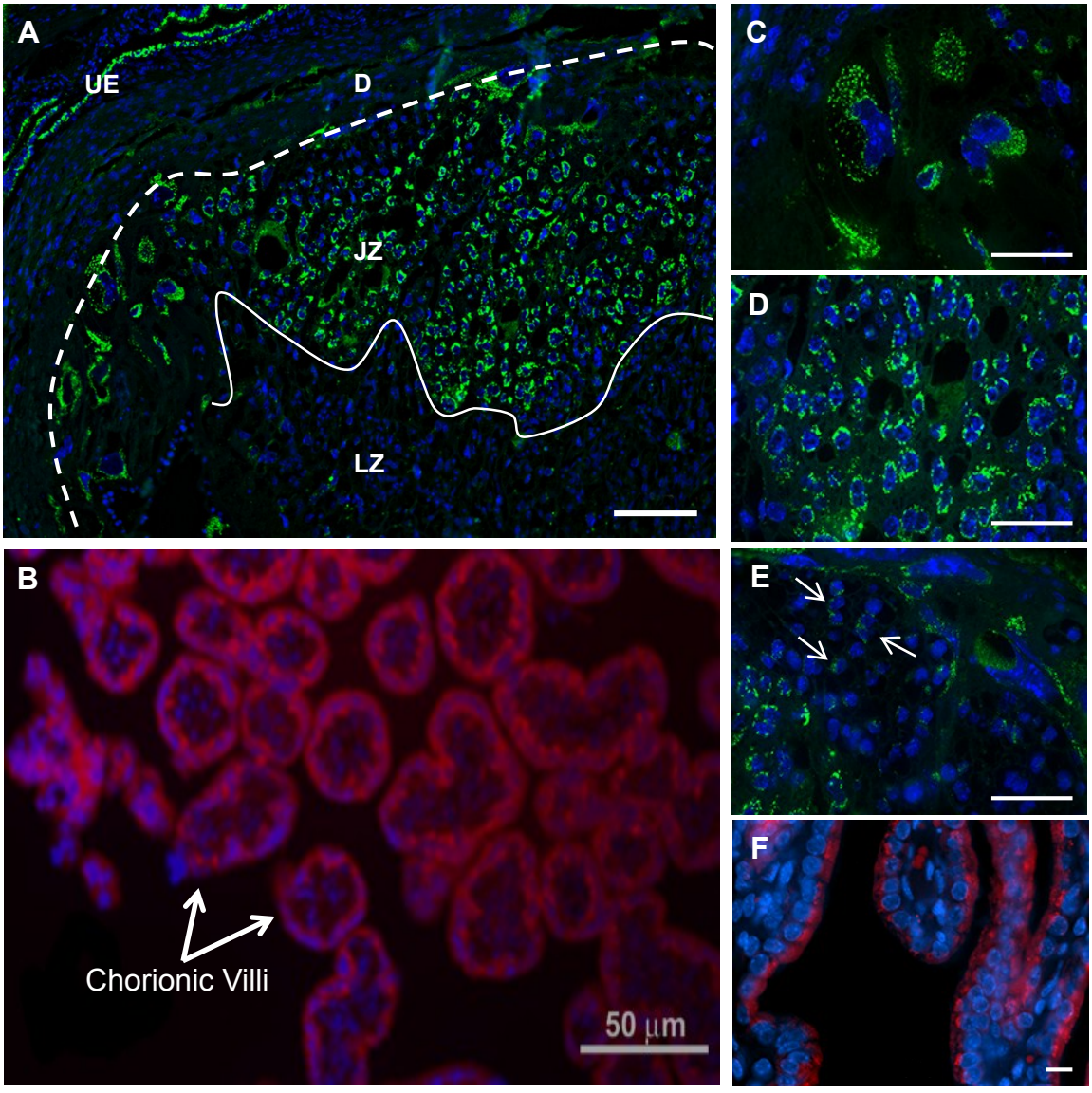

Figure 4.2: Irf6 expression in the placenta.

Figure 4.2 (cont'd)

A) Irf6 is expressed in the mouse placenta (green; Nuclei – blue, scale bar represents 100μm) . B) Irf6 expression is observed in the synctiotrophoblast of the chorionic villi of human placenta (red; Nuclei – blue). In the mouse placenta, punctate Irf6 expression in trophoblast giant cells (C) and spongiotrophoblasts (D) is observed. E) Irf6 was expressed in trophoblast glycogen cells (white arrows). F) Apical expression of Irf6 (red) in uterine luminal epithelium. Scale bar represents 10μm. B) Irf6 is expressed in the human placenta (red). UE – Uterine epithelium, D – Decidua, JZ – Junctional Zone, LZ – Labyrinth zone. Scale bars represent 50μm in B,C,D, and E.

found in the labyrinth zone of mouse placenta (see Fig 4.2B). Unlike the mouse, IRF6 expression in the mouse persists until late gestational stages. Immunostaining for Irf6 in human placental tissue was done by Dr. Anuja Dokras. Expression of IRF6 in the human placenta suggest that Irf6 function in the placenta is conserved across mammals.

Loss of Irf6 does not alter placental morphology:

To determine the role of Irf6 in placental development, we assessed a common metric, area of placental zones. Many knock out mouse models with impaired placental development exhibit defective placental growth as measured by the area of the entire placenta or the specific zones of placenta (Sferruzzi-Perri *et al.*, 2009; Tunster *et al.*, 2010; Wu *et al.*, 2003). The placental zones of $Irf6^{+/+}$ and $Irf6^{gt/gt}$ placentas were measured and compared. At E14.5, we analyzed 13 $Irf6^{+/+}$ and 14 $Irf6^{gt/gt}$ placentas. There was no difference in the area of the whole placenta, LZ, or JZ (Fig. 4.3A). At E17.5, we analyzed eight $Irf6^{+/+}$ and seven $Irf6^{gt/gt}$ placentas. Similarly, we found no difference in the area of whole placenta or any of the placental zones (Fig 4.3B). In addition, there was no difference in wet weights of the placenta or the embryo at both time points assessed (see Fig 4.4).

Loss of Irf6 does not alter glycogen content or localization:

Irf6 was expressed in trophoblast glycogen cells. To analyze the effect of loss of *Irf6* on trophoblast glycogen cell development and function, we utilized Periodic Acid-Schiff (PAS), a histological stain used to detect glycogen. Placental sections at E14.5 were stained with PAS and the number of glycogen clusters localized to the labyrinth zone was counted. Ten $Irf6^{+/+}$ and twelve $Irf6^{gt/gt}$ placenta were analyzed. There was no

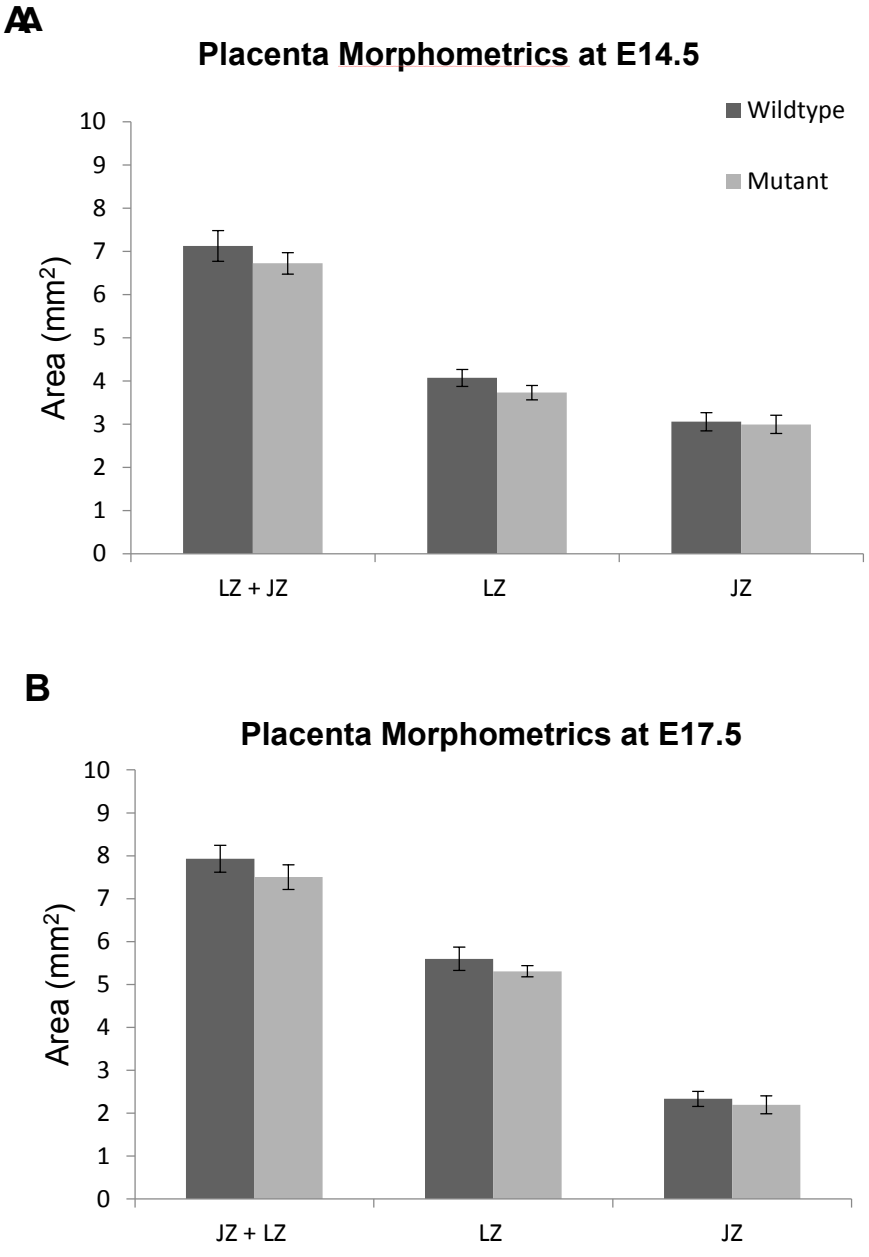

Figure 4.3: Loss of Irf6 does not alter placental morphology.

Figure 4.3 (cont'd)

'Wildtype' refers to *Irf6*$^{+/+}$ placenta. 'Mutant' refers to *Irf6*$^{gt/gt}$ placenta. A) Area measurements of placental zones at E14.5. Data represent 13 Wildtype and 14 Mutant placentas. (JZ+LZ: Wildtype – 7.12 ± 0.36, Mutant – 6.72 ± 0.25. LZ: Wildtype – 4.07 ± 0.19, Mutant – 3.73 ± 0.17. JZ: Wildtype – 3.05 ± 0.21. Mutant – 2.99 ± 0.21). B) Area measurements of placental zones at E17.5. Data represent measurements from eight Wildtype and seven Mutant placentas. (JZ+LZ: Wildtype – 7.92 ± 0.31, Mutant – 7.50 ± 0.29. LZ: Wildtype – 5.60 ± 0.27, Mutant – 5.31 ± 0.13. JZ: Wildtype – 2.33 ± 0.17, Mutant – 2.19 ± 0.21.) Error bars represent standard errors. A student's T-test was used to test for statistically significant differences between groups.

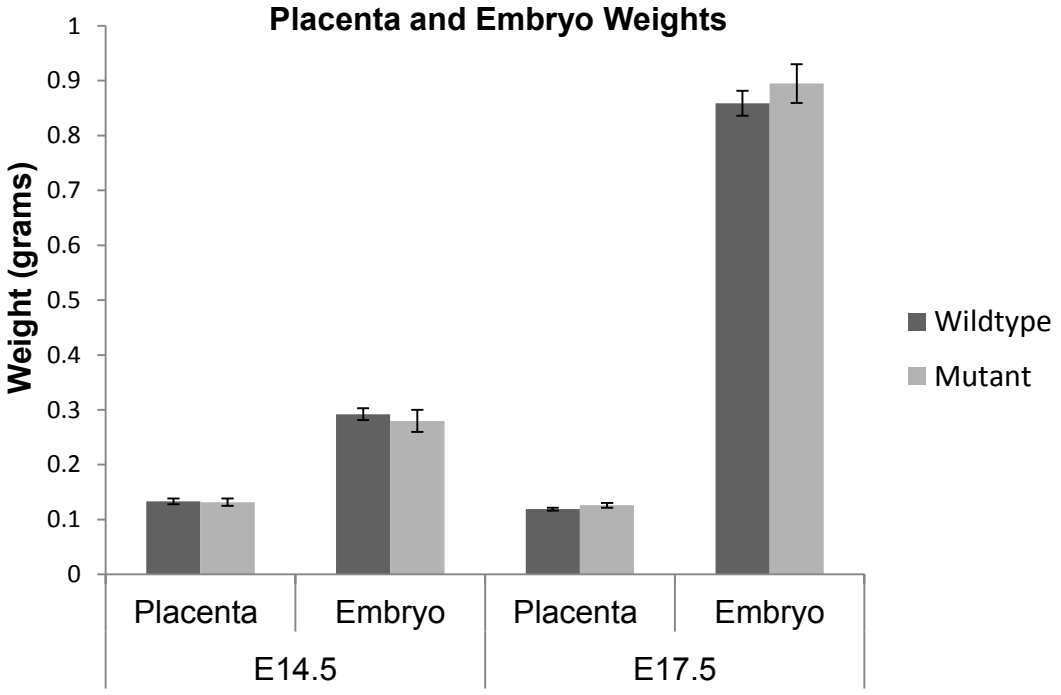

Figure 4.4: **Loss of *Irf6* does not alter placental and embryo wet weights**.

Figure 4.4 (cont'd)

Wet weights were collected at E14.5 and E17.5. Light bars representing wildtype animals were either *Irf6*$^{+/+}$ or *Irf6*$^{gt/+}$. Dark bars represent *Irf6*$^{gt/gt}$ embryos. Data at E14.5 represents average placenta and embryo weights for 25 wildtype and 12 mutant animals. (E14.5 Placenta: Wildtype – 0.13 ± 0.005, Mutant – 0.13 ± 0.007. E14.5 Embryo: Wildtype – 0.29 ± 0.01, Mutant – 0.28 ± 0.02). Data at E17.5 represents average placenta and embryo weights for 19 wildtype and seven animals. (E17.5 Placenta: Wildtype – 0.18 ± 0.002, Mutant – 0.13 ± 0.004. E17.5 Embryo: Wildtype – 0.86 ± 0.02, Mutant – 0.89 ± 0.04. Error bars represent standard error. A student's T-test was used to assess statistical significance.

significant difference in the number of trophoblast glycogen cells localized to the labyrinth zone (Student's T-test; p = 0.99, see Fig 4.5C)

While there was no difference in the number of trophoblast glycogen clusters between *Irf6*$^{+/+}$ and *Irf6*$^{gt/gt}$ placenta, PAS staining appeared to be more intense in *Irf6*-deficient placenta (see Fig4.5 A-B). Glycogen was extracted from whole placentas, and its concentration was measured at E14.5. We observed no significant difference in glycogen content between *Irf6*$^{+/+}$ and *Irf6*$^{gt/gt}$ placenta (n=3; p = 0.42, see Fig 4.5D).

DISCUSSION:

Irf6 is a critical regulator of epithelial differentiation and proliferation. The trophoblast lineage is epithelial in nature. Recent studies indicate that Irf6 is expressed in the trophectoderm of ovine embryos (Fleming *et al.*, 2009). We detected Irf6 in the murine trophectoderm. Unexpectedly, this Irf6 appeared to be localized to the nucleus. While Irf6 is a transcription factor, it has predominantly been detected in the cytoplasm. This can be due to the transient nature of Irf6 activation. Phosphorylation of IRF family members serves as an activation signal allowing for translocation into the nucleus. Concomitantly, phosphorylation also acts as a signal for degradation. While phosphorylation of Irf6 has not been shown to result in nuclear translocation, it does serve as a signal for degradation (Bailey *et al.*, 2008). The nuclear localization observed in blastocysts suggests that Irf6 functions within the nucleus, presumably as a transcriptional regulator. Fleming et al (2009) found that Irf6 acts as a transcriptional activator in trophoblast cell lines (Fleming *et al.*, 2009). Gene expression and ChIP analysis would be required to determine if *Irf6* plays a similar role in the trophoblast lineage of mouse.

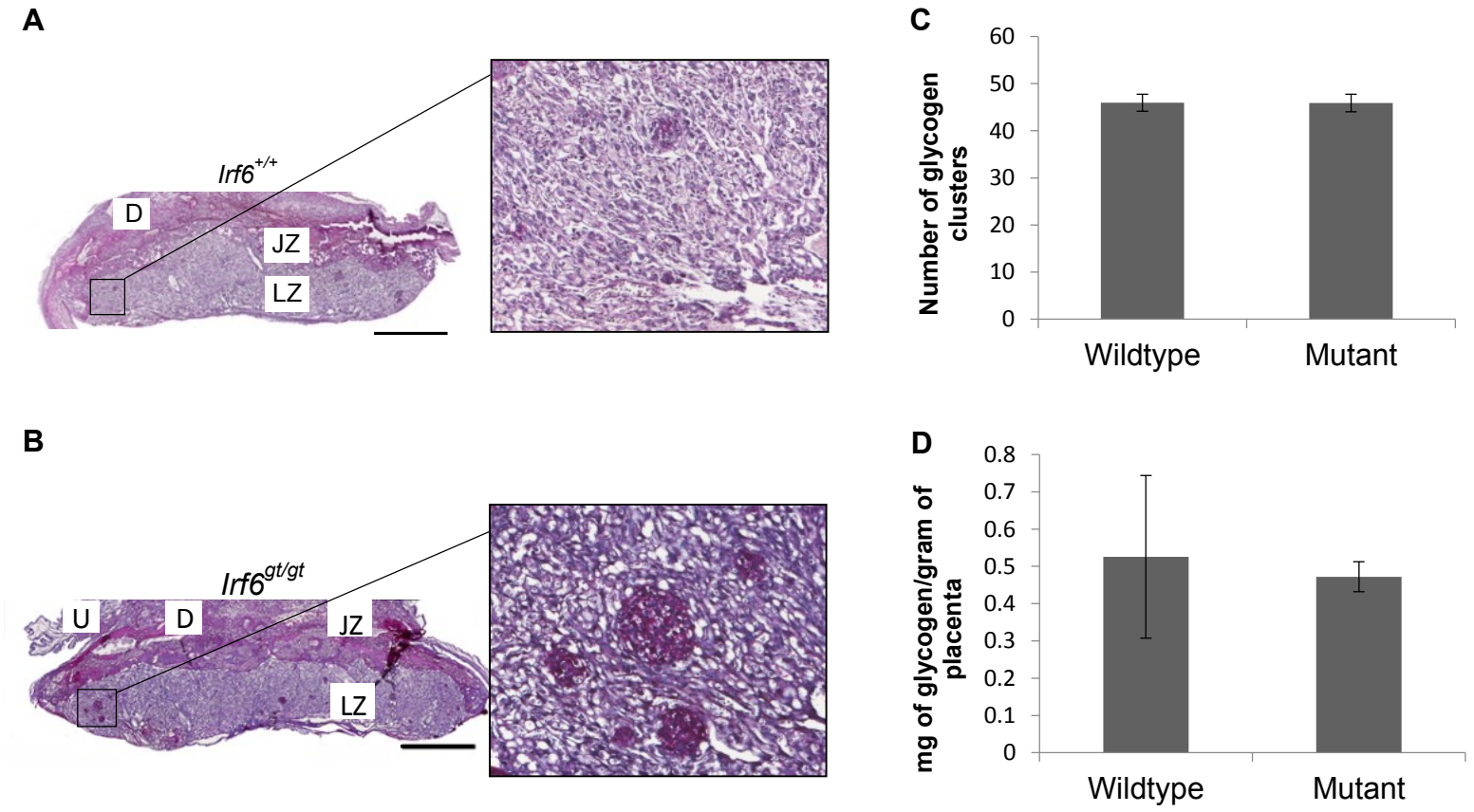

Figure 4.5: Loss of Irf6 does not affect trophoblast glycogen cell localization or content.

Figure 4.5 (cont'd)

PAS staining of placenta from wildtype (A) and mutant (B) placenta suggested an increase in trophoblast glycogen cells localized to the LZ. In addition, mutant placenta appeared to display more intense staining. C) Trophoblast glycogen cells localized to the LZ were counted at E14.5. Data represent counts from ten wildtype and 12 mutant placentas. (Wildtype – 45.96 ± 1.82, Mutant – 45.91 ± 1.82, $p = 0.45$). There was no statistical difference between wildtype and mutant glycogen cell localization. D) Total glycogen content in placenta at E14.5. Data represents glycogen content from three wildtype and three mutant placenta. (Wildtype – 0.53 ± 0.22, Mutant – 0.47 ± 0.04; $p=0.42$) For all graphs, error bars represent standard deviations and a Student's T-test was used to determine statistical significance

In the mouse, we observed Irf6 expression in spongiotrophoblast and trophoblast giant cells. In human placenta, Irf6 was detected in the chorionic villi of human placenta. Irf6 was localized to the cytoplasm in these cell types. In the mouse, the spongiotrophoblast and trophoblast giant cells express numerous members of the prolactin hormone family, including placental lactogens, and growth hormone (Hu and Cross, 2010; Lu *et al.*, 1994). Unlike the chorionic villi in the mouse, the chorionic villi of the human placenta also serve as a source of pregnancy specific hormones (Haig, 2008). Given the endocrine function of these cells, Irf6 may play a conserved role in regulating these hormones in the placenta.

To determine the function of Irf6 in the murine placenta, placental morphology was examined in $Irf6^{+/+}$ and $Irf6^{gt/gt}$ placenta. Differences in placental morphology are indicative of placental dysfunction. We found no differences in the area of any of the placental zones between $Irf6^{+/+}$ and $Irf6^{gt/gt}$. In addition, there was no difference in body or placental weights of $Irf6^{gt/gt}$ animals when compared to wildtype counterparts. These data suggest a non-essential role for Irf6 in placental development. In support of a non-essential role for Irf6 in placental development, we observed no change in trophoblast glycogen cell content or localization despite expression in these cell types.

The physiological relevance of placenta-produced hormones is ill-defined. Pregnancy can occur without complication in the absence of growth hormone and placental lactogens in humans (Nielsen *et al.*, 1979; Rygaard *et al.*, 1998). In the mouse, PLP-A, a member of the prolactin family of hormones was dispensable in normal laboratory settings with unlimited access to food and water as well as routine hygienic maintenance. However, in hypoxic conditions, *PLP-A* null mice were unable to

maintain pregnancies due to placentation failure and impaired nutrient flow (Ain *et al.*, 2004). Similarly, if the function of Irf6 is to regulate placental hormones, we hypothesize that an observable phenotype will be observed under conditions of physiological stress, such as hypoxia or nutrient limitation.

Alternately, as the IRF family is a nine-member family of transcription factors, other family members may be performing redundant function in the placenta (Tamura *et al.*, 2008). For example, *Irf1* is expressed in numerous placental cell types, including the trophoblast giant cells. *Irf1*- deficient placenta and pups are smaller than wildtype counterparts (Ashkar *et al.*, 2003). These data indicate a critical role for *Irf1* in placenta development. Therefore, *Irf1* function may compensate for loss of *Irf6* in the murine placenta. To address functional redundancy between IRF family members multi-gene knockouts must be generated.

Lastly, Irf6 was localized to the apical domain of the luminal epithelium during gestation. *Irf6* mRNA was also expressed in the luminal and glandular epithelium of the ovine uterus (Fleming *et al.*, 2009). In addition, Irf6 was also localized to the apical membrane of mammary epithelium and subsequently secreted into breast milk (Bailey *et al.*, 2009). Apical Irf6 in the uterine epithelium may be secreted into amniotic fluid. The function of secreted Irf6 is unknown. The use of the conditional allele of Irf6 in combination with Cre drivers specific to uterine tissues are required to determine the function of this apically localized Irf6.

In summary, we assessed Irf6 expression in the murine placenta and conducted a morphological analysis using tissue from Irf6-null embryos. While Irf6 was expressed in the trophectoderm and murine placenta, we conclude that the role of Irf6 during

placentation is dispensable. This is the first study to document Irf6 expression in the mouse placenta. Further studies must be conducted to determine the compound effects of loss of Irf6 in the presence of physiological stressors.

REFERENCES

REFERENCES

Ain R, Dai G, Dunmore JH, Godwin AR, Soares MJ. 2004. A prolactin family paralog regulates reproductive adaptations to a physiological stressor. Proc Natl Acad Sci U S A 101: 16543-16548.

Ananth CV, Keyes KM, Wapner RJ. 2013. Pre-eclampsia rates in the United States, 1980-2010: age-period-cohort analysis. BMJ 347: f6564.

Ashkar AA, Black GP, Wei Q, He H, Liang L, Head JR, Croy BA. 2003. Assessment of requirements for IL-15 and IFN regulatory factors in uterine NK cell differentiation and function during pregnancy. J Immunol 171: 2937-2944.

Bailey CM, Abbott DE, Margaryan NV, Khalkhali-Ellis Z, Hendrix MJ. 2008. Interferon regulatory factor 6 promotes cell cycle arrest and is regulated by the proteasome in a cell cycle-dependent manner. Mol Cell Biol 28: 2235-2243.

Bailey CM, Margaryan NV, Abbott DE, Schutte BC, Yang B, Khalkhali-Ellis Z, Hendrix MJ. 2009. Temporal and spatial expression patterns for the tumor suppressor Maspin and its binding partner interferon regulatory factor 6 during breast development. Dev Growth Differ 51: 473-481.

Ben J, Jabs EW, Chong SS. 2005. Genomic, cDNA and embryonic expression analysis of zebrafish IRF6, the gene mutated in the human oral clefting disorders Van der Woude and popliteal pterygium syndromes. Gene Expr Patterns 5: 629-638.

Chavez DJ, Enders AC, Schlafke S. 1984. Trophectoderm cell subpopulations in the periimplantation mouse blastocyst. J Exp Zool 231: 267-271.

Coan PM, Conroy N, Burton GJ, Ferguson-Smith AC. 2006. Origin and characteristics of glycogen cells in the developing murine placenta. Dev Dyn 235: 3280-3294.

Cross JC. 2006. Placental function in development and disease. Reprod Fertil Dev 18: 71-76.

de la Garza G, Schleiffarth JR, Dunnwald M, Mankad A, Weirather JL, Bonde G, Butcher S, Mansour TA, Kousa YA, Fukazawa CF, Houston DW, Manak JR, Schutte BC, Wagner DS, Cornell RA. 2013. Interferon regulatory factor 6 promotes differentiation of the periderm by activating expression of Grainyhead-like 3. J Invest Dermatol 133: 68-77.

Fan X, Hagos EG, Xu B, Sias C, Kawakami K, Burdine RD, Dougan ST. 2007. Nodal signals mediate interactions between the extra-embryonic and embryonic tissues in zebrafish. Dev Biol 310: 363-378.

Faye-Petersen OM. 2008. The placenta in preterm birth. J Clin Pathol 61: 1261-1275.

Fleming JA, Song G, Choi Y, Spencer TE, Bazer FW. 2009. Interferon regulatory factor 6 (IRF6) is expressed in the ovine uterus and functions as a transcriptional activator. Mol Cell Endocrinol 299: 252-260.

Georgiades P, Ferguson-Smith AC, Burton GJ. 2002. Comparative developmental anatomy of the murine and human definitive placentae. Placenta 23: 3-19.

Haig D. 2008. Placental growth hormone-related proteins and prolactin-related proteins. Placenta 29 Suppl A: S36-41.

Hu D, Cross JC. 2010. Development and function of trophoblast giant cells in the rodent placenta. Int J Dev Biol 54: 341-354.

Ingraham CR, Kinoshita A, Kondo S, Yang B, Sajan S, Trout KJ, Malik MI, Dunnwald M, Goudy SL, Lovett M, Murray JC, Schutte BC. 2006. Abnormal skin, limb and craniofacial morphogenesis in mice deficient for interferon regulatory factor 6 (Irf6). Nat Genet 38: 1335-1340.

Kunath T, Strumpf D, Rossant J. 2004. Early trophoblast determination and stem cell maintenance in the mouse--a review. Placenta 25 Suppl A: S32-38.

Linzer DI, Fisher SJ. 1999. The placenta and the prolactin family of hormones: regulation of the physiology of pregnancy. Mol Endocrinol 13: 837-840.

Lu XJ, Deb S, Soares MJ. 1994. Spontaneous differentiation of trophoblast cells along the spongiotrophoblast cell pathway: expression of members of the placental prolactin gene family and modulation by retinoic acid. Dev Biol 163: 86-97.

Malassine A, Frendo JL, Evain-Brion D. 2003. A comparison of placental development and endocrine functions between the human and mouse model. Hum Reprod Update 9: 531-539.

Muglia LJ, Katz M. 2010. The enigma of spontaneous preterm birth. N Engl J Med 362: 529-535.

Ness RB, Sibai BM. 2006. Shared and disparate components of the pathophysiologies of fetal growth restriction and preeclampsia. Am J Obstet Gynecol 195: 40-49.

Nielsen PV, Pedersen H, Kampmann EM. 1979. Absence of human placental lactogen in an otherwise uneventful pregnancy. Am J Obstet Gynecol 135: 322-326.

Richardson RJ, Dixon J, Jiang R, Dixon MJ. 2009. Integration of IRF6 and Jagged2 signalling is essential for controlling palatal adhesion and fusion competence. Hum Mol Genet 18: 2632-2642.

Richardson RJ, Dixon J, Malhotra S, Hardman MJ, Knowles L, Boot-Handford RP, Shore P, Whitmarsh A, Dixon MJ. 2006. Irf6 is a key determinant of the keratinocyte proliferation-differentiation switch. Nat Genet 38: 1329-1334.

Rossant J, Cross JC. 2001. Placental development: lessons from mouse mutants. Nat Rev Genet 2: 538-548.

Rygaard K, Revol A, Esquivel-Escobedo D, Beck BL, Barrera-Saldana HA. 1998. Absence of human placental lactogen and placental growth hormone (HGH-V) during pregnancy: PCR analysis of the deletion. Hum Genet 102: 87-92.

Sabel JL, d'Alencon C, O'Brien EK, Van Otterloo E, Lutz K, Cuykendall TN, Schutte BC, Houston DW, Cornell RA. 2009. Maternal Interferon Regulatory Factor 6 is required for the differentiation of primary superficial epithelia in Danio and Xenopus embryos. Dev Biol 325: 249-262.

Sferruzzi-Perri AN, Macpherson AM, Roberts CT, Robertson SA. 2009. Csf2 null mutation alters placental gene expression and trophoblast glycogen cell and giant cell abundance in mice. Biol Reprod 81: 207-221.

Sibai B, Dekker G, Kupferminc M. 2005. Pre-eclampsia. Lancet 365: 785-799.

Tamura T, Yanai H, Savitsky D, Taniguchi T. 2008. The IRF family transcription factors in immunity and oncogenesis. Annu Rev Immunol 26: 535-584.

Tesser RB, Scherholz PL, do Nascimento L, Katz SG. 2010. Trophoblast glycogen cells differentiate early in the mouse ectoplacental cone: putative role during placentation. Histochem Cell Biol 134: 83-92.

Tunster SJ, Tycko B, John RM. 2010. The imprinted Phlda2 gene regulates extraembryonic energy stores. Mol Cell Biol 30: 295-306.

Wu L, de Bruin A, Saavedra HI, Starovic M, Trimboli A, Yang Y, Opavska J, Wilson P, Thompson JC, Ostrowski MC, Rosol TJ, Woollett LA, Weinstein M, Cross JC, Robinson ML, Leone G. 2003. Extra-embryonic function of Rb is essential for embryonic development and viability. Nature 421: 942-947.

Zybina EV, Zybina TG, Stein GI. 2000. Trophoblast cell invasiveness and capability for the cell and genome reproduction in rat placenta. Early Pregnancy 4: 39-57.

CHAPTER FIVE:

Summary and Future Directions

SUMMARY AND FUTURE DIRECTIONS

Interferon Regulatory Factor 6 is known for its role in pathogenesis of cleft lip and palate. Mutations in *IRF6* cause two Mendelian clefting disorders (Kondo *et al.*, 2002). DNA variation in *IRF6* contributes risk for isolated cleft lip and palate (Rahimov *et al.*, 2008). Mice deficient for *Irf6* display severe skin, limb, and craniofacial defects (Ingraham *et al.*, 2006; Richardson *et al.*, 2006) . However, some studies have implicated Irf6 in development of the oocyte and the extra-embryonic lineage. Namely, irf6 is expressed in and required for normal development of the superficial epithelium in zebrafish and frog, a tissue with anatomical and molecular similarities to the trophectoderm (Sabel *et al.*, 2009). *Irf6* is expressed in the ovine trophectoderm and acts as a transcriptional activator in ovine trophoblast cell lines (Fleming *et al.*, 2009). In addition, *Irf6* is expressed in the bovine oocyte (Regassa *et al.*, 2011). Given these data, we hypothesized that *Irf6* was critical for proper trophectoderm development and that maternally expressed *Irf6* is required for early embryonic development in the mouse. To test this hypothesis, we generated and characterized a novel genetic tool as well as utilized a conventional *Irf6* knockout mouse model.

In this work, we generated a novel conditional allele of *Irf6* allowing for *Cre*-mediated recombination. This was particularly useful because mice deficient for *Irf6* die shortly after birth (Ingraham *et al.*, 2006), impeding the study of *Irf6* function in postnatal development and disease. This conditional allele was susceptible to Cre-mediated recombination. In addition, recombination of this allele was sufficient to produce a null allele of *Irf6*. Thus, the conditional allele can be used for deletion of *Irf6* in a tissue specific fashion. This conditional model is especially relevant in cases where *Irf6*

function remains undefined due to perinatal lethality. For example, the expression of Irf6 in mammary epithelium is rather unique. Irf6 is localized to the apical membrane of mammary epithelial cells during lactation and secreted into breast milk (Bailey *et al.*, 2009). This is atypical localization and behavior for a transcription factor. The use of a mammary specific Cre- line, such as MMTV-Cre or WAP-Cre (Wagner *et al.*, 1997), would allow for analysis of Irf6 function in mammary epithelium. In the context of this work, future studies should employ the conditional allele to explore the function of Irf6 in uterine luminal epithelium, where apical localization is also observed, and in granulosa cells of ovarian follicles.

While recombination of the conditional allele produced a null allele, it is important to note that the efficiency of this recombination event differed based on the transgenic *Cre* line being used. *CAG-Cre* and *Ella-Cre* mediated recombination of the conditional allele with different efficiency, despite being expressed at the same time point of development. Similarly, our collaborators have reported incomplete recombination of the conditional allele in the palate (*Tgfβ3-Cre*), skin (*K14-Cre-ER*), and macrophages (*LysM-Cre*). Incomplete recombination when using Cre transgenic lines is not uncommon and is most likely due to positional effects at the transgene integration site or incomplete promoter fragments upstream of the *Cre* gene. However, such mosaicism may affect interpretation of data. One strategy to overcome such problems is to utilize the conditional allele in combination with a null allele of *Irf6*. In this case, only one recombination event will be required per cell.

Methylation of the target locus has also been shown to inhibit Cre recombinase activity (Long and Rossi, 2009). A CpG island near the *IRF6* promoter was shown to be

methylated. This methylation is associated with reduced IRF6 expression (Botti *et al.*, 2011). To determine if methylation affects recombination efficiency, bisulfite sequencing should be conducted to determine the methylation status of *Irf6* in different cell types in question. These data would aid in selection of appropriate *Cre* drivers and also provide insight into mechanisms of *Irf6* regulation in different cell types.

In the research reported here, we utilized the conditional allele to generate mice with oocyte specific deletion of *Irf6.* This was motivated by the findings that *Irf6* is maternally deposited in the oocyte in zebrafish, frog, and cow and that maternal irf6 protein is required for normal early embryonic development. We utilized the *Gdf9-Cre* to drive *Cre* expression in primordial follicles as early as postnatal day 3 (Lan *et al.*, 2004). *Gdf9-Cre* mediated recombination of the conditional allele occurred at high efficiency and prior to completion of meiosis I during oogenesis.

For protein expression analysis in the ovary, we utilized a number of antibodies against Irf6. The first antibody was produced in rabbit and published by *Ingraham et al* (2006). With this antibody, we observed Irf6 signal in the oocyte (punctate throughout the cytoplasm) and in granulosa cells. However, due to lack of availability, we were not able to test this antibody in ovaries from experimental females. The second antibody tested was a commercial antibody produce in rabbit against amino acids 441 – 455 (Sigma-Aldrich, St. Louis, MO). While this antibody replicated the staining patterns of that published by *Ingraham et al (2006*) in both wildtype and *Irf6*-deficient skin, we were unable to detect a signal in ovaries from control or experimental animals. Therefore, this antibody was not used for further experiments. Lastly, we tested rabbit anti-Irf6 antibody generated by our lab (Irf6-SPEA). In wildtype embryonic skin, this antibody

replicated the expression pattern published by Ingraham et al (2006). However, immunofluorescent signal was also observed in skin from mice deficient for Irf6.

Protein expression analysis on oocytes collected from experimental females was conducted using the Irf6-Akira antibody. The immunizing peptide mapped to exon six of the Irf6 protein. Immunofluorescent and Western blot analysis of oocytes from experimental females indicate ineffective deletion of Irf6 protein, despite genetic evidence of recombination. While immunofluorescent signal for Irf6 is not lost in Irf6-deficient control tissues (skin), the findings in the oocyte have been confirmed with real-time PCR analysis. Specifically, only a 30% reduction in *Irf6* mRNA in oocytes from experimental females was observed. While this reduction may be statistically significant, it may have little biological relevance.

The observed mRNA and protein can be explained by a unique feature of the oocyte, the storage of mRNA and proteins to drive early embryonic development. We utilized an in vivo system to generate oocyte specific deletion of Irf6. However, such experiments are routinely done in vitro by injection of mature oocytes with siRNAs against maternal effect genes. In some cases, this approach has been complicated by persistence of stored maternal mRNAs and proteins. In fact, a new technique in which oocytes are collected at postnatal day 12 and injected with siRNA followed by in vitro maturation has been developed to overcome the effects of stored maternal gene products (Inoue *et al.*, 2014).

The data presented here suggests that Irf6 expression precedes that of *Gdf9-Cre.* Therefore, future studies utilizing the *VASA-Cre* transgenic mouse line, which would mediate gene deletion in germ cells as early as embryonic day 15 (Gallardo *et*

al., 2007), may provide more effective gene deletion, thus being a better model for studying the function of Irf6 in oogenesis. Use of the VASA-Cre line may provide a more robust phenotype during oogenesis as stores of Irf6 would not be available to aid in development. In addition, effective deletion of *Irf6* in oogenesis may result in a phenotype during early embryonic development as most stored gene products are activated for function following fertilization.

Irf6 is expressed in primordial germ cells however, it unclear at what time point this expression starts. Irf6 mRNA was also detected in the testes (Kondo *et al.*, 2002). These data suggest that *Irf6* may also play a role in development of the male germ cell, the sperm. Further gene expression analysis must be conducted to confirm the expression of Irf6 in sperm. Because *VASA-Cre* has been documented to drive *Cre* expression during embryogenesis, this transgenic line can be used to study a potential role of *Irf6* in spermatogenesis.

Despite the conflicting deletion data, we observed two novel phenotypes. First, experimental females had increased litter size. This increase was accompanied by an increase in the number of eggs ovulated. Future studies should be aimed at elucidating the underlying mechanism of this increased fertility. Ovulation in mammals is regulated is in part regulated by complex interactions between the oocyte and surrounding granulosa cells. At the core of these interactions is Gdf-9 and BMP-15, two oocyte specific factors and members of the TGFβ superfamily. These paracrine factors are known to regulate ovulation in both mice and sheep. Notably, sheep carrying mutations in either gene display increased fertility (Otsuka *et al.*, 2011). In addition, novel variants in GDF9 are overrepresented in mothers of dizygotic twins (Palmer *et al.*,

2006). *Irf6* is regulated by *Tgfβ3* signaling in the palate (Iwata *et al.*, 2013). It is possible that *Irf6* is regulated by Gdf9 and Bmp15 signaling in oocytes. To test this hypothesis, mice with mutations in *Gdf9* or *Bmp15* should be crossed with our experimental females to determine if epistatic relationships exist. Also, levels of *Irf6* mRNA and protein should be assessed in mice deficient for *Gdf9* or *Bmp15*. For future studies, it would also be interesting to examine associations between variants in IRF6 and rates of dizygotic twinning.

The second novel phenotype we observed was multiple oocyte follicles (MOF). As with ovulation, mice homozygous for null mutations of *Bmp15* and heterozygous for a null mutation of *Gdf9* develop multiple oocyte follicles (Yan *et al.*, 2001). Furthermore, Notch signaling is also implicated in MOF formation (Xu and Gridley, 2013). Irf6 expression is regulated by Notch signaling in keratinocytes (Restivo *et al.*, 2011). We hypothesize that these pathways regulate *Irf6* expression in the oocyte. To test this hypothesis, *Irf6* mRNA and protein levels should be assessed in the Gdf9/Bmp15 double mutants and in models with ablated Notch signaling (Notch2 and Lunatic Fringe).

Irf6 expression was also observed in the granulosa cells, the somatic cells surrounding the oocyte. These cells play critical roles in oocyte health and maturation. Future experiments studying the role of Irf6 in the granulosa cells may provide further insight into the molecular communication network that exist between the oocyte and granulosa cells. Specifically, females with a granulosa cell specific deletion of *Irf6* can be generated using the Cyp19-Cre transgenic line. Granulosa cells are epithelial in nature. *Irf6* is required for proper differentiation of epithelial cell types (Biggs *et al.*,

2012; Ingraham *et al.*, 2006). Therefore, loss of *Irf6* in the granulosa cells may result in impaired differentiation and subsequently, female infertility. It has been documented that oocyte- or granulosa- specific loss of certain genes results in opposing phenotypes (Adhikari *et al.*, 2010; Huang *et al.*, 2013).

While the incidence of MOFs is intriguing, the physiological relevance of MOFs remains to be determined. However, the potential connections between *Tgfβ* signaling, Notch signaling and Irf6 present an opportunity to explore more fundamental aspects of *Irf6* biology. Irf6 is regulated by *MCS9.7*, an enhancer element 9.7kb upstream of the transcriptional start site (Rahimov *et al.*, 2008). Common DNA variants in this enhancer element contribute significant risk for isolated cleft lip and palate. However, this enhancer element is not active in the medial edge epithelium of the palate, where *Irf6* is regulated by *Tgfβ3 (*Fakhouri *et al.,* 2012*;* Richardson *et al.,* 2009*).* These data suggest that Irf6 is regulated by a second enhancer element and that *Tgfβ* signals through this enhancer. Our preliminary assessments of *MCS9.7* activity in the ovary indicate that it is not active.

A second putative enhancer element, characterized by enrichment of monomethylation of histone H3 lysine 4, has been identified. This element lies ~1 to 4.5 kb upstream of the transcriptional start site. In addition, canonical binding sites for Notch and SMAD (downstream of *Tgfβ* signaling) within this element have verified in skin (Iwata *et al.*, 2013; Restivo *et al.*, 2011). Therefore, the ovary/oocyte may provide a valuable tissue in the characterization of a novel *Irf6* enhancer element. Much like *MCS9.7*, this enhancer element may have significant clinical relevance as DNA variants may increase risk for skin disorders in which Irf6 is involved, including squamous cell

carcinoma and wound healing. In the context of this work, DNA variants in this novel enhancer may be associated with increased incidence of reproductive phenotypes. Mice with oocyte specific excision of Irf6 produce more offspring per pregnancy due to increase number of eggs ovulated. Therefore, future experiments aimed at characterizing the activity of this enhancer in the ovary and sequencing populations with high twinning rates may provide a new candidate for twinning.

The last portion of this work was aimed at elucidating the role of *Irf6* in placental development. The staining pattern of Irf6 in mouse and human placenta could indicate a role in hormone production. To test this hypothesis, real-time PCR should be conducted to assess expression of different placenta-specific hormones in wildtype and *Irf6*-deficient placenta. If differences are identified, then it would be necessary to examine placental development following exposure to physiological stressors.

The data presented in this work provide a novel role for Irf6 in reproductive processes. The future work described here will provide further insight into the molecular mechanisms governing these phenotypes. In addition, deciphering these mechanisms will allow for generation and testing of hypotheses in human populations.

REFERENCES

REFERENCES

Adhikari D, Zheng W, Shen Y, Gorre N, Hamalainen T, Cooney AJ, Huhtaniemi I, Lan ZJ, Liu K. 2010. Tsc/mTORC1 signaling in oocytes governs the quiescence and activation of primordial follicles. Hum Mol Genet 19: 397-410.

Bailey CM, Margaryan NV, Abbott DE, Schutte BC, Yang B, Khalkhali-Ellis Z, Hendrix MJ. 2009. Temporal and spatial expression patterns for the tumor suppressor Maspin and its binding partner interferon regulatory factor 6 during breast development. Dev Growth Differ 51: 473-481.

Biggs LC, Rhea L, Schutte BC, Dunnwald M. 2012. Interferon regulatory factor 6 is necessary, but not sufficient, for keratinocyte differentiation. J Invest Dermatol 132: 50-58.

Botti E, Spallone G, Moretti F, Marinari B, Pinetti V, Galanti S, De Meo PD, De Nicola F, Ganci F, Castrignano T, Pesole G, Chimenti S, Guerrini L, Fanciulli M, Blandino G, Karin M, Costanzo A. 2011. Developmental factor IRF6 exhibits tumor suppressor activity in squamous cell carcinomas. Proc Natl Acad Sci U S A 108: 13710-13715.

Fakhouri WD, Rhea L, Du T, Sweezer E, Morrison H, Fitzpatrick D, Yang B, Dunnwald M, Schutte BC. 2012. MCS9.7 enhancer activity is highly, but not completely, associated with expression of Irf6 and p63. Dev Dyn 241: 340-349.

Fleming JA, Song G, Choi Y, Spencer TE, Bazer FW. 2009. Interferon regulatory factor 6 (IRF6) is expressed in the ovine uterus and functions as a transcriptional activator. Mol Cell Endocrinol 299: 252-260.

Gallardo T, Shirley L, John GB, Castrillon DH. 2007. Generation of a germ cell-specific mouse transgenic Cre line, Vasa-Cre. Genesis 45: 413-417.

Huang L, Wang ZB, Jiang ZZ, Hu MW, Lin F, Zhang QH, Luo YB, Hou Y, Zhao Y, Fan HY, Schatten H, Sun QY. 2013. Specific disruption of Tsc1 in ovarian granulosa cells promotes ovulation and causes progressive accumulation of corpora lutea. PLoS One 8: e54052.

Ingraham CR, Kinoshita A, Kondo S, Yang B, Sajan S, Trout KJ, Malik MI, Dunnwald M, Goudy SL, Lovett M, Murray JC, Schutte BC. 2006. Abnormal skin, limb and craniofacial morphogenesis in mice deficient for interferon regulatory factor 6 (Irf6). Nat Genet 38: 1335-1340.

Inoue A, Sunaga K, Aoki F, Zhang Y. 2014. siRNA-mediated depletion of stable proteins in mouse oocytes.

Iwata J, Suzuki A, Pelikan RC, Ho TV, Sanchez-Lara PA, Urata M, Dixon MJ, Chai Y. 2013. Smad4-Irf6 genetic interaction and TGFbeta-mediated IRF6 signaling cascade are crucial for palatal fusion in mice. Development 140: 1220-1230.

Kondo S, Schutte BC, Richardson RJ, Bjork BC, Knight AS, Watanabe Y, Howard E, de Lima RL, Daack-Hirsch S, Sander A, McDonald-McGinn DM, Zackai EH, Lammer EJ, Aylsworth AS, Ardinger HH, Lidral AC, Pober BR, Moreno L, Arcos-Burgos M, Valencia C, Houdayer C, Bahuau M, Moretti-Ferreira D, Richieri-Costa A, Dixon MJ, Murray JC. 2002. Mutations in IRF6 cause Van der Woude and popliteal pterygium syndromes. Nat Genet 32: 285-289.

Lan ZJ, Xu X, Cooney AJ. 2004. Differential oocyte-specific expression of Cre recombinase activity in GDF-9-iCre, Zp3cre, and Msx2Cre transgenic mice. Biol Reprod 71: 1469-1474.

Long MA, Rossi FM. 2009. Silencing inhibits Cre-mediated recombination of the Z/AP and Z/EG reporters in adult cells. PLoS One 4: e5435.

Otsuka F, McTavish KJ, Shimasaki S. 2011. Integral role of GDF-9 and BMP-15 in ovarian function. Mol Reprod Dev 78: 9-21.

Palmer JS, Zhao ZZ, Hoekstra C, Hayward NK, Webb PM, Whiteman DC, Martin NG, Boomsma DI, Duffy DL, Montgomery GW. 2006. Novel variants in growth differentiation factor 9 in mothers of dizygotic twins. J Clin Endocrinol Metab 91: 4713-4716.

Rahimov F, Marazita ML, Visel A, Cooper ME, Hitchler MJ, Rubini M, Domann FE, Govil M, Christensen K, Bille C, Melbye M, Jugessur A, Lie RT, Wilcox AJ, Fitzpatrick DR, Green ED, Mossey PA, Little J, Steegers-Theunissen RP, Pennacchio LA, Schutte BC, Murray JC. 2008. Disruption of an AP-2alpha binding site in an IRF6 enhancer is associated with cleft lip. Nat Genet 40: 1341-1347.

Regassa A, Rings F, Hoelker M, Cinar U, Tholen E, Looft C, Schellander K, Tesfaye D. 2011. Transcriptome dynamics and molecular cross-talk between bovine oocyte and its companion cumulus cells. BMC Genomics 12: 57.

Restivo G, Nguyen BC, Dziunycz P, Ristorcelli E, Ryan RJ, Ozuysal OY, Di Piazza M, Radtke F, Dixon MJ, Hofbauer GF, Lefort K, Dotto GP. 2011. IRF6 is a mediator of Notch pro-differentiation and tumour suppressive function in keratinocytes. EMBO J 30: 4571-4585.

Richardson RJ, Dixon J, Jiang R, Dixon MJ. 2009. Integration of IRF6 and Jagged2 signalling is essential for controlling palatal adhesion and fusion competence. Hum Mol Genet 18: 2632-2642.

Richardson RJ, Dixon J, Malhotra S, Hardman MJ, Knowles L, Boot-Handford RP, Shore P, Whitmarsh A, Dixon MJ. 2006. Irf6 is a key determinant of the keratinocyte proliferation-differentiation switch. Nat Genet 38: 1329-1334.

Sabel JL, d'Alencon C, O'Brien EK, Van Otterloo E, Lutz K, Cuykendall TN, Schutte BC, Houston DW, Cornell RA. 2009. Maternal Interferon Regulatory Factor 6 is required for the differentiation of primary superficial epithelia in Danio and Xenopus embryos. Dev Biol 325: 249-262.

Wagner KU, Wall RJ, St-Onge L, Gruss P, Wynshaw-Boris A, Garrett L, Li M, Furth PA, Hennighausen L. 1997. Cre-mediated gene deletion in the mammary gland. Nucleic Acids Res 25: 4323-4330.

Xu J, Gridley T. 2013. Notch2 is required in somatic cells for breakdown of ovarian germ-cell nests and formation of primordial follicles. BMC Biol 11: 13.

Yan C, Wang P, DeMayo J, DeMayo FJ, Elvin JA, Carino C, Prasad SV, Skinner SS, Dunbar BS, Dube JL, Celeste AJ, Matzuk MM. 2001. Synergistic roles of bone morphogenetic protein 15 and growth differentiation factor 9 in ovarian function. Mol Endocrinol 15: 854-866.